

Quantification of the thioredoxin system

by

Letrisha Padayachee

MSc (Genetics)

Submitted in fulfilment of the academic requirements for the degree of Doctor of Philosophy
in Genetics

School of Life Sciences

College of Agriculture, Engineering and Science

University of KwaZulu-Natal

Pietermaritzburg

South Africa

July 2017

Preface

The research contained in this thesis was completed by the candidate while based in the Discipline of Genetics, School of Life Sciences of the College of Agriculture, Engineering and Science, University of KwaZulu-Natal, Pietermaritzburg, South Africa.

The contents of this work have not been submitted in any form to another university and, except where the work of others is acknowledged in the text, the results reported are due to investigations by the candidate.

Name: Dr C.S Pillay

Signed: _____

Date: _____

Declaration 1: Plagiarism

I, Letrisha Padayachee, declare that:

(i) the research reported in this dissertation, except where otherwise indicated or acknowledged, is my original work;

(ii) this dissertation has not been submitted in full or in part for any degree or examination to any other university;

(iii) this dissertation does not contain other persons' data, pictures, graphs or other information, unless specifically acknowledged as being sourced from other persons;

(iv) this dissertation does not contain other persons' writing, unless specifically acknowledged as being sourced from other researchers. Where other written sources have been quoted, then:

a) their words have been re-written but the general information attributed to them has been referenced;

b) where their exact words have been used, their writing has been placed inside quotation marks, and referenced;

(v) where I have used material for which publications followed, I have indicated in detail my role in the work;

(vi) this dissertation is primarily a collection of material, prepared by myself, published as journal articles or presented as a poster and oral presentations at conferences. In some cases, additional material has been included;

(vii) this dissertation does not contain text, graphics or tables copied and pasted from the Internet, unless specifically acknowledged, and the source being detailed in the dissertation and in the References sections.

Name: Letrisha Padayachee

Signed: _____

Date: _____

List of publications and presentations

Publications:

- Padayachee, L. and Pillay, C. S. 2016. The thioredoxin system and not the Michaelis–Menten equation should be fitted to substrate saturation datasets from the thioredoxin insulin assay. *Redox Report*, 21, 170-179.
- Padayachee, L. and Pillay, C. S. 2017. Multiple measures of the thioredoxin system. *Manuscript in preparation*.
- Padayachee, L., Rohwer, J. M. and Pillay, C. S. 2017. Quantification of the thioredoxin system using the thioredoxin redox charge as a surrogate measure for flux. *Manuscript in preparation*.

Presentations:

- South African Genetics and Bioinformatics Society conference, Kwalata Game Reserve, Pretoria (2014).
- ESF-EMBO Thiol-Based Redox Switches in Life Sciences conference, Sant Feliu de Guixols, Spain (2015).
- South African Genetics and Bioinformatics Society conference, Nelson Mandela School of Medicine, Durban (2016).

Abstract

The thioredoxin system consisting of thioredoxin, thioredoxin reductase and NADPH plays a significant role in a large number of redox-dependent processes including DNA synthesis and anti-oxidant defense. Perturbations of this system have been associated with a number of diseases but contradictory descriptions of thioredoxin as both an enzyme and a redox couple have complicated the quantification of the system in these pathologies with Michaelis-Menten parameters, activity measurements, redox potentials and redox ratios all being used to describe the thioredoxin system *in vitro* and *in vivo*. To clarify these discrepancies, the thioredoxin system from *Saccharomyces cerevisiae* was cloned, expressed and purified and computational modeling as well as *in vitro* studies were used to show that accurate parameter sets for thioredoxin reduction reactions can be obtained by fitting the thioredoxin system, rather than the Michaelis-Menten equation to substrate saturation datasets. It was also confirmed that substrate saturation in the insulin reduction assay was due to the saturation of the thioredoxin redox cycle caused by limiting thioredoxin reductase concentrations, the progressive redistribution of the thioredoxin moiety into its oxidized form or both. Validation of this mechanism then enabled the use of computational models of the thioredoxin system to identify the minimum, experimentally tractable, parameter set needed to quantitatively describe the steady state behaviour of this system under stress conditions. The flux through the system represents a comprehensive description of the state of the system, but currently there are no methods available to measure this flux *in vivo* and therefore core and realistic models based on the thioredoxin system were used to determine how the existing measures of thioredoxin activity corresponded to the flux of the system under reductive supply and oxidative demand conditions. Computational modeling using a basic model of the *E. coli* thioredoxin system and comprehensive, *in vivo* computational models systematically tested all of the measures of the Trx system and revealed that a novel measure, the thioredoxin redox charge, may be a useful surrogate measure of the flux within the system. This result was confirmed by *in vitro* reductive supply and oxidative demand assays and western blot analysis using the reconstituted yeast peroxiredoxin system. Collectively, these results propose a novel, independent and experimentally tractable surrogate measure for flux through the Trx system allowing for the quantification of changes in this *system* associated with pathological conditions.

Acknowledgements

I would like to express my sincere gratitude to the following people for their contribution to this thesis.

My supervisor, Dr Ché Pillay, for having me as a student. Thank you for your unending guidance and support. Thank you for allowing me to stay in the 'cloud' for as long as I needed to and for helping me get out of it when I didn't know how to. You have been a remarkable mentor and I am truly grateful for the opportunity to have worked with you.

Prof. Armindo Salvador (University of Coimbra) for helping me with COPASI and for so generously supplying the red blood cell model used in our analysis.

Dr Elizabeth Veal (Newcastle University) for the *S. pombe* model and for all her help with the redox western blotting experiments - our first beautiful blot after weeks of failure!

Prof. Johann Rohwer for his advice and suggestions on all things computational.

Thank you to Mampo for generously sharing her TRR1 babies with me as well as Bea for her TSA1 clones.

Jess and Megan for the use of equipment and especially Goodman Zondi for all his help and willing involvement no matter the task. You have always gone the extra mile for the lab and for that I am eternally grateful.

To Lauren, thank you for helping us with the chickens ;), something we could have never done without you. All your help and advice is truly appreciated!

Pat Joubert for assisting me with lab orders and always being so cheerful no matter how gloomy the situation was.

To Charmaine Ahrens, Natalie Jones and Tanya Karalic for all their admin help.

The National Research Foundation and the Faculty of Science and Agriculture for generous scholarships during my post-graduate years.

My sisters Mary, Milly-la, Lee, Nargis, Nicole and Erasha who were always there offering love and support no matter the distance that separated us- you guys are amazing!

To Bea, thank you for being one of my greatest friends on and off campus. You truly made the time we spent in the lab so memorable with our daily sing-offs and ‘road trips’. Thank you also for our sushi outings and for introducing me to OITNB and AHS binge-watching.

To Nolyn John, thank you for always being my sounding board, for allowing me to bounce ideas off you, no matter how busy you were. I truly appreciate the time, effort and thought you put into our brainstorming sessions. I will especially miss our random chats about the “book of questions”!

To Di and Sophia, thank you for the entertaining conversations and all the laughs!

To Angie and Dedee, I will miss you two cuties most of all. Thank you for all the fun and laughter you jam-packed into our short visits. You guys are simply precious!

I would also like to thank my family especially my mum Sharlene, Twanisha, Russell, Calvin and Jody for supporting me throughout all my studies and for never questioning my decision to pursue what I love.

To the 3 greatest joys in my life, Caitlyn, Caillym and Camden, you guys have filled my life with so much of love and have made all my days so bright. Thank you for all the warm hugs and all the silly moments. I cherish each of you immensely.

To Jody, thank you for your patience and endless love. Thank you for always being there, offering support and motivation and knowing exactly when I needed it the most. Thank you especially for making our trip to Barcelona so memorable with all things ‘magical’. Aquí está el comienzo de nuestro feliz para siempre- deja que empiece la magia!

To my parents-in-law, thank you for being such special people, so warm and welcoming. Thank you for your unwavering love and support throughout the years.

And finally, my mum, to whom this thesis is dedicated, how do I put into words the enormous gratitude I have for everything you have done for me? Thank you for always being my biggest supporter, for always encouraging me to dream bigger and to work harder. All that I am or could ever hope to be, I owe to you!

List of abbreviations

AEBSF	4-(2-aminoethyl)benzenesulfonyl fluoride hydrochloride
AIS	Acute ischemic stroke
ASD	Autism spectrum disorders
BSA	Bovine serum albumin
CAD	Coronary artery disease
ddH ₂ O	Milli-Q water
dH ₂ O	Distilled water
DTNB	5, 5'-dithiobis(2-nitrobenzoic acid)
DTT	Dithiothreitol
EDTA	Ethylene diamine tetraacetic acid
FiTC–insulin	Fluorescein isothiocyanate-labeled insulin
H ₂ O ₂	Hydrogen peroxide
IPTG	Isopropyl β-D-1-thiogalactopyranoside
LB	Luria Bertani
NADPH	β-nicotinamide adenine dinucleotide phosphate
PCR	Polymerase Chain Reaction
PEG	Polyethylene glycol
PEG-maleimide	Methoxypolyethylene glycol maleimide
PySCeS	Python Simulator of Cellular Systems
SDS-PAGE	Sodium dodecyl sulfate-polyacrylamide gel electrophoresis
Sec	Selenocysteine
SGD	<i>Saccharomyces</i> genome database
TCA	Trichloroacetic acid
TEMED	N,N,N', N'-tetramethylethylenediamine
Trx	Thioredoxin
YPD	Yeast peptone dextrose

Contents

Preface.....	i
Declaration 1: Plagiarism.....	ii
List of publications and presentations.....	iii
Abstract.....	iv
Acknowledgements.....	v
List of abbreviations.....	viii
List of Tables.....	xiii
List of Figures.....	xiv
Chapter 1.....	1
1.1 Introduction.....	1
1.2 The thioredoxin system.....	2
1.2.1 Thioredoxin reductase.....	2
1.2.2 Thioredoxin.....	3
1.3 Connectivity of the thioredoxin system.....	4
1.4 Measurement of the thioredoxin system.....	7
1.4.1 Approach 1: Enzyme assays.....	7
1.4.2 Approaches 2 and 3: Redox states and redox potentials.....	14
1.4.3 Approach 4: Transcript and protein levels.....	17
1.5 Limitations with the current quantification methods for the thioredoxin system: could a systems biology approach be the solution?.....	20
1.6 Aims of study.....	23
Chapter 2: Purification of the yeast thioredoxin system.....	24
2.1 Introduction.....	24
2.2 Materials.....	24
2.3 Preparation of common reagents.....	25

2.3.1 DTT.....	25
2.3.2 Bovine pancreas insulin	25
2.3.3 DTNB.....	26
2.3.4 NADPH.....	26
2.3.5 IPTG stock solution	26
2.3.6 Kanamycin stock solution.....	26
2.3.7 Ampicillin stock solution.....	26
2.3.8 Bacterial growth media	27
2.4 The yeast thioredoxin activity assay	28
2.4.1 Methods to determine Trx activity.....	28
2.5 The yeast thioredoxin reductase activity assay	29
2.5.1 Methods to determine thioredoxin reductase activity.....	29
2.6 Cloning of Trx.....	30
2.6.1 Isolation of genomic DNA from <i>S. cerevisiae</i>	30
2.6.2 PCR.....	30
2.6.3 Mini-prep procedure for purification of plasmid DNA	31
2.6.4 Restriction Digestion	31
2.6.5 Gel purification and Ligation.....	31
2.6.6 Plasmid DNA extraction of pET28a.....	32
2.6.7 Gel purification and Ligation.....	32
2.6.8 Preparation of competent cells using the calcium chloride method	32
2.6.9 Transformation of <i>E. coli</i> BL21 (DE3) with pET28a.....	33
2.6.10 Colony PCR.....	33
2.6.11 Agarose gel electrophoresis	33
2.6.12 DNA quantification.....	34
2.6.13 Induction and optimization of expression.....	34

2.6.14 Tris-Tricine sodium dodecyl sulfate polyacrylamide gel electrophoresis (SDS-PAGE).....	34
2.7 Cloning of thioredoxin reductase.....	35
2.7.1 Colony PCR.....	35
2.7.2 Induction and expression.....	36
2.8 Recombinant purification of Trx and thioredoxin reductase.....	36
2.8.1 Preparation of Trx and thioredoxin reductase crude extract for purification.....	36
2.8.2 Ni-NTA affinity purification.....	37
2.8.3 Concentration of protein samples.....	37
2.9 Results.....	37
2.9.1 Developing a cheaper and faster Trx activity assay.....	37
2.9.2 The development of the thioredoxin reductase assay.....	38
2.9.3 The successful cloning and expression of <i>TRX1</i>	41
2.9.4 The purification of recombinant thioredoxin reductase and Trx by affinity chromatography.....	48
2.10 Discussion.....	50
Chapter 3: The thioredoxin system and not the Michaelis-Menten equation should be fitted to substrate saturation datasets from the thioredoxin insulin assay.....	52
3.1 Introduction.....	52
3.2 Materials.....	55
3.3 Methods.....	55
3.3.1 Kinetic modeling.....	55
3.3.2 Thioredoxin insulin reduction assay.....	56
3.3.3 Determination of the redox state of Trx.....	57
3.4 Results.....	58
3.4.1 Computational models with thioredoxin described either as an enzyme, or as a redox couple, have contrasting kinetic properties.....	58
3.4.2 Assay of the yeast thioredoxin system.....	61

3.4.3 Thioredoxin reductase activity is limiting in the insulin reduction assay.....	62
3.4.4 Saturation of the redox cycle and redistribution of the thioredoxin moiety	64
3.5 Discussion.....	66
Chapter 4: The thioredoxin redox charge as a surrogate measure for flux	68
4.1 Introduction.....	68
4.2 Materials	70
4.3 Methods.....	70
4.3.1 Kinetic modeling.....	70
4.3.2 Antibody preparation	71
4.3.3 Recombinant purification of TSA.....	73
4.3.4 His-tag cleavage of recombinant thioredoxin reductase and peroxiredoxin.....	74
4.3.5 Kinetic assays.....	74
4.3.6 Western blot.....	75
4.4 Results.....	76
4.4.1 Comparative analysis of the thioredoxin redox charge and the existing <i>in vivo</i> measures of the Trx system.....	76
4.4.2 The thioredoxin redox charge tracks changes in the thioredoxin reductive supply and oxidative demand <i>in vitro</i>	83
4.4.3 Realistic models illustrated the general applicability of the thioredoxin redox charge as a surrogate measure for flux	91
4.5 Discussion.....	94
Chapter 5: Conclusion.....	98
5.1 General discussion	98
5.2 Future work.....	101
5.3 Final remarks	101
References.....	103
Appendix.....	125

List of Tables

Table 2.1 Preparation of the resolving and stacking gels for Tris-tricine SDS-PAGE.....	35
Table 2.2 Comparison of the rates obtained by the modification of two Trx activity assays..	39
Table 2.3 Comparison of the rates obtained by utilizing various thioredoxin reductase activity assays.	40
Table 3.1 Kinetic parameters and species concentrations used for building computational models of the <i>E. coli</i> and baker's yeast thioredoxin systems.	56
Table 3.2 The Michaelis-Menten parameters and second-order rate constants (k_2) for insulin reduction from computational modeling of the <i>E. coli</i> thioredoxin system at varying thioredoxin reductase (TR) concentrations.	61
Table 3.3 The Michaelis-Menten parameters and second-order rate constants (k_2) for insulin reduction by the baker's yeast thioredoxin system at varying thioredoxin reductase (TR) concentrations.	61

List of Figures

- Figure 1.1 The thioredoxin system. Reduced Trx (TrxSH) directly reduces oxidized proteins and is oxidized (TrxSS). The regeneration of Trx from its oxidized form is catalyzed by thioredoxin reductase (TR) using NADPH (Lillig and Holmgren, 2007).2
- Figure 1.2 Mechanism by which thioredoxin catalyses the reduction of protein disulfides. Reduced thioredoxin (Trx-(SH)₂) binds to an oxidized target protein (X-S₂) via its hydrophobic surface patch. Nucleophilic attack by the thiolate of Cys32 results in formation of a transient mixed disulfide, which is followed by a nucleophilic attack of the deprotonated Cys35 generating oxidized thioredoxin (Trx-S₂) and the reduced protein (X-(SH)₂) (Holmgren, 1995). (Reprinted with permission from the Elsevier publishing company)4
- Figure 1.3 Quantification of thioredoxin (Trx) and/or thioredoxin reductase (TR) in various pathologies. Perturbations of thioredoxin and/or thioredoxin reductase have been associated with various pathologies and several quantification methods have been used to determine the role played by the system components in each disease.8
- Figure 1.4 Measurement of the thioredoxin system. Perturbations in the thioredoxin system have been quantified using several approaches including enzyme assays (A), redox states (B), redox potentials (C) as well as transcript and protein levels (D). The thioredoxin system components, thioredoxin and/or thioredoxin reductase, are usually measured independently (indicated by the red line, A and D respectively) and surprisingly, little or no information is available for the quantitative measurement of the complete thioredoxin system *in vivo*.9
- Figure 1.5 Thioredoxin mediated insulin reduction assay. This assay involves the reduction of insulin by thioredoxin which can be monitored either by following the aggregation of the free β -chain at 650 nm (A) or by coupling the reaction to NADPH and monitoring the oxidation of NADPH at 340 nm (B).10
- Figure 1.6 Proposed mechanism for the reaction between thioredoxin and Mito-Naph. A fluorescence off-on change is induced by thioredoxin mediated disulfide cleavage of the probe, resulting in a subsequent intramolecular cyclization by the released thiolate to give a fluorescent product which can be measured at 540 nm. (Reprinted with permission from Lee, M. H., Han, J. H., Lee, J.-H., Choi, H. G., Kang, C. & Kim, J. S. 2012. Mitochondrial Thioredoxin-Responding Off-On Fluorescent Probe. *Journal of the American Chemical Society*, 134, 17314-17319. Copyright (2012), American Chemical Society.)13
- Figure 1.7 Proposed mechanism of the activation of the TRFS-green probe by thioredoxin reductase and NADPH. TRFS-green contains a five-membered, cyclic disulfide scaffold

which can be selectively cleaved by thioredoxin reductase in the presence of NADPH. Upon reduction, the nucleophilic thiolate subsequently attacks the amide carbonyl carbon driven by the formation of a five-membered cyclic carbamate, which simultaneously releases the quenched fluorophore naphthalimide to activate the green fluorescent signal. (Reprinted with permission from Zhang, L., Duan, D., Liu, Y., Ge, C., Cui, X., Sun, J. & Fang, J. 2014. Highly Selective Off–On Fluorescent Probe for Imaging Thioredoxin Reductase in Living Cells. *Journal of the American Chemical Society*, 136, 226-233. Copyright (2014), American Chemical Society.)..... 14

Figure 2.1 Genomic DNA isolation and PCR amplification of the *TRX1* gene. Genomic DNA was isolated from *S. cerevisiae* using the Bustin Grab procedure (Harju *et al.*, 2004) (A). PCR of the DNA was undertaken using *TRX1*-specific primers (B). The PCR product was gel purified using the Fermentas gel purification kit (C). The gels have been cropped to fit the figures into this thesis but no other bands were observed in the non-MWM lanes.42

Figure 2.2 Confirming that the pTZ57R/T clones contained *TRX1*. pTZ57R/T DNA was isolated from *E. coli* JM109 cells using a standard mini-prep procedure a was restricted with BamHI to linearize the plasmid (B). In addition, PCR of the plasmid DNA was undertaken using *TRX1*-specific primers to confirm the presence of the insert (C). Restriction digestion of the cloning vector pTZ57R/T-*TRX1* showing the release of the *TRX1* fragment (D). Some gels have been cropped to fit the figures into this thesis but no other bands were observed in the non-MWM lanes.44

Figure 2.3 pET28a expression vector isolation and restriction endonuclease digestion. pET28a was isolated from *E. coli* BL21 (DE3) cells using a standard mini-prep procedure (A). Restriction digestion of the expression vector (B). The gels have been cropped to fit the figures into this thesis but no other bands were observed in the non-MWM lanes.44

Figure 2.4 Transformation of *E. coli* BL21 (DE3) with pLPTrxA/B/C. pLPTrxA/B/C DNA was isolated from *E. coli* BL21 (DE3) cells using a standard mini-prep procedure (A). PCR performed on pLPTrxA/B/C clones to verify success of transformation (B). Single restriction digestion of pLPTrxA/B/C clones was undertaken with HindIII to size the clones (C) and double digestion with HindIII and NdeI was undertaken to release the *TRX1* gene (D). The gels have been cropped to fit the figures into this thesis but no other bands were observed in the non-MWM lanes.45

Figure 2.5 Alignment of the pLPTrxA/B/C (A) promoter sequences and (B) terminator sequences with the *TRX1* sequence and reverse complement of the *TRX1* sequence from *S. cerevisiae* (NCBI Reference Sequence: NC_001144.5), respectively. Identical residues are

denoted with an asterisk. The overall percentage identity between each promoter and reference sequence as well as each terminator and reference sequence was 100 %.....46

Figure 2.6 Expression and specific activity of *TRX1* at various time points (2-19 hours). Recombinant *TRX1* expression was induced with 0.5 mM IPTG for 0-19 hours and analyzed by SDS-PAGE (A). The specific activity of induced fractions (B) was also determined. Duplicate biological samples were assayed at a given time point and the standard error is indicated.....47

Figure 2.7 Induction of *TRR1*. Recombinant *TRR1* expression was induced with 0.5 mM isopropyl β -D-1-thiogalactopyranoside (IPTG) for various time intervals (0-6 hours) and analyzed by SDS-PAGE (A) and the DTNB reduction assay (B). Duplicate biological samples were assayed at each time point and the standard error is indicated.....49

Figure 2.8 Ni-NTA affinity purification of recombinant TRX1 (A) and TRR1 (B). *TRX1* expression was induced for 6 hours and the cells processed as described in Section 2.8.1 to yield pure TRX1 (A). *TRR1* was induced for 1 hour and the cells processed as described in Section 2.8.1 to yield pure TRR1 (B). The gels were stained with Coomassie blue.....50

Figure 3.1 The Michaelis-Menten equation and the thioredoxin redox couple model both fit an *in vitro* insulin reduction dataset (Holmgren, 1979a) but the resulting kinetic models show distinct responses to thioredoxin reductase concentration and substrate saturation. In (A) the Michaelis-Menten equation and the thioredoxin redox couple kinetic model (black line) both showed excellent fits ($r^2 \geq 0.996$) to an insulin substrate saturation dataset (●). Increasing the thioredoxin reductase concentration (0.05 μ M) in the thioredoxin redox couple model to 0.15 (blue) or 0.25 μ M (green) increased the flux within the system at a given insulin concentration. Substrate saturation (black) within a fitted thioredoxin redox couple model (0.05 μ M thioredoxin reductase) was accompanied by the redistribution of thioredoxin from its reduced (blue) to oxidized (red) form (B). In (C) disulfide bond rather than insulin concentration was used to determine the kinetic parameters for thioredoxin-dependent insulin reduction.59

Figure 3.2 Similar rates were obtained when the thioredoxin insulin assay was initiated with thioredoxin reductase or NADPH. Insulin reduction by the thioredoxin system was initiated with either thioredoxin reductase (A) or NADPH (B) and a decrease in absorbance was monitored over negative and positive scales, respectively. The assay contained insulin (80 μ M), thioredoxin reductase (0.05 μ M), thioredoxin (1.5 μ M) and NADPH (150 μ M) and was performed in duplicate.....62

Figure 3.3 Changing the thioredoxin reductase concentration altered the kinetic profile and parameters obtained with the yeast thioredoxin insulin reduction assay. The flux obtained for a given insulin concentration increased as the thioredoxin reductase concentration was increased over the range 0.05 (●), 0.15 (■) and 0.25 μM (◆). The Michaelis-Menten equation and the redox couple model were both fitted to these datasets using either insulin concentration (A) or the disulfide bond concentration (B). All assays were performed in triplicate with standard errors shown.63

Figure 4.1 A model of the *E. coli* thioredoxin system illustrating the reductive supply and oxidative demand activities on the system. The reduction of oxidized thioredoxin (TrxSS) is catalyzed by thioredoxin reductase (TR) and NADPH, and in turn reduced thioredoxin (TrxSH) serves as an electron donor for the reduction of methionine sulfoxide (MetSO) and 3'-phosphoadenosine-5'-phosphosulfate (PAPS) by methionine sulfoxide and PAPS reductase respectively. Also included is the reduction of the peroxiredoxin (Tpx) by thioredoxin and its oxidation by hydrogen peroxide (H_2O_2) as well as the reduction of protein disulfides (PSS) (Adapted from Pillay *et al.*, 2011).69

Figure 4.2 The reductive thioredoxin redox charge correlated with the flux as the reductive supply from NADPH and thioredoxin reductase increased. Varying concentrations of NADPH and thioredoxin reductase (TR) were used to determine the relationship between the flux (blue) and redox potential (cyan, A and E), redox ratio (TrxSH/TrxSS) (green, B and F), oxidative thioredoxin redox charge (TrxSS/Trx Total) (red, C and G) and reductive thioredoxin redox charge (TrxSH/Trx Total) (magenta, D and H).78

Figure 4.3 The oxidative thioredoxin redox charge corresponded with the flux as the oxidative demand increased. The relationship between the flux (blue) and existing measures of the thioredoxin system including the redox potential (cyan, A and E), redox ratio (TrxSH/TrxSS) (green, B and F), oxidative thioredoxin redox charge (TrxSS/Trx Total) (red, C and G) and reductive thioredoxin redox charge (TrxSH/Trx Total) (magenta, D and H) were evaluated with varying concentrations of H_2O_2 and Tpx, respectively.79

Figure 4.4 The flux through the thioredoxin system correlated with the log transformation of the thioredoxin redox ratio. Models with varying concentrations of NADPH (A-B) and H_2O_2 (C-D) were simulated and the effect on the flux (blue) and the thioredoxin redox ratio, (TrxSH/TrxSS) (A and C, green) or (TrxSS/TrxSH) (B and D, green) was investigated. The log transformation of the respective redox ratio (red) was simultaneously plotted.80

Figure 4.5 Co-response analysis confirms that the reductive and oxidative thioredoxin redox charge correlated with the flux under reductive supply and oxidative demand conditions,

respectively. Co-response plots were generated for NADPH (-) and thioredoxin reductase (-) (A-D) as well as H₂O₂ (-) and peroxiredoxin (-) (E-H) perturbations and the relationship with the redox potential (A and E), redox ratio (TrxSH/TrxSS) (B and F), oxidative thioredoxin redox charge (TrxSS/Trx Total) (C and G) and reductive thioredoxin redox charge (TrxSH/Trx Total) (D and H) was determined. Each y-axis was scaled according to the range of output values for each measure.....81

Figure 4.6 The reductive thioredoxin redox charge correlated with the flux with varying concentrations of a competitive inhibitor. Simulations were performed with varying concentrations of Ebselen and the relationship between the flux (blue) and redox potential (cyan, A), redox ratio (TrxSH/TrxSS) (green, B), oxidative thioredoxin redox charge (TrxSS/Trx Total) (red, C) and reductive thioredoxin redox charge (TrxSH/Trx Total) (magenta, D) was tested. The effect of the inhibitor on the concentration of reduced thioredoxin (black, A-D) was also determined. It should be noted that the reductive thioredoxin redox charge plot was superimposed on the reduced thioredoxin plot (D).....83

Figure 4.7 Ni-NTA affinity purification of recombinant TSA1. *TSA1* expression was induced for 2 hours and the cells processed as described in Section 2.8.1 to yield pure TSA1. The gel was stained with Coomassie blue.84

Figure 4.8 Nickel affinity purification of His-tag cleaved recombinant TSA1 and TRR1 (A) and western blot analysis confirming the specificity of the anti-Trx1 antibodies (B and C). His-tags from TSA1 and TRR1 were cleaved using the Thrombin CleanCleave kit and the extract was mixed with Ni-NTA agarose. The proteins cleaved to completion eluted as the unbound fractions and ran at a lower molecular weight when analyzed by SDS-PAGE. The gel in this figure was stained with Coomassie blue (A). Western blotting analysis confirmed that the cleavage removed the His-tag (B) and the polyclonal antibodies specifically recognised thioredoxin (Ox Trx1) (C). The gels have been cropped to fit the figures into this thesis but no other bands were observed in the non-MWM lanes.85

Figure 4.9 The rate of NADPH oxidation was measured at 340 nm at various concentrations of thioredoxin reductase (0-700 nM) (A) and peroxiredoxin (0-4000 nM) (B). The reaction mixture contained in a final volume of 1 ml, 150 μM NADPH, 1 μM Trx, reaction buffer (25 mM potassium phosphate, 1 mM EDTA, 100 mM ammonium sulfate, pH 7.0), 100 nM TRR1 for varying TSA1 assays (A) and 250 nM TSA1 for varying TRR1 assays (B). Experiments were performed in triplicate and the standard error bars are indicated.86

Figure 4.10 The effect of perturbations of the reductive supply and oxidative demand on the thioredoxin redox poise. For the alkylation studies, purified thioredoxin was used as an

oxidative control (Ox Trx) and PEG-maleimide treatment increased the molecular weight of this control. In an assay control to ensure the reduction of Trx by thioredoxin reductase, incubation of thioredoxin (1 μM) with thioredoxin reductase (0.1 μM) and NADPH (150 μM) resulted in the appearance of reduced thioredoxin at 47 kDa (A) which was confirmed by DTT-pretreatment of oxidized thioredoxin (B). The kinetic assay samples containing NADPH (150 μM), thioredoxin (1 μM) and varying concentrations of thioredoxin reductase (TRR1) (C) or TSA1 (D) were alkylated with PEG-maleimide and the reduced thioredoxin concentration was detected using polyclonal chicken anti-thioredoxin antibodies. All bands were quantified with Image J. A reduced Trx fraction could not be detected in the 1 nM TRR1 experiment (C) and therefore this fraction was assigned a nominal value of 0.1%. The gels have been cropped to fit the figures into this thesis but no other bands were observed in the non-MWM lane.....90

Figure 4.11 The reductive thioredoxin redox charge correlated with the flux as the reductive supply from thioredoxin reductase increased while the oxidative thioredoxin redox charge correlated with the flux with increasing peroxiredoxin concentrations. *In vitro* assays with varying concentrations of thioredoxin reductase and peroxiredoxin were performed to determine the relationship between the flux (blue) and redox potential (cyan, A and E), redox ratio (TrxSH/TrxSS) (green, B and F), oxidative thioredoxin redox charge (TrxSS/Trx Total) (red, C and G) and reductive thioredoxin redox charge (TrxSH/Trx Total) (magenta, D and H).90

Figure 4.12 Co-response plots generated from *in vitro* assay and western blot data confirmed that the reductive thioredoxin redox charge correlated with the flux with perturbations in reductive supply and the oxidative thioredoxin redox charge correlated with the flux with perturbations in oxidative demand. Co-response plots were generated with varying concentrations of thioredoxin reductase (A-D) and peroxiredoxin (E-H) and the relationship with the redox potential (A and E), redox ratio (TrxSH/TrxSS) (B and F), oxidative thioredoxin redox charge (TrxSS/Trx Total) (C and G) and reductive thioredoxin redox charge (TrxSH/Trx Total) (D and H) was determined.....91

Figure 4.13 A large scale realistic model of the red blood cell supports the use of the thioredoxin redox charge as a surrogate measure for flux. Plots with the flux (blue) and redox potential (cyan, A), redox ratio (TrxSH/TrxSS) (green, B), oxidative thioredoxin redox charge (TrxSS/Trx Total) (red, C) and reductive thioredoxin redox charge (TrxSH/Trx Total) (magenta, D) were generated with varying concentrations of hydrogen peroxide. Using this respective data, co-response plots were then generated (E-H).93

Figure 4.14 A realistic model of the *in vivo* oxidation of *S. pombe* peroxiredoxin supported the use of the thioredoxin redox charge as a surrogate measure for flux. Plots with the flux (blue) and redox potential (cyan, A), redox ratio (TrxSH/TrxSS) (green, B), oxidative thioredoxin redox charge (TrxSS/Trx Total) (red, C) and reductive thioredoxin redox charge (TrxSH/Trx Total) (magenta, D) were generated with varying concentrations of H₂O₂. Co-response plots were then generated (E-H) using this respective data.....94

Figure 5.1 A timeline of the computational models of redoxin systems. Several computational models have been developed to elucidate the behavior of redoxin networks in Jurkat T-cells (Adimora *et al.*, 2010), the red blood cell (Benfeitas *et al.*, 2014), HeLa (Lim *et al.*, 2015) and lens epithelial cells (Dwivedi and Kemp, 2012) as well as *E. coli* (Pillay *et al.*, 2011), *Trypanosoma cruzi* (Olin-Sandoval *et al.*, 2012), *Candida albicans* (Komalapriya *et al.*, 2015) and *S. pombe* (Tomalin *et al.*, 2016).....99

Chapter 1

1.1 Introduction

The rise in planetary oxygen levels as a by-product of cyanobacterial photosynthesis approximately 2.5 billion years ago had a dramatic effect on the development of living systems, leading to a massive extinction event which displaced obligate anaerobes as the primary life form on the planet (Sessions *et al.*, 2009, Planavsky *et al.*, 2014). This space was occupied by aerobic organisms which used oxygen as a terminal electron acceptor in cellular respiration and consequently gained a vastly more efficient energy metabolism together with novel biochemical pathways. Nonetheless this improved energy metabolism came at a price. In a series of classical papers McCord and Fridovich showed that living cells actively catalyze the dismutation of superoxide to molecular oxygen and hydrogen peroxide (McCord and Fridovich, 1969a, McCord and Fridovich, 1969b, McCord and Fridovich, 1970). The development of this assay together with several other assays revealed that living systems have evolved a barrage of enzymes and metabolites to protect themselves against the damaging effects of oxygen-derived species. This and other work led to the Free Radical Theory of Disease in which posited that reactive oxygen species (ROS) were an unavoidable consequence of aerobic metabolism and that when present in excess, result in several pathologies (Harman, 1956). The use of antioxidant regimens in the prevention and treatment of these disease states was therefore widely embraced but clinical studies have since shown that antioxidant therapy is associated with accelerated disease progression and other detrimental effects (Steinhubl, 2008, Persson *et al.*, 2014, Sayin *et al.*, 2014, Le Gal *et al.*, 2015).

These studies have revealed the complexity of redox homeostasis with ROS appearing to play dual roles as toxins and as essential signalling molecules (Jones, 2006, D'Autreaux and Toledano, 2007, Pham-Huy *et al.*, 2008). Aerobic metabolism is now considered a finely constructed network with multiple and discrete connections, redox signaling pathways and circuits (Jones, 2006). A key mediator in this network is the thioredoxin system composed of thioredoxin (Trx), NADP(H), and thioredoxin reductase (Figure 1.1). In this system, thioredoxin reductase uses NADPH to reduce thioredoxin, which in turn reduces a wide array

of protein and non-protein targets, forming a large redox-regulated network (Collet and Messens, 2010, Jones and Go, 2011). This network provides reducing equivalents for key cellular metabolic processes including DNA synthesis, antioxidant defense and the regulation of redox signal transduction (Arnér and Holmgren, 2000b, Toledano *et al.*, 2007). The components of the system will be described below.

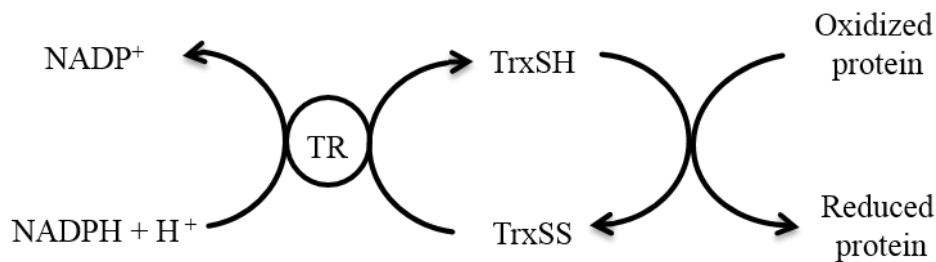


Figure 1.1 The thioredoxin system. Reduced Trx (TrxSH) directly reduces oxidized proteins and is oxidized (TrxSS). The regeneration of Trx from its oxidized form is catalyzed by thioredoxin reductase (TR) using NADPH (Lillig and Holmgren, 2007).

1.2 The thioredoxin system

1.2.1 Thioredoxin reductase

Thioredoxin reductase is a member of a family of pyridine nucleotide-disulfide oxidoreductases (Williams, 1995, Arnér and Holmgren, 2000b). Members of this family are homodimeric flavoproteins, in which each subunit has an NADPH binding site, a redox-active disulfide bond and a tightly bound flavin adenine dinucleotide (FAD) prosthetic group (Williams, 1995, Zhong *et al.*, 2000) which mediates the transfer of reducing equivalents from NADPH to its own disulfide bond, and then to the disulfide bond of the substrate (Holmgren and Bjornstedt, 1995, Williams, 1995). Thioredoxin reductase is responsible for the reduction of oxidized Trx and is also able to reduce non-disulfide substrates such as hydrogen peroxide albeit at a significantly lower rate than specialized peroxidases (Takemoto *et al.*, 1998).

Thioredoxin reductases can be classified into two types, based on size. The first type has a higher molecular mass of approximately 55 kDa and is generally found in animals (Gasdaska *et al.*, 1995) and protozoa such as the malaria parasite (Krnajski *et al.*, 2001), and is more closely related to glutathione reductase than to bacterial thioredoxin reductase. This reductase also has a broader substrate specificity (Mustacich and Powis, 2000) and contains the rare

amino acid selenocysteine (Sec) in its active site in place of the conserved cysteine (Cys) found in bacterial thioredoxin reductase (Arnér and Holmgren, 2000b, Zhong *et al.*, 2000). This Sec residue is essential for the catalytic activity of thioredoxin reductase because either its removal (Nordberg *et al.*, 1998) or modification (Gorlatov and Stadtman, 1998, Nordberg *et al.*, 1998) leads to inactivation of the enzyme. Sec participates in the reaction mechanism of thioredoxin reductase in two important thiol/disulfide exchange reactions; first, the selenolate of Sec acts as the electron donor to thioredoxin and second, as part of the selenosulfide bond found in the C-terminus of the enzyme, selenium accepts electrons from the oxidation of NADPH in the N-terminal redox center of thioredoxin reductase (Lothrop *et al.*, 2014).

The second type of thioredoxin reductase is present in archaea, bacteria and eukarya including fungi, plants and the protozoan intestinal parasite *Entamoeba*. This enzyme has a lower molecular mass of 35 kDa (Williams, 1995, Hirt *et al.*, 2002) and is related to the alkyl hydroperoxide reductase (AhpF) (Poole *et al.*, 2000). There is approximately 20% sequence identity between high molecular weight thioredoxin reductase and its low molecular weight counterpart in the region where they can be reliably aligned. Further, unlike the high molecular weight thioredoxin reductase that has a redox-active centre located in the FAD-binding domain, the redox-active disulfide of the low molecular weight thioredoxin reductase is located in the NADPH domain showing the significant variation between the two types of thioredoxin reductase (Hirt *et al.*, 2002). Enzyme catalysis also involves two redox reactions with the formation of disulfide bonds following the reduction of Trx and reducing equivalents are obtained from NADPH oxidation.

1.2.2 Thioredoxin

Trx is a low molecular weight (12 kDa), thermostable and ubiquitous protein that can be localized in the cytoplasm, nucleus or in mitochondrial cell fractions (Das *et al.*, 1999). The key to the redox activity of this protein is the presence of two cysteine residues (Cys32 and Cys35) separated by two amino acids (Gly-Pro) in its conserved active site. These cysteines exist as a dithiol (-SH)₂ or as a disulfide (-S)₂ in the reduced and oxidized states, respectively. Thioredoxin reductase reduces the disulfide bond forming reduced Trx which can then form a complex with an oxidized substrate via a hydrophobic surface patch (Collet and Messens, 2010). Upon the formation of this complex, thiol-disulfide exchange generates

oxidized Trx and the reduced substrate (Figure 1.2) (Holmgren, 1985) ultimately linking the activities of both Trx and thioredoxin reductase.

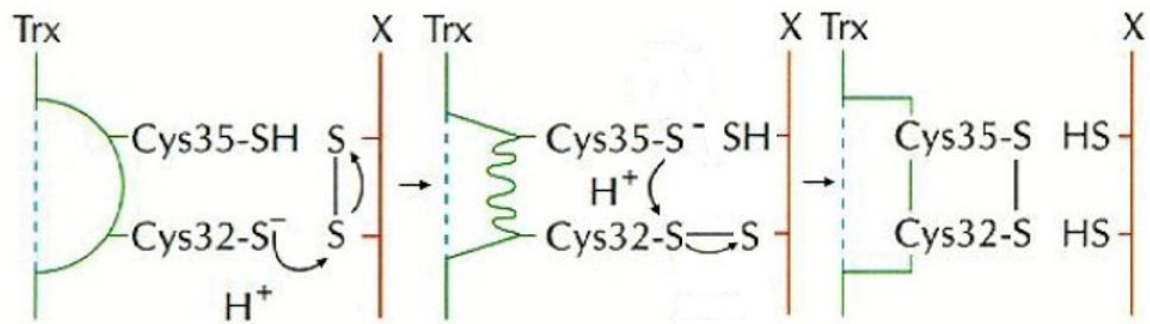


Figure 1.2 Mechanism by which thioredoxin catalyses the reduction of protein disulfides. Reduced thioredoxin (Trx-(SH)₂) binds to an oxidized target protein (X-S₂) via its hydrophobic surface patch. Nucleophilic attack by the thiolate of Cys32 results in formation of a transient mixed disulfide, which is followed by a nucleophilic attack of the deprotonated Cys35 generating oxidized thioredoxin (Trx-S₂) and the reduced protein (X-(SH)₂) (Holmgren, 1995). (Reprinted with permission from the Elsevier publishing company)

1.3 Connectivity of the thioredoxin system

The biosynthetic reactions in which Trx has been implicated include providing reducing equivalents to ribonucleotide reductase, thioredoxin peroxidase (Pigiet and Conley, 1977), methionine sulfoxide reductases (Sengupta and Holmgren, 2012), the regeneration of oxidatively damaged proteins and scavenging reactive oxygen species as well as other free radicals (Das and Das, 2000). Several transcription factors are also redox regulated by Trx which modulates their DNA binding activities and/or their retention within the nucleus (Holmgren and Lu, 2010, Karlenius and Tonissen, 2010). In mammalian cells, Trx directly modulates the activity of various transcription factors such as AP-1 and p53 (Mukherjee and Martin, 2008) while some transcription factors can be indirectly affected by Trx. For example, Ref-1 (redox factor-1) is reduced by Trx which in turn activates other redox-regulated transcription factors that are responsible for the activation of many genes responsible for promoting cell viability in response to oxidative stress and hypoxia (Demple *et al.*, 1991, Robson and Hickson, 1991, Robson *et al.*, 1991, Hawkes *et al.*, 2014). Interestingly, Ref-1 functions not only as a major redox-signaling factor but is also a DNA-repair endonuclease, and is involved in the base excision repair (BER) pathway which is responsible for restoring apurinic/apyrimidinic (AP) sites in DNA, a major end product in

reactive oxygen species (ROS) damage (Demple *et al.*, 1991, Hawkes *et al.*, 2014). Additionally, Trx plays pivotal roles in the regulation of redox signalling as it senses and responds to environmental oxidative stress as well as ROS generated by cellular respiration and metabolism. Trx is responsible for modulating the redox state, function, and activity of its target signalling proteins. Trx controls the mitogen-activated protein kinase (MAPK) cascades through the redox state-dependent association and dissociation with apoptosis signal-regulating kinase 1 (ASK1), an upstream regulator of the cascades. In unstimulated cells, ASK1 forms an inactive complex with reduced Trx (Fujino *et al.*, 2006). However, exposure to ROS causes the oxidation of Trx leading to the dissociation of Trx from ASK1, which consequently converts the inactive form of ASK1 to an active kinase (Matsuzawa and Ichijo, 2008). Trx also regulates other kinases or components of signalling pathways. The phosphatase PTEN functions as a terminator of the Akt signalling pathway which plays a central role in cell growth and survival. Trx directly interacts with PTEN inhibiting its phosphatase activity and membrane binding resulting in the activation of the Akt pathway (Meuillet *et al.*, 2004).

In plants, the thioredoxin system provides a crucial link between the activities of electron transport and carbon assimilation (Meyer *et al.*, 2008). Approximately 500 proteins had been identified as potential or established Trx targets in land plants and oxygenic photosynthetic microorganisms (Montrichard *et al.*, 2009). Plant Trxs are involved in multiple processes such as photorespiration, lipid and hormone metabolism, membrane transport, ATP synthesis (Balmer *et al.*, 2004) and seed germination (Joudrier *et al.*, 2005). In the chloroplast, the activities of a number of enzymes including four enzymes of the Benson-Calvin cycle, fructose biphosphatase, sedoheptulose biphosphatase, ribulose-5-P kinase and glyceraldehyde-3-phosphate dehydrogenase are all regulated by Trx (Dey and Harborne, 1997). Other chloroplastic enzymes regulated by Trx include NADP-malate dehydrogenase, phenylalanine ammonia lyase and glucose-6-phosphate dehydrogenase (Dey and Harborne, 1997). A Trx isoform, Trx h has been associated in the reduction of seed α -amylase and trypsin inhibitors from several sources (Jiao *et al.*, 1992).

In addition to the Trx-dependent reactions outlined above, a large variety of other potential substrates that interact intracellularly with Trx have been identified through omic techniques and methods. For example, the C-terminal cysteine of the catalytic site of Trx which is essential for resolving the mixed disulfide complex that results in the release of a reduced

substrate protein and oxidized Trx (Figure 1.2) can be mutated to an alanine (Balmer *et al.*, 2004) allowing the formation of stable complexes between Trx and its substrates (Depuydt *et al.*, 2009). Using this approach in combination with affinity chromatography, 50 potential Trx-linked proteins functional in 12 processes including electron transport, transformation, translation, protein assembly and folding, were identified from photosynthetic and heterotrophic mitochondrial sources (Balmer *et al.*, 2004).

An alternate approach involved the purification of proteins bound to Trx using Tandem Affinity Purification (TAP) followed by MS/MS mass spectrometry analysis. The procedure involves a TAP-tag being appended to the C-terminus of *Escherichia coli* Trx1 and thereafter the Trx-substrate complexes were purified using two affinity chromatography steps. Using this method, a total of 80 *E. coli* proteins have been identified, implicating Trx1 in approximately 26 cellular processes including transcriptional regulation, cell division, energy transduction, and several biosynthetic pathways (Kumar *et al.*, 2004).

Another approach to identify Trx substrates involves differential thiol-labeling (Leichert and Jakob, 2004). In this approach, accessible thiol groups are carbamidomethylated (CAM) with iodoacetamide (IAM) and blocked for the subsequent reduction and alkylation steps. DTT is used to reduce the disulfide bonds and the newly accessible thiols are then labeled with radioactive iodoacetamide (^{14}C -IAM). A radioactive label is therefore incorporated into the proteins that originally contained disulfide bonds. Proteins that require Trx for reduction can be identified through a comparison of cellular extracts prepared from wild-type and Trx-knockout strains. Using this approach, a considerable number of redox-sensitive cytoplasmic proteins containing significantly oxidized thiol groups were identified in strains lacking thioredoxin. These included detoxifying enzymes as well as several metabolic enzymes with active-site cysteines that were previously unknown substrates of thioredoxin (Leichert and Jakob, 2004).

Thus the thioredoxin system has multiple interactions with several cellular processes creating a complex and interconnected redox network. Perturbations of this network have, not surprisingly, been correlated with several oxidative stress-associated acute and chronic diseases (Figure 1.3). However, quantifying the contribution of this system in redox regulation depends on the quality of the assays available for the system.

1.4 Measurement of the thioredoxin system

Confusingly, a number of approaches and consequently several distinct measures including Michaelis-Menten parameters, redox potentials, redox ratios as well as protein and transcript levels have been used to describe the thioredoxin system *in vitro* and *in vivo* (Figure 1.4). The most commonly utilized approaches and assays used to characterize the thioredoxin system components in relation to their roles in disease states are critically reviewed below.

1.4.1 Approach 1: Enzyme assays

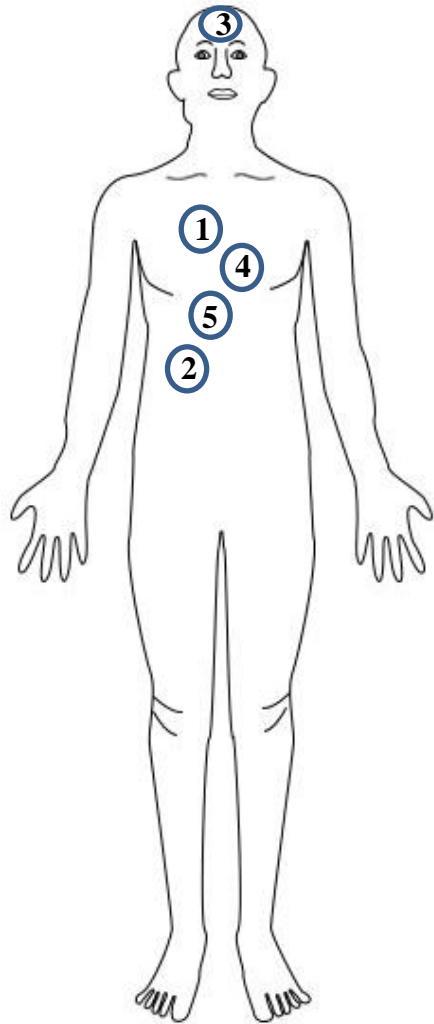
Several spectrophoto- and spectrofluorometric methods involving the use of insulin, DTNB or FiTC-insulin as a substrate have been developed for the quantification of changes in thioredoxin and/or thioredoxin reductase activity which are considered valuable indicators in a number of clinical conditions. For example, alterations in activity due to changes in cellular redox homeostasis have been reported in cancer (Yoo *et al.*, 2010, Ahrens *et al.*, 2015) and HIV infection (Nakamura *et al.*, 1996, Burke-Gaffney *et al.*, 2005).

Organ: Lungs **1**
Pathology: Cancer
Measure: TR and Trx protein levels
Method: Immunohistochemistry, Western blot
Reference: Park *et al.* (2006)

Pathology: Cancer
Measure: (1) Trx and TR mRNA levels
(2) Trx and TR protein levels
Method: (1) RT-PCR
(2) Immunohistochemistry, Western blot
Reference: Soini *et al.* (2001)

Pathology: Asthma
Measure: Serum Trx levels
Method: Sandwich ELISA
Reference: Yamada *et al.* (2003)

Organ: Liver **2**
Pathology: Cancer
Measure: (1) Trx mRNA levels
(2) Trx protein levels
Method: (1) Northern blot analysis
(2) Immunohistochemistry
Reference: Kawahara *et al.* (1996)



3 **Organ:** Brain
Pathology: Alzheimer's disease
Measure: TR activity
Method: End-point insulin assay
Reference: Lovell *et al.* (2000)

Pathology: Parkinson's disease
Measure: TR activity
Method: Mito-TRFS fluorescent probe
Reference: Liu *et al.* (2016)

4 **Organ:** Heart
Pathology: Coronary artery disease
Measure: (1) TR and Trx activities
(2) TR and Trx protein levels
Method: (1) End-point insulin assay
(2) Western blot
Reference: Wu *et al.* (2010)

5 **Organ:** Stomach
Pathology: Cancer
Measure: Trx protein levels
Method: Immunohistochemistry
Reference: Grogan *et al.* (2000)

Figure 1.3 Quantification of thioredoxin (Trx) and/or thioredoxin reductase (TR) in various pathologies. Perturbations of thioredoxin and/or thioredoxin reductase have been associated with various pathologies and several quantification methods have been used to determine the role played by the system components in each disease.

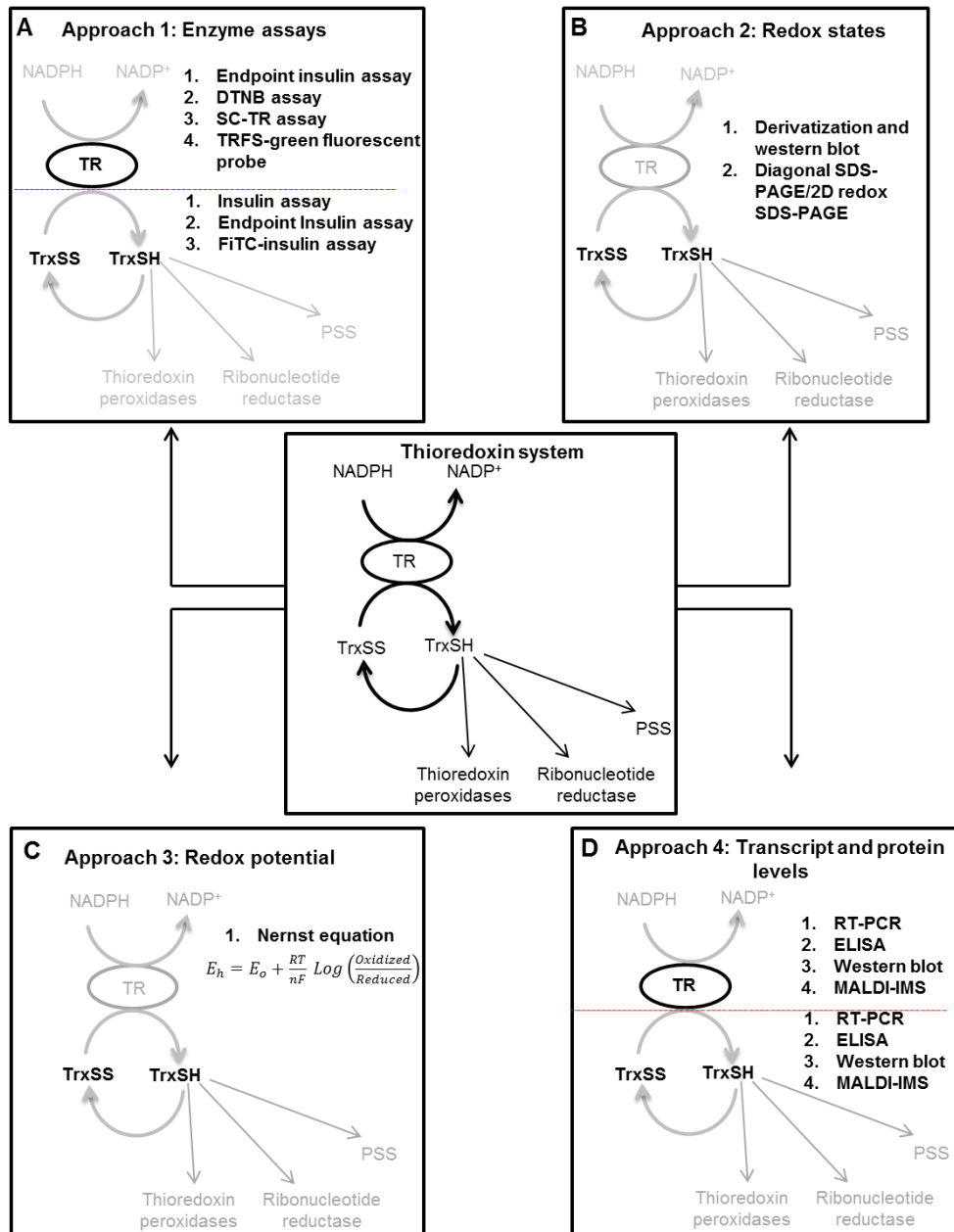


Figure 1.4 Measurement of the thioredoxin system. Perturbations in the thioredoxin system have been quantified using several approaches including enzyme assays (A), redox states (B), redox potentials (C) as well as transcript and protein levels (D). The thioredoxin system components, thioredoxin and/or thioredoxin reductase, are usually measured independently (indicated by the red line, A and D respectively) and surprisingly, little or no information is available for the quantitative measurement of the complete thioredoxin system *in vivo*.

1.4.1.1 Spectrophotometric assays

1.4.1.1.1 Insulin activity assay

Thioredoxins possess insulin disulfide reductase activity and this assay (Holmgren, 1979a) has been used to characterize the thioredoxins of several species (Alger *et al.*, 2002, Jeon and Ishikawa, 2002, Akif *et al.*, 2008, Grimaldi *et al.*, 2008, Yang and Ma, 2010). The assay involves the reduction of insulin by thioredoxin which can be monitored turbidimetrically by following the aggregation of the free β -chain (Holmgren, 1979b) or by coupling the reaction to NADPH oxidation (Holmgren, 1979a, Arnér and Holmgren, 2000a) (Figure 1.5). Although commonly used, a key limitation with this assay for biological samples such as tissue extracts is that NADPH-metabolizing enzymes can interfere with the assay resulting in a high background (Arnér and Holmgren, 2000a). Further, because the Trx system is coupled, it may not be immediately apparent if an increase in reported activity is caused by increases in Trx and/or thioredoxin reductase.

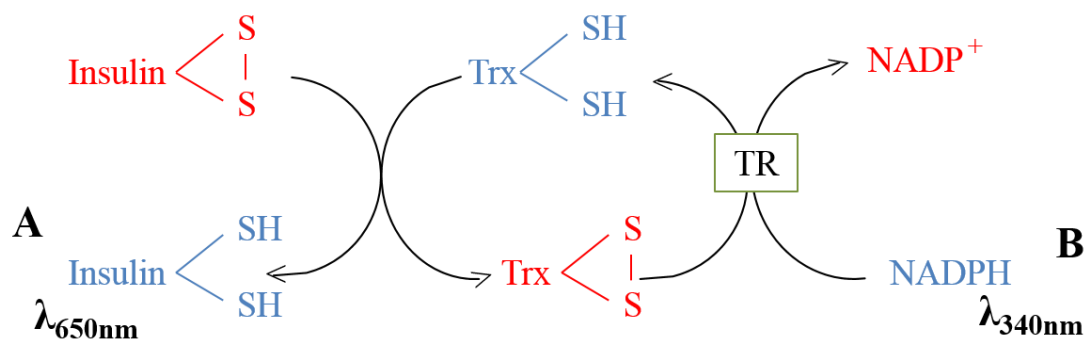


Figure 1.5 Thioredoxin mediated insulin reduction assay. This assay involves the reduction of insulin by thioredoxin which can be monitored either by following the aggregation of the free β -chain at 650 nm (A) or by coupling the reaction to NADPH and monitoring the oxidation of NADPH at 340 nm (B).

1.4.1.1.2 End-point insulin activity assay

Due to the small amounts of thioredoxin and/or thioredoxin reductase present in complex biological samples, a modified version of the insulin assay was subsequently developed in which the thioredoxin system reduces the disulfide bonds of insulin and the reaction is stopped by guanidine hydrochloride (Arnér and Holmgren, 2000a). The reduced thiol groups of insulin then react with DTNB which upon reduction to 5-thio-2-

nitrobenzoic acid (TNB) produces a yellow color and has an absorption maximum at 412 nm which can be monitored spectrophotometrically.

1.4.1.1.3 DTNB assay

The DTNB calorimetric assay has also been used to determine the thioredoxin reductase activity in mammalian cells and tissues. However, the key limitation with this assay is that it is not ideal for cell lysates as these fractions contain other NADPH oxidoreductases including lipoamide dehydrogenase and glutathione reductase that are also capable of reducing DTNB (Brigelius *et al.*, 1983, Biewenga *et al.*, 1996). The contribution of the activities of these enzymes to the total DTNB reduction may be quantified by using a thioredoxin reductase inhibitor such as aurothiomalate or auranofin (Saccoccia *et al.*, 2014) which significantly increases the cost of the assay.

1.4.1.1.4 SC-TR assay

The SC-TR assay uses selenocystine, a commercially available diselenide-bridged amino acid as a substrate that can only be reduced by high molecular weight thioredoxin reductase. In this continuous assay, the activity of thioredoxin reductase is determined by monitoring NADPH consumption at 340 nm as thioredoxin reductase reduces selenocystine (Cunniff *et al.*, 2013). This assay was used to compare thioredoxin reductase activity in malignant mesothelioma cells compared to control LP9 mesothelial cells and it was found that the malignant mesothelioma cell lines had twice the thioredoxin reductase activity when compared to the control cells (Cunniff *et al.*, 2013).

The SC-TR assay offers several advantages in comparison to the traditional assays used to determine thioredoxin reductase activity. First, the assays can be performed using traditional spectrophotometry or adapted for use in a 96-well plate format, allowing for the analysis of multiple experimental parameters at once. Second, this assay is more versatile than other methods using cell lysates as it is compatible with the use of non-ionic detergents that are commonly used in buffers to lyse mammalian cells (Holden and Horton, 2009, Ji, 2010). Third, the assay is both direct and continuous. Fourth, unlike DTNB, selenocystine is specifically reduced by thioredoxin reductase and is not a substrate for other NADPH cellular reductases making this assay suitable for complete cell lysates. Finally, as the assay uses a direct substrate of thioredoxin reductase, there is no need to supply exogenous thioredoxin, insulin and DTNB to the reaction mixture. However, a key limitation of this assay is that it is

only applicable to mammalian thioredoxin reductase and cannot be used to measure the low molecular weight thioredoxin reductase.

1.4.1.2 Spectrofluorometric methods

1.4.1.2.1 Fluorescein isothiocyanate-labeled insulin (FiTC–insulin) assay

In an attempt to acquire a more sensitive and reproducible assay for the analysis of thioredoxin and thioredoxin reductase activities in clinical samples, the fluorescein isothiocyanate-labeled insulin (FiTC–insulin) assay was developed (Montano *et al.*, 2014). This modified version of the original insulin assay (Heuck and Wolosiuk, 1997b, Heuck and Wolosiuk, 1997a) involved the synthesis of fluorescent derivatives of bovine pancreas insulin for a spectrofluorometric assay (Montano *et al.*, 2014). FiTC–insulin emits fluorescence at 520 nm after excitation at 480 nm (Heuck and Wolosiuk, 1997b, Heuck and Wolosiuk, 1997a) and the fluorescence increases when the disulfide bonds between the insulin A and B chains are reduced. The advantage of this assay compared to the traditional insulin assay is that Trx has a higher affinity for FiTC-insulin than insulin. Additionally, due to its high sensitivity, this assay only requires small sample amounts for activity measurements making it suitable for clinical studies (Montano *et al.*, 2014). However like insulin, FiTC–insulin is not a physiological substrate for thioredoxin and thus the relevance of a high or low reductive activity in this assay may not be readily apparent.

1.4.1.2.2 Thioredoxin Mito-NAPH off–on fluorescent probe

The Mito-NAPH probe was developed to visualize mitochondrial thioredoxin activity in cells where a fluorescence off-on change is induced by a thioredoxin-mediated disulfide cleavage of the probe which can be measured at 540 nm (Figure 1.6). The main advantage of this probe is that Trx activity can be detected at concentrations as low as 50 nM which is well below its physiological level and the probe can be directed to the mitochondria increasing the specificity of the assay. Although innovative, a limitation with this probe is that although it preferentially reacts with Trx, other biological sulfur species such as GSH are present at relatively high concentrations and the probe also displays a response towards them (Lee *et al.*, 2012).

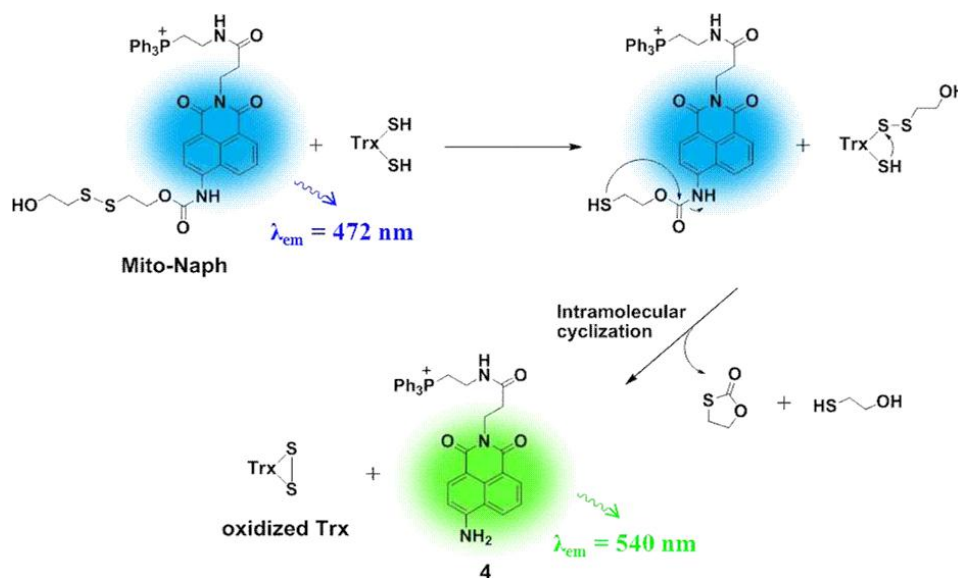


Figure 1.6 Proposed mechanism for the reaction between thioredoxin and Mito-Naph. A fluorescence off-on change is induced by thioredoxin mediated disulfide cleavage of the probe, resulting in a subsequent intramolecular cyclization by the released thiolate to give a fluorescent product which can be measured at 540 nm. (Reprinted with permission from Lee, M. H., Han, J. H., Lee, J.-H., Choi, H. G., Kang, C. & Kim, J. S. 2012. Mitochondrial Thioredoxin-Responding Off-On Fluorescent Probe. *Journal of the American Chemical Society*, 134, 17314-17319. Copyright (2012), American Chemical Society.)

1.4.1.2.3 Thioredoxin reductase fluorogenic substrate (TRFS)-green fluorescent probe

TRFS-green was designed and synthesized for monitoring mammalian thioredoxin reductase activity (Zhang *et al.*, 2014) and has been used to image the thioredoxin reductase activity in various types of live cells (Liu *et al.*, 2014, Zhang *et al.*, 2015a, Peng *et al.*, 2015b, Peng *et al.*, 2015a). Thioredoxin reductase 2 and its respective substrate thioredoxin 2 are known to regulate mitochondrial ROS levels and therefore monitoring the activity of thioredoxin reductase 2 is of significance for the etiology of various neurodegenerative diseases including Parkinson's disease (Lopert *et al.*, 2012, Perier and Vila, 2012, Subramaniam and Chesselet, 2013, Hu and Wang, 2016) and Alzheimer's disease (Arodin *et al.*, 2014) which are associated with mitochondrial dysfunction.

The probe contains a 1,2-dithiolane scaffold with a quenched naphthalimide fluorophore and displays a green fluorescence off-on change that is induced by a thioredoxin reductase mediated disulfide cleavage. This results in an intramolecular cyclization that liberates the masked naphthalimide fluorophore (Figure 1.7). The ability to trigger the fluorescent signal

by cellular protein extracts correlated well with the endogenous thioredoxin reductase activity in different cells (Zhang *et al.*, 2014). A major advantage of this probe is that it shows high selectivity towards thioredoxin reductase over other related enzymes. However a key limitation with the TRFS-green probe is that it does not accumulate exclusively in the mitochondria and instead appears to be evenly distributed in the cytosol (Liu *et al.*, 2016).

1.4.2 Approaches 2 and 3: Redox states and redox potentials

Due to its crucial role in regulating normal cellular behaviour, redox status has been recognized as a key parameter of biological research in several pathologies. Most procedures to measure the redox states of thioredoxin 1 and 2 consist of three main parts: derivatization, redox western blotting and the calculation of redox potentials which are described below.

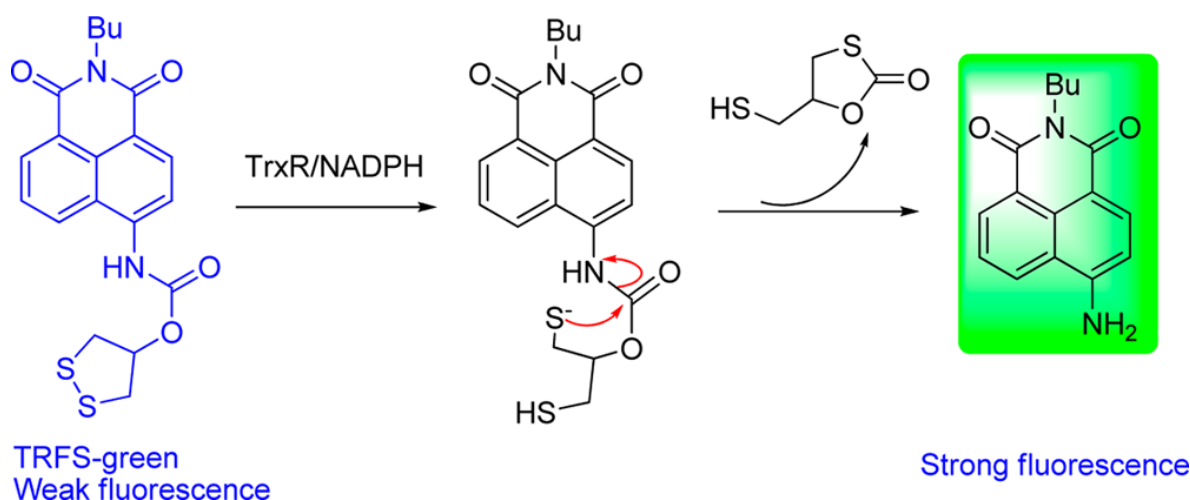


Figure 1.7 Proposed mechanism of the activation of the TRFS-green probe by thioredoxin reductase and NADPH. TRFS-green contains a five-membered, cyclic disulfide scaffold which can be selectively cleaved by thioredoxin reductase in the presence of NADPH. Upon reduction, the nucleophilic thiolate subsequently attacks the amide carbonyl carbon driven by the formation of a five-membered cyclic carbamate, which simultaneously releases the quenched fluorophore naphthalimide to activate the green fluorescent signal. (Reprinted with permission from Zhang, L., Duan, D., Liu, Y., Ge, C., Cui, X., Sun, J. & Fang, J. 2014. Highly Selective Off-On Fluorescent Probe for Imaging Thioredoxin Reductase in Living Cells. *Journal of the American Chemical Society*, 136, 226-233. Copyright (2014), American Chemical Society.)

1.4.2.1 Derivatization and redox western blot

When determining the redox state of a protein, samples have to be quenched to trap the prevailing thiol-disulfide status. Two approaches are commonly used; the first entails

blocking free thiols with a cell-permeable alkylating agent and the second method involves the quenching of thiol-disulfide exchange with an acid. As both methods pose advantages and disadvantages, the optimal procedure for quenching the thiol-disulfide state was identified to be a combination of the two strategies where samples are first quenched with TCA followed by alkylation of thiols (Hansen and Winther, 2009). This method allows for the separation of the reduced and the oxidized forms of proteins based on their molecular masses using SDS-PAGE or charge using native or urea PAGE. This procedure is generally used in conjunction with western blotting to probe the redox state within cells.

The redox western analysis of thioredoxin, currently the gold standard, provides a convenient tool to estimate the redox state of different compartments and improve the understanding of redox signalling (reviewed in Go and Jones (2001)). Labelling with thiol reagents containing biotin allows selection and/or detection with streptavidin and can enhance assay flexibility. However, the major drawback of this approach is that it can be difficult to calibrate because of multiple thiols in proteins, non-linear responses and epitope changes with thiol oxidation or alkylation (Go and Jones, 2013). Also, the derivatization procedure involves tissue destruction and the lysis of cells which may compromise recovery. Further, it is difficult to measure redox ratios in different organelles other than by cumbersome fractionation of sub-cellular structures. In principle, genetically encoded redox probes (Ren and Ai, 2013) could overcome many of these limitations but to the best of our knowledge probes specific for Trx are yet to be synthesised.

1.4.2.2 Diagonal SDS-PAGE/2D redox SDS-PAGE

Diagonal SDS-PAGE, originally used to analyse intermolecular disulfide bonds artificially generated between ribosomal proteins in *E. coli* (Sommer and Traut, 1974), is a proteomic method that allows for a global analysis of the redox state of cellular proteins. This method does not require protein purification and can therefore be used in a high-throughput manner using cell lysates (Xia *et al.*, 2007). The first step in determining the *in vivo* thiol/disulfide state of proteins involves the rapid blocking of all free thiol groups to prevent unwanted thiol-disulfide exchange reactions. This is achieved by addition of a membrane permeable thiol trapping reagent either to the intact cells shortly before lysis or to the protein extract immediately after cell lysis (Zander *et al.*, 1998). The alkylated protein extract is then separated by SDS-PAGE in the first dimension under non-reducing conditions. Upon completion of the run, the entire lane is excised, reduced and is applied horizontally to

another gel. Following electrophoresis and after staining the gel, three groups of proteins can be distinguished. Proteins without disulfide bonds are recovered on the diagonal line because their migration behaviour is identical in both dimensions, while proteins with intra- and intermolecular disulfides migrate above and below the diagonal line respectively (Cumming *et al.*, 2004, Leichert and Jakob, 2004). This method in combination with mass spectrometry was used to identify several known disulfide bonded cytoplasmic proteins such as peroxiredoxins, thioredoxin reductase, nucleoside-diphosphate kinase and ribonucleotide-diphosphate reductase that undergo disulfide bond formation upon exposure of cells to oxidative stress. Unexpectedly, a significant number of previously unknown disulfide bonded proteins were also found including those involved in molecular chaperoning, translation and glycolysis (Cumming *et al.*, 2004).

1.4.2.3 Determining the cellular redox potential using the Nernst equation

Redox states are often quantified in terms of the steady-state redox potential (E_h) because the rates of oxidation and reduction of individual thiols in cells are difficult to measure (Go and Jones, 2013). The most common way to determine the cellular Trx redox potential is through the Nernst equation (equation 1.1) which incorporates the relative *in vivo* concentrations of the redox couple determined by redox western blotting (Section 1.4.2.1) (Hansen *et al.*, 2006, Jones, 2010, Wouters *et al.*, 2010):

$$E_h = E^\circ + \frac{RT}{nF} \log_{10} \frac{\text{Oxidized Trx}}{\text{Reduced Trx}} \quad (1.1)$$

where E° represents the standard redox potential, R is the universal gas constant, T is the absolute temperature in Kelvin, n is the number of moles of electrons transferred and F is the Faraday constant.

The cellular redox potential provides a general overview of the thiol disulfide redox state of a cellular redox couple and can change dramatically with oxidative influences or deficiencies in the cellular redox-balancing systems (Leichert and Jakob, 2004). Several advantages have been associated with the use of redox potentials for quantifying the Trx system. First, the redox potential follows from studies looking at the redox regulation of proteins *in vitro*, and in some instances a precise relationship could be observed between changes in the redox potential of a given redox couple and the *in vivo* activity of a protein.

Second, changes observed in the cellular redox potential have indeed been correlated to physiological changes within some cells and tissues (Pillay *et al.*, 2013).

1.4.3 Approach 4: Transcript and protein levels

The presence of elevated concentrations of thioredoxin and/or thioredoxin reductase in biological fluids and tissues can be useful as a biomarker of oxidative stress in disease states (Quiñonez-Flores *et al.*, 2016). Thioredoxin and/or thioredoxin reductase have been shown to be over-expressed in many cancers and cancer cell lines (Miyazaki *et al.*, 1998, Arner and Holmgren, 2006, Yoo *et al.*, 2007, Hedström *et al.*, 2009) as well as asthma (Yamada *et al.*, 2003) and neurodegenerative diseases such as Alzheimer's disease (Arodin *et al.*, 2014). The most common methods used to derive the transcript and/or protein expression levels of the thioredoxin system components are discussed below.

1.4.3.1 Reverse transcription polymerase chain reaction (RT-PCR)

Reverse transcription polymerase chain reaction (RT-PCR) is commonly used to assess gene transcription in cells or tissues. Using this method, patients with non-small cell primary lung tumors showed significantly increased levels of thioredoxin mRNA compared to the thioredoxin mRNA levels in paired normal lung tissue (Gasdaska *et al.*, 1994) and half of human primary colorectal carcinomas examined had increased thioredoxin mRNA compared to adjacent normal colonic mucosa from the same subject (Berggren *et al.*, 1996).

RT-PCR has many advantages including high specificity, sensitivity and speed. However, the main limitation with this method is that a gene's transcript level does not necessarily predict its protein level as there is considerable discrepancy between mRNA and protein expression, both at steady state expression levels and in response to perturbations (Pascal *et al.*, 2008). Quantifying the relationship between protein and mRNA levels can be problematic, and previous efforts to find correlations have found variable success. For example, Stark *et al.* (2006) compared the mRNA and protein expression of the p53 gene in breast cancer brain metastases versus primary tumors and found that the mRNA level of p53 was significantly lower in brain metastases but the comparison of the protein levels was insignificant. Therefore findings of mRNA expression need to be validated by protein and activity measurements.

1.4.3.2 Northern blot

The northern blot technique is a classical way of analyzing the presence of a specific RNA sequence in a sample and has been used to identify differences in the genetic expression patterns between healthy and diseased tissues (Josefsen and Nielsen, 2011). Although this method is relatively inexpensive, simple to perform and still currently in use (see for example Brown *et al.* (2013), Ikeh *et al.* (2016)), it has a lower sensitivity when compared to RT-PCR and requires a large amount of target RNA sample.

1.4.3.3 Enzyme-linked immunosorbent assay (ELISA)

The enzyme-linked immunosorbent assay (ELISA) is the most commonly used method to determine the thioredoxin system component levels in human plasma and serum (Miyazaki *et al.*, 1998, Park *et al.*, 2014, Wu *et al.*, 2014, Li *et al.*, 2015, Zhang *et al.*, 2015a). The clinical significance of serum thioredoxin levels was assessed in acute ischemic stroke (AIS) patients using solid-phase sandwich enzyme-linked immunosorbent assay (ELISA) in which two highly specific antibodies to the human thioredoxin protein were utilized. Using this method, it was found that the serum thioredoxin levels were significantly increased in first-ever stroke patients compared with those in normal controls and it was concluded that the serum thioredoxin levels might be used as an independent diagnostic marker of AIS (Wu *et al.*, 2014). This method was also used to measure the serum levels of thioredoxin in patients diagnosed with hepatocellular carcinoma (Li *et al.*, 2015) as well as to assess the clinical significance of serum thioredoxin levels in children with autism spectrum disorders (ASD) where it was observed that the thioredoxin levels were significantly higher in children with ASD when compared to typically developing children (Zhang *et al.*, 2015b).

The key advantage of this assay is that it provides a convenient method for the analysis of a large number of samples within a single run and requires significantly less sample volume compared to other techniques such as northern blotting (Frijhoff *et al.*, 2015). However, an important limitation is that human serum samples also contain immunoglobulins that affect the results of immunoassays by binding to reagent antibodies used in the assay leading to false positive signals (Zhang *et al.*, 2009). In addition, quantifying protein levels yields no insights into the redox state of the protein. Finally, elevated thioredoxin levels have been associated with multiple conditions and therefore increased serum levels of this protein may not necessarily be a marker of a specific pathology.

1.4.3.4 Mass spectrometry

Mass spectrometric peptide mapping used in conjunction with protein database searching is becoming a popular choice for the rapid identification of proteins. A typical protein identification experiment involves the separation of proteins of interest by one-dimensional or two dimensional polyacrylamide gel electrophoresis. The bands containing the proteins of interest are then excised and are in-gel digested by a protease such as trypsin. The resulting proteolytic peptides are analyzed by matrix-assisted laser desorption/ionization (MALDI) imaging mass spectrometry to yield a peptide mass map. Identification of proteins is achieved by searching for the best match between the experimentally determined masses in the peptide map and those calculated by theoretical cleavage of each of the proteins in an appropriate sequence database (Aebersold, 2003). Extensive application of mass spectrometric methods to neurodegenerative diseases such as Alzheimer's disease and Parkinson's disease, as well as other human diseases and animal models, have established the value of these approaches in improving our mechanistic understanding of redox biology and human disease (Butterfield *et al.*, 2006).

1.4.3.4 Redox proteomics

In contrast to the measurement of individual biomarkers, proteomic analysis aims to identify a panel of complementary biomarkers that are either up- or downregulated with altered post-translational modifications which differ in pathological and normal states and can therefore give extensive information regarding a disease. This approach has an advantage over mRNA expression analysis as it directly focuses on the actual biological effector molecules and provides more accurate functional information about biological systems (Shiio and Aebersold, 2006).

Redox proteomics is a rapidly advancing area of proteomics focused on identifying and quantifying redox-based changes within the proteome during redox signaling and under oxidative stress conditions (Rinalducci *et al.*, 2008). It also aims to broaden the information available concerning potential biomarkers for disease diagnosis and provide insights into perturbed redox metabolic networks and potential targets for modulation of disease progression by means of drug therapy. In addition to the methods previously mentioned (Section 1.3), a number of other redox proteomics methods have been developed. An example of a redox proteomics approach involves the use of isotope-coded affinity tags (ICATs) with three functional moieties: a cysteine reactive moiety, a linker containing either

a heavy (contains eight deuteriums) or light (contains eight hydrogens) isotope resulting in a mass difference between the two, and a biotin affinity tag used to isolate ICAT-labeled peptides. Using this technique, the cysteine side chains in complex mixtures of proteins from two different states of a cell population such as normal and disease conditions are labeled with isotopically light and heavy ICAT reagents. The two mixtures are then combined and after tryptic digestion to form peptides, the labelled peptides are affinity-purified using an avidin column and are then analyzed by mass spectrometry. The quantitative information based on the relative abundance of the light and heavy isotopes is obtained and the identification of proteins is determined from the peptide molecular mass and amino acid sequence (Gygi *et al.*, 1999, Aebersold *et al.*, 2007).

The ICAT technique has significantly expanded the range of proteins that can be analyzed including low-abundance, hydrophobic or highly charged proteins, and also allows accurate quantification and concurrent sequence identification of individual proteins in complex mixtures (Shiio and Aebersold, 2006). While the ICAT approach provides a widely applicable means to compare quantitatively global protein expression in cells and tissues (Gygi *et al.*, 1999), it displays insufficient proteome coverage and it is estimated that only 10-20% of the whole cell proteome can be analyzed in a single ICAT experiment (Shiio and Aebersold, 2006).

1.5 Limitations with the current quantification methods for the thioredoxin system: could a systems biology approach be the solution?

In addition to the methodological limitations within each approach outlined above, several limitations have been identified with the actual measures chosen to characterize the thioredoxin system. For example, the enzyme assay approach is limited as a number of inconsistencies exist in the description of thioredoxin as an enzyme. In contrast to the catalytic cycles of conventional enzymes, thioredoxins become oxidized and therefore inactive after reacting with their substrates. A separate enzyme-catalysed reaction is required to return thioredoxin to its active form (Figure 1.1-1.2) and a varying turnover number has been reported for the reduction of insulin by thioredoxin suggesting that Michaelis-Menten parameters should not be used to quantify thioredoxin activity (Pillay *et al.*, 2009). Further, monitoring changes in thioredoxin reductase activity alone, may also be an inadequate

measure of the thioredoxin system which is comprised of several subsystems that can affect each other through the Trx redox cycle (Pillay *et al.*, 2011).

On the other hand, data from cultured cells and tissues had suggested that redoxins should be characterized as redox couples (Trotter and Grant, 2003, Watson *et al.*, 2004), and quantified with redox ratios and potentials and not by enzyme kinetic parameters and activity measurements which has further complicated the quantification of the Trx system. However, theoretical studies have also questioned the validity and usefulness of cellular redox potentials and have suggested that kinetic rather than thermodynamic regulation may be a more important consideration because the Nernst equation only provides a measure of the thermodynamic potential. The equation gives no indication of whether reactions actually occur or the rates of these reactions within a given system and thus while the Nernst equation may have some correlative value to physiological changes, its predictive capacity has been limited (Flohé, 2010, Flohé, 2013, Pillay *et al.*, 2013).

Although measurement of protein levels has been informative, this data is inherently incomplete as elevations in these levels can be ambiguous as they may reflect either an increase in protein production or a decrease in turnover. As described above, a major limitation with the analysis of transcript levels alone is that these levels may not be able to predict the corresponding protein levels. The isolated assessment of protein levels is also inadequate as it provides no information regarding protein activity and therefore it might be best to concurrently measure the catalytic activity of the protein.

Given the multiple approaches taken to quantify the Trx system and the limitations associated with each one, it is unclear which measure provides the most accurate description of the role played by the *system* in pathological states (Figure 1.3). Also, efforts aimed at alleviating pathologies associated with Trx system perturbations may have been limited as these diseases involve a large variety and number of elements that interact via complex networks and nonlinear interactions (Wang, 2010). Therefore, analysis and quantification of system constituents in isolation or knocking out a single target molecule in a biochemical pathway may be insufficient for analysing the role of the Trx system in a pathology (Hornberg *et al.*, 2006, Wang, 2010). It is increasingly believed that a systems approach, rather than the current gene-centric view could solve these problems (Wang, 2010, Loscalzo and Barabasi, 2011) because developing an understanding of the complex systems involved

in various pathologies might make it possible to develop more efficient therapeutic strategies which could lead to significant advances in the treatment of disease (Wang, 2010). Consequently utilizing a *system* measure such as flux may provide better insight into the steady state behaviour of the thioredoxin network as a whole. However as measuring flux *in vivo* is experimentally challenging, computational modeling has often been used (Sauer, 2006).

Computational methods allow for the generation of *in silico* models of cells, tissues and organs with the aim of simulating the steady state and dynamic properties of a system. Using this approach, several computational models of the thioredoxin system have been developed to elucidate the behavior of the system (Adimora *et al.*, 2010, Pillay *et al.*, 2011, Benfeitas *et al.*, 2014, Tomalin *et al.*, 2016). An advantage of this approach is that the flux can be estimated through computational model-based interpretation of experimental data (Sauer, 2006). However a limitation with this inference approach is that it relies on data fitting experiments and therefore the development of accurate models.

In this regard, a major hurdle faced during thioredoxin computational modeling studies was whether to describe thioredoxin as an enzyme or as a redox couple as conflicting measures of thioredoxin activity have been reported in the biochemical literature (detailed in Pillay *et al.* (2009), Pillay *et al.* (2013)). Specifically, if thioredoxin was modeled as an enzyme, then it should appear in the rate vector (v) of the kinetic model equation (equation (1.2), but if it was modeled as a redox couple, then it should appear in the stoichiometric matrix (N) of that equation (Terzer *et al.*, 2009, Pillay *et al.*, 2013):

$$\frac{ds_i}{dt} = N \cdot v \tag{1.2}$$

where s_i refers to the species within the kinetic model.

Using computational modeling, it was proposed that thioredoxin should be modeled as a redox couple, that mass action kinetics were sufficient to describe thioredoxin activity and that the Michaelis-Menten parameters assigned to thioredoxin were unreliable. It was also proposed that the *in vitro* enzymatic properties attributed to thioredoxin resulted from the saturation of the thioredoxin redox cycle and not thioredoxin itself (Pillay *et al.*, 2009). A number of computational models have subsequently been built using this approach (Adimora

et al., 2010, Pillay *et al.*, 2011, Benfeitas *et al.*, 2014, Tomalin *et al.*, 2016). However, prior and subsequent kinetic fitting studies from other groups support the description of thioredoxin and indeed other redoxins as enzymes (Holmgren, 1979a, Juttner *et al.*, 2000, Bao *et al.*, 2009, Maeda *et al.*, 2010, Obiero *et al.*, 2010, Chen *et al.*, 2014) which has questioned the applicability of the computational modeling approach.

1.6 Aims of study

Given the ambiguous description of thioredoxin activity, the first aim of this research was to confirm the kinetic mechanism of the thioredoxin system in order to accurately model this network for system biology applications. This aim involved computational and molecular methods including the cloning, expression and purification of the thioredoxin system from *Saccharomyces cerevisiae* and the generation of substrate saturation curves using insulin as a model substrate. As model inference is currently the only available way to obtain a flux through the system, finding an independent and experimentally tractable surrogate measure for this flux would represent a significant advance and was therefore the second aim of this study. To achieve this objective, simulations of thioredoxin system computational models as well as *in vitro* assays were performed to determine which of the measures of the thioredoxin system was a surrogate measure for flux under conditions of perturbed oxidative demand and reductive supply.

Chapter 2: Purification of the yeast thioredoxin system

2.1 Introduction

The initial step in the isolation of a protein is to choose a method of measuring the presence of the protein and of distinguishing it from all other proteins that might be present in the same material. This is achieved by an activity assay which measures the unique activity of the protein and allows various materials to be analyzed so that the one containing the largest amount of the desired protein, can be used as the starting material (Dennison, 2003). Usually, the more specific the assay, the more effective the purification is (Berg *et al.*, 2002).

Once a source material has been selected, the protein must be extracted in a soluble form suitable for manipulation. The object of extraction is to get the target protein out of the cellular material where it is located and into solution so that it can be manipulated. This can be achieved by homogenisation, which disrupts the tissues and breaks open the cells to release their contents. The extract can then be clarified by either filtration or centrifugation. The crude extracts containing the desired protein are thereafter purified on the basis of characteristics such as solubility, size, charge and specific binding affinity (Dennison, 2003).

The original methods employed in the purification of Trx and thioredoxin reductase were tedious and time consuming (Williams *et al.*, 1967) and were replaced with cloning technologies which were simpler and faster (Gasdaska *et al.*, 1995, Miranda-Vizuete *et al.*, 1997, Serrato *et al.*, 2002, Kim *et al.*, 2005). The sections below describe the materials and methods used to isolate the Trx system. The methods section is divided into separate sub-sections with descriptions because of the range of techniques covered. All the results are presented in a single section (Section 2.9).

2.2 Materials

TEMED, ammonium persulfate, Coomassie brilliant blue R-250 powder, dithiothreitol (DTT), bovine pancreas insulin, 5, 5'-dithiobis(2-nitrobenzoic acid) (DTNB), β -nicotinamide

adenine dinucleotide phosphate (NADPH), bovine serum albumin (BSA), isopropyl β -D-1-thiogalactopyranoside (IPTG), kanamycin, ampicillin and 4-(2-aminoethyl)benzenesulfonyl fluoride hydrochloride (AEBSF) were obtained from Sigma (Capital Labs, South Africa) while RNase A was obtained from Roche (South Africa). A Rapid DNA Ligation Kit, the ThermoScientific Gel Extraction Kit, the InsTAclone™ PCR cloning kit, TransformAid™ Bacterial Transformation Kit and Taq™ DNA polymerase were obtained from Inqaba Biotech (Johannesburg, South Africa) while the QIAquick™ Gel Extraction Kit, agarose for gel electrophoresis and Ni-NTA agarose were obtained from Whitehead Scientific (Pty) Ltd (Cape Town, South Africa). The New England Biolabs HindIII, NdeI and BamHI restriction enzymes were obtained from The Scientific Group (Midrand, South Africa) and Acrylamide-Bis ready to use solution (37.5:1) and Polyethylene glycol (PEG) 20,000 were obtained from Merck (South Africa). All other common chemicals were obtained from Saarchem (Merck, South Africa) and were of the highest purity available. pET28a was generously donated by Professor Dean Goldring (Biochemistry, UKZN) and the thioredoxin reductase clones (pMPTRRA, B, C and D) were generously supplied by Miss M.M Photolo (Genetics, UKZN).

2.3 Preparation of common reagents

The preparation of all common reagents has been described in the text below whilst the preparation of specialized reagents will be described later in the chapter.

2.3.1 DTT

A fresh stock solution of DTT (1 M) was prepared at the time of use by dissolving DTT powder (0.154 g) in ddH₂O (1 ml). 200 μ l of this stock solution was made up to 2 ml with ddH₂O and the resulting DTT solution (final concentration 100 mM) was used in the Trx activity assay.

2.3.2 Bovine pancreas insulin

A 1.6 mM stock solution of insulin was prepared by suspending insulin (50 mg) in 0.5 ml 100 mM potassium phosphate buffer (pH 6.5). The pH was adjusted to 2-3 with 1 M HCl to dissolve the protein completely and was thereafter titrated back to the original pH of the

buffer (pH 6.5) with NaOH (1 M). Finally, the volume was adjusted to 5 ml with ddH₂O. The clear insulin solution was stored at – 20°C.

2.3.3 DTNB

A stock solution of DTNB (62.1 mM, final concentration) was freshly prepared by dissolving DTNB powder (0.025 g) in 99% ethanol (1 ml). The resulting solution was stored in the dark as DTNB is light sensitive.

2.3.4 NADPH

Stock vials were prepared by keeping 10 mg portions of NADPH (dry) in separate small microcentrifuge tubes at -20°C. At the time of use, a single tube was dissolved in ddH₂O (250 µl) and the final concentration was spectrophotometrically confirmed at 340 nm using the extinction coefficient (6,220 M⁻¹ cm⁻¹).

2.3.5 IPTG stock solution

A stock solution (100 mM) was prepared by dissolving IPTG powder (0.238 g) in dH₂O and the volume was made up to 10 ml. This suspension was filter sterilized using a 0.2 µm filter (Merck, South Africa).

2.3.6 Kanamycin stock solution

A stock solution (30 mg/ml) was prepared by dissolving kanamycin sulphate (0.3 g) in dH₂O. The volume was made up to 10 ml. This suspension was filter sterilized using a 0.2 µm filter (Merck, South Africa) and stored in 1 ml aliquots at -20°C.

2.3.7 Ampicillin stock solution

A stock solution (25 mg/ml) was prepared by dissolving ampicillin sodium salt (0.25 g) in dH₂O. The volume was made up to 10 ml. This suspension was filter sterilized using a 0.2 µm filter (Merck, South Africa) and stored in 1 ml aliquots at -20°C.

2.3.8 Bacterial growth media

2.3.8.1 Luria Bertani (LB) broth

Tryptone (1% (w/v)), yeast extract (0.5% (w/v)) and NaCl (0.5% (w/v)) were dissolved in dH₂O and the solution was made up to the desired volume. The solution was autoclaved and stored at room temperature. When necessary, the appropriate antibiotic, either kanamycin (30 µg/ml, final concentration) or ampicillin (50 µg/ml, final concentration) was added.

2.3.8.2 Luria Bertani (LB) agar

Tryptone (1% (w/v)), yeast extract (0.5% (w/v)), NaCl (0.5% (w/v)) and bacteriological agar (1.5% (w/v)) were dissolved in dH₂O and the solution was made up to the desired volume. The solution was autoclaved and upon cooling, media was poured into petri dishes. When necessary, the appropriate antibiotic, either kanamycin (30 µg/ml, final concentration) or ampicillin (50 µg/ml, final concentration) was added. The plates were stored at 4°C.

2.3.8.3 Yeast Peptone Dextrose (YPD)

Yeast extract (1% (w/v)), peptone (2% (w/v)) and dextrose (2% (w/v)) were dissolved in dH₂O and the solution was made up to the desired volume. The solution was autoclaved and stored at room temperature.

2.3.8.4 SOC media

Yeast extract (0.5% (w/v)), tryptone (2% (w/v)), NaCl (10 mM), KCl (2.5 mM) and MgCl₂ (10 mM) were dissolved in dH₂O and the solution was made up to the desired volume. The solution was autoclaved and once cooled, glucose (20 mM, final concentration) was added. The glucose solution (1 M) was sterilized by passing it through a 0.2 µm filter. The SOC media was then stored at 4°C.

2.3.8.5 2xYT media

Tryptone (1.6% (w/v)), yeast extract (1% (w/v)) and NaCl (0.5% (w/v)) were dissolved in dH₂O. The pH was adjusted to 7.0 with NaOH and the volume was made up with dH₂O. The solution was sterilized by autoclaving and thereafter stored at room temperature.

2.4 The yeast thioredoxin activity assay

There are a number of assays that have been developed to test the activity of Trx (Chapter 1). However, many of these assays require thioredoxin reductase (Luthman and Holmgren, 1982, Jeon and Ishikawa, 2002, Grimaldi *et al.*, 2008) and commercial Trx assay kits are relatively expensive. Current assays for Trx are therefore constrained by the cost and availability of pure enzyme and it was important to develop a novel Trx activity assay that was inexpensive and allowed for the rapid identification of the target molecules in crude extracts.

Holmgren (1979b) showed that the rate of the reduction of insulin disulfides by DTT was low but the addition of *E. coli* Trx to the reaction mixture increased the rate of reduction significantly. These findings could be used as the basis for an activity assay for Trx and as pure thioredoxin reductase was no longer needed, the cost of the assay was greatly reduced. However, a potential problem with this assay was that it took over 20 min before a result was obtained (Holmgren, 1979b).

2.4.1 Methods to determine Trx activity

To determine the activity of Trx, a number of assay conditions were tested based on data in Holmgren (1979b) which included variations in insulin (0.01 mM and 0.13 mM) and DTT (0.33 mM and 1 mM) concentrations as well as the pH of the potassium phosphate buffer (pH 6.5 and 7.0). Each reaction mixture contained 2 mM EDTA and proceeded at 25°C (Holmgren, 1979b). A modified version of the original assay (Holmgren, 1979b) involving the incubation of all components for 20 min at 25°C prior to absorbance readings being taken, was also attempted (Sigma-Aldrich, 1994). However in this study, a method involving the reduction of the Trx by preincubating 0.1 M DTT (10 µl) with the Trx containing crude extract for 10 min at 25°C was developed. A master mix containing 84 mM potassium phosphate buffer (pH 7.0), EDTA (2.67 mM) and insulin (0.21 mM) was made into a final volume of 9 ml. Thereafter the reaction was initiated by addition of the preincubated suspension (250 µl) to the master mix (750 µl). The final reaction mixture contained 63 mM potassium phosphate buffer (pH 7.0), EDTA (2 mM), insulin (0.01 mM) and DTT (1 mM) in a final volume of 1 ml. The change in absorbance at 650 nm was directly monitored using a

sample without the addition of the crude extract as the reference cuvette. Absorbance measurements were made with a UV-1800 Shimadzu Spectrophotometer.

2.5 The yeast thioredoxin reductase activity assay

The thioredoxin reductase assay involves monitoring either NADPH oxidation or direct reduction of a substrate such as 5, 5'-dithiobis(2-nitrobenzoic acid) (DTNB). In the former assay, the oxidation of NADPH is monitored spectrophotometrically in a mixture containing potassium phosphate, KCl, EDTA and NADPH as well as oxidized Trx and thioredoxin reductase,. However, the limitation with this method is that purified Trx is required. Trx, the natural substrate of thioredoxin reductase, is very expensive and difficult to obtain so the activity of thioredoxin reductase is usually assayed using an alternate substrate.

The alternative assay to measure the activity of thioredoxin reductase is by monitoring the change in absorbance at 412 nm occurring as a result of the reduction of DTNB to TNB which has proven to be sufficiently specific (Arnér and Holmgren, 2000a, Štefanková *et al.*, 2006). It was also shown that the use of univalent cations in this assay significantly increased the rate of reduction (Lim and Lim, 1995). It has been proposed that these cations may induce a conformational change in *E. coli* thioredoxin reductase in which its closed conformation is converted to an open conformation thereby exposing the active site (Lim and Lim, 1995).

2.5.1 Methods to determine thioredoxin reductase activity

To determine the activity of thioredoxin reductase, a number of assay conditions were tested including DTNB (1 mM - 5 mM) and NADPH (0.3 mM - 0.5 mM) concentrations, the pH of the potassium phosphate buffer (pH 7.0 and 7.2) (Arnér and Holmgren, 2000a, Štefanková *et al.*, 2006) and the effect of including univalent cations (NaCl) within the reaction (Lim and Lim, 1995). The final reaction mixture used in this study contained 0.1 M Tris-Cl (pH 8.0), 0.5 mM DTNB, 0.24 mM NADPH, 0.01% BSA, 0.5 M NaCl and crude extract containing TrxR in a final volume of 1 ml. The reaction was initiated by the addition of the crude extract and proceeded at 25°C with the change in absorbance at 412 nm being directly monitored using a sample without the crude extract as the reference cuvette. Absorbance measurements were made with a UV-1800 Shimadzu Spectrophotometer.

2.6 Cloning of Trx

2.6.1 Isolation of genomic DNA from *S. cerevisiae*

Yeast genomic DNA was isolated utilizing the Bust 'N Grab method (Harju *et al.*, 2004). Briefly, two 1.5 ml samples of a 16 hour yeast culture grown in YPD were pelleted by centrifugation (20,000 x *g*, 5 min, room temperature). The pellet was completely resuspended in 200 µl of lysis buffer (2% (v/v) Triton X-100, 1% (w/v) SDS, 100 mM NaCl, 10 mM Tris-HCl (pH 8.0) and 1 mM EDTA (pH 8.0)) by gentle inversion of the tubes. The tubes were then incubated at -75°C until the contents was completely frozen (5 min) and were then rapidly transferred to a 95°C water bath (1 min) to allow the contents to thaw. This process was repeated three times and thereafter the tubes were vortexed for 30 seconds. Chloroform (200 µl) was added to each tube followed by vortexing (2 min). Upon centrifugation (20,000 x *g*, 5 min, room temperature), three distinct layers could be seen and the upper aqueous phase was transferred to a clean eppendorf tube containing 400 µl ice-cold 100% ethanol. The tubes were gently inverted and incubated for 5 min at -20°C for precipitation of the DNA. The precipitated DNA was pelleted by centrifugation (20,000 × *g*, 5 min, room temperature), washed with 70% (v/v) ethanol (0.5 ml), air-dried and re-suspended in 50 µl TE buffer (10 mM Tris-HCl (pH 8.0), 1 mM EDTA (pH 8.0)). These samples were assayed at 260 nm and 280 nm to determine DNA concentration and purity (Section 2.6.12) and were also analyzed by agarose gel electrophoresis (Section 2.6.11).

2.6.2 PCR

To amplify the *TRX1* gene, PCR was performed using yeast *TRX1* specific primers, 5'-AGCCCATATGGTTACTCAATTCAA^{AA}ACTGCC-3' and 5'-ACGAAGCTTAAGCATTAGCAGCAATGGC-3' (NdeI and HindIII sites are underlined, respectively). These primers were designed using Primer3 (<http://frodo.wi.mit.edu>) and the Trx sequence was obtained from the *Saccharomyces* genome database (SGD) (<http://www.yeastgenome.org>, Gene ID 850732). The primers were designed so that there was an overlap between the start codon and the restriction site of NdeI whilst the HindIII restriction site overlapped with the stop codon. This design ensured that more of the coding sequence was included in the primer, increasing the accuracy of the PCR. The PCR reaction mixture consisted of TaqTM DNA polymerase (0.5 U), reaction buffer (1X), a dNTP mix (0.2 mM), the forward and reverse primers (250 nM each) and DNA (0.01-1 µg) in 25 µl. The following PCR cycling conditions were used: 95°C,

3 min (initial denaturation); 95°C, 30 sec; 55°C, 30 sec; 72°C, 30 sec (30 cycles) and a final extension at 72°C, 7 min. For all PCR experiments a no template control was included in order to check for contamination and the PCR products were analyzed by gel electrophoresis (Section 2.6.11).

2.6.3 Mini-prep procedure for purification of plasmid DNA

Plasmid DNA was purified using the standard mini-prep procedure (Sambrook *et al.*, 1989). Two 10 ml samples of an overnight culture grown in LB (containing the appropriate antibiotic) were centrifuged (7,250 x g, 5 min, 4°C). The pellet was resuspended in 200 µl GTE solution (25 mM Tris-Cl (pH 8.0), 10 mM EDTA, 50 mM glucose), RNase A (2 µl) was added and the suspension was incubated at room temperature for 5 min before being transferred to a sterile eppendorf tube. 400 µl NaOH/SDS solution (0.2 M NaOH, 1% (w/v) SDS) was added to lyse the cells and the suspension was mixed by gentle finger tapping followed by incubation on ice for 5 min. 3 M potassium acetate solution (300 µl) was added and the suspension was incubated on ice for 5 min before being centrifuged (12,000 x g, 5 min, room temperature). Isopropanol (600 µl) was added to the supernatant (800 µl) and incubated at -20°C for 30 min. The suspension was centrifuged (12,000 x g, 5 min, room temperature) and the pellet was washed with ice-cold 70% ethanol (500 µl) to remove salt. The pellet was then resuspended in 50 µl TE buffer (10 mM Tris-HCl (pH 8.0), 1 mM EDTA (pH 8.0)).

2.6.4 Restriction Digestion

Plasmid DNA was routinely restricted with either BamHI or HindIII to linearise the DNA for sizing. In these reactions, plasmid DNA (1 µg), restriction enzyme (2 U), buffer (1 X) and for a BamHI digest, BSA (0.1 µg/ µl) were incubated at 37°C for 2 hours. For cloning experiments, plasmid DNA was restricted with HindIII and NdeI to liberate the *TRX1* fragment. In these reactions, plasmid DNA (37.5 µg), restriction enzyme (2 U each) and nuclease free water were all incubated with 1X NEBuffer 2 at 37°C for 4 hours.

2.6.5 Gel purification and Ligation

The amplified *TRX1* fragment was gel purified using the QIAquick™ Gel Extraction Kit and thereafter ligated with the pTZ57R/T vector using the InsTAclone™ PCR cloning kit to yield the pTrxA, pTrxB and pTrxC clones. A typical reaction mixture contained the pTZ57R/T vector DNA (0.165 µg), purified PCR fragment (at 3: 1 molar excess over vector),

Ligation buffer (1 X), T4 DNA Ligase (5U/ μ l) and nuclease free water. The pTZ57R/T vector was transformed into *E. coli* JM109 cells using a TransformAid™ Bacterial Transformation Kit according to the manufacturer's instructions. As a positive control for competent cell growth, *E. coli* JM109 competent cells were plated onto a LB agar plate with no antibiotic and as a negative control, untransformed cells were plated onto LB plates containing ampicillin (50 μ g/ml). To purify the recombinant pTZ57R/T DNA, a plasmid mini-prep procedure was performed (Section 2.6.3). PCR (Section 2.6.2) using the purified recombinant plasmid as a template was done to confirm the presence of the *TRX1* insert. A restriction digestion using BamHI was also performed to linearise the vector for sizing and the vector was digested with HindIII and NdeI to liberate the *TRX1* fragment.

2.6.6 Plasmid DNA extraction of pET28a

The expression vector, pET28a, was isolated from *E. coli* BL21 (DE3) cells using a plasmid DNA extraction procedure (Section 2.6.3). A_{260} and A_{280} readings of the samples were taken to determine DNA concentration and purity and these samples were also analyzed by agarose gel electrophoresis (Section 2.6.11).

2.6.7 Gel purification and Ligation

Restriction digested pET28a (section 2.6.4) and the liberated *TRX1* fragment were both gel purified using a Fermentas Gel Extraction Kit. The gel-extracted *TRX1* fragment and restricted pET28a expression vector were subsequently ligated using a Rapid DNA Ligation Kit (Fermentas) to form the expression plasmids pLPTrxA, pLPTrxB and pLPTrxC. A typical ligation mixture contained vector DNA (10 – 100 ng), insert DNA (at 3: 1 molar excess over vector), 1X Rapid Ligation Buffer, T4 DNA Ligase (5U/ μ l) and nuclease free water. The mixture was incubated at 4°C overnight and was then used for transformation.

2.6.8 Preparation of competent cells using the calcium chloride method

A calcium chloride (CaCl_2) method (Sabel'nikov *et al.*, 1977) was used to make *E. coli* BL21 (DE3) competent cells. *E. coli* BL21 (DE3) cells were cultured in 2xYT medium until an OD_{600} (0.3-0.4) was reached. Two 10 ml samples were transferred to ice-cold sterile tubes, incubated on ice for 10 min and thereafter centrifuged (4,500 x g, 10 min, 4°C). The pellet was resuspended in ice-cold 0.1 M calcium chloride (10 ml). The suspension was centrifuged (4,500 x g, 10 min, 4°C) and the pellet was resuspended in ice-cold 0.1 M calcium

chloride (2 ml) followed by a 30 min incubation on ice. These competent cells were then used for transformation.

2.6.9 Transformation of *E. coli* BL21 (DE3) with pET28a

The ligation mix (1 μ l) was added to the competent cells (20 μ l) and incubated on ice (30 min). This mixture was then heat shocked (42°C, 90 sec) and immediately placed on ice (2 min). Pre-warmed (37°C) SOC media (80 μ l) was added to the cells and the cells were incubated for 1 hour at 37°C in a shaking water bath. The transformation mix (50 μ l) was plated onto LB agar plates containing kanamycin (30 μ g/ml) and incubated at 37°C overnight. As a control for competent cell growth, *E. coli* BL21 (DE3) competent cells were plated onto a LB agar plate (no antibiotic) whilst in the control for antibiotic activity, untransformed *E. coli* BL21 (DE3) competent cells were plated onto the selective medium. As a control for the competency, *E. coli* BL21 (DE3) cells were transformed with the pET28a expression vector (70 ng). To confirm the identity of the clones obtained, a colony PCR using the reaction conditions described above (Section 2.6.2) was done and the plasmid DNA was purified and restricted with HindIII to linearize the vector for sizing.

2.6.10 Colony PCR

Sections of single colonies from the transformation plate were selected, dissolved in autoclaved distilled water (25 μ l) and incubated in a water bath (2 min, 100°C). This mixture was centrifuged (13,000 \times g, 2 min, room temperature) and 2 μ l of the supernatant was used to perform a PCR using the conditions described above (Section 2.6.2).

2.6.11 Agarose gel electrophoresis

Analysis of isolated genomic and plasmid DNA was carried out on 1 % (w/v) agarose gels while restriction digestion and PCR products were carried out on 2 % (w/v) agarose gels. Gels were prepared by dissolving agarose in 50 ml 1 x TAE buffer (40 mM Tris, 20 mM acetic acid, 1 mM EDTA, pH 8.0) by gentle heating over a bunsen burner. Once cooled, 2 μ l of ethidium bromide (10 mg/ml) was added, the gel was poured into the casting tray and allowed to polymerize (30 min). Gels were run at 90 V until the bromophenol blue in the loading buffer (30% (v/v) glycerol, 0.25% (m/v) bromophenol blue) had migrated approximately $\frac{3}{4}$ down the gel and thereafter photographed under ultraviolet light. A standard curve, relating log molecular weight to the distance travelled by each fragment (mm) was constructed and used to determine the size of the bands of interest, through extrapolation.

2.6.12 DNA quantification

The NanoDrop™ 2000 UV-Vis Spectrophotometer (Thermo Scientific, South Africa) was used to determine the purity and concentration of the DNA. The concentration was measured in ng/μl.

2.6.13 Induction and optimization of expression

Protein expression of the pET28a clones (pLPT_{rx}A, B, C) was induced by culturing selected clones in LB media (30 μg/ml of kanamycin) until an OD₆₀₀ (0.3-0.4) was reached. Isopropyl β-D-1-thiogalactopyranoside (IPTG, final concentration 0.5 mM) was added to cultures which were incubated at 37°C in a shaking waterbath. Following IPTG addition, samples were taken every 30 min and an OD₆₀₀ was measured. To optimize expression, samples were also taken at 2, 4, 6, 17 and 19 hours and an OD₆₀₀ was measured. All samples were centrifuged (12,000 × g, 10 min, 4°C) and re-suspended in water to a final OD₆₀₀ of 10. This step ensured that approximately equal concentrations of protein were compared over the course of the induction experiment. An equal volume of 2 × sample buffer (125mM Tris-HCl, 4% (m/v) SDS, 20% (v/v) glycerol, 10% (v/v) mercaptoethanol, 0.01% (m/v) bromophenol blue, pH 6.8) was added to 20 μl of the re-suspended samples and the samples were analyzed by SDS-PAGE (Section 2.3). For the optimization experiments, cells were also sonicated, centrifuged (15,000 × g, 20 min, 4°C) and thereafter the supernatant was subjected to the insulin activity assay (Section 2.4.1). The activity of each sample was calculated and this was used to determine the optimal expression time for purification.

2.6.14 Tris-Tricine sodium dodecyl sulfate polyacrylamide gel electrophoresis (SDS-PAGE)

Tricine SDS-PAGE is commonly used to resolve smaller proteins in the mass range 1-100 kDa which are sometimes poorly resolved by the conventional Laemmli SDS-PAGE system (Schägger, 2006). In this system, tricine is used as the trailing ion in the stacking phase and allows a resolution of small proteins at lower acrylamide concentrations than in glycine SDS-PAGE systems (Schägger and von Jagow, 1987). Protein samples, prepared in either reducing or non-reducing treatment buffer (125mM Tris-HCl, 4% (m/v) SDS, 20% (v/v) glycerol, 0.01% (m/v) bromophenol blue, 10% (v/v) 2- mercaptoethanol (only present in reducing buffer), pH 6.8) and boiled for 5 minutes prior to loading, were visualised on a 15% Tris-Tricine gels (Table) which comprised of acrylamide: bis (37:5:1) ready to use

solution, Gel Buffer (3 M Tris-HCl, 0.3% (m/v) SDS, pH 8.45) and dH₂O. Polymerisation was initiated with TEMED and freshly prepared ammonium persulfate (10% (w/v)). The gels were run at 42 mA with unlimited voltage using cathode (0.1 M Tris-HCl, 0.1 M Tricine, 0.1% (m/v) SDS, pH 8.25) and anode buffer (0.2 M Tris-HCl, pH 8.9) and were stopped when the tracking dye reached the bottom of the gel. Upon completion of electrophoresis, gels were soaked in Coomassie blue stain (0.125% (m/v) Coomassie brilliant blue R-250, 50% (v/v) methanol and 10% (v/v) acetic acid) overnight at room temperature with gentle agitation. The stain was then removed and the gels were soaked in destain I solution (50% (v/v) methanol, 10% (v/v) acetic acid) on a shaker until background staining was reduced. Gels were then transferred to destain II (5% (v/v) methanol, 7% (v/v) acetic acid) and thereafter photographed under white light.

Table 2.1 Preparation of the resolving and stacking gels for Tris-tricine SDS-PAGE

Reagents	Resolving gel (ml)	Stacking gel (ml)
Monomer	8.0	0.67
Gel Buffer	4.0	1.25
dH ₂ O	3.71	3.00
Ammonium persulfate	0.240	0.050
TEMED	0.016	0.010

2.7 Cloning of thioredoxin reductase

2.7.1 Colony PCR

Clones of thioredoxin reductase (pMPTRRA, B, C and D) were obtained from Miss M.M Photolo (Genetics, UKZN). These clones had been sequenced confirming that they were native *TRR1*. These were then tested to confirm the presence of the *TRR1* gene by performing a colony PCR (Section 2.6.10) using yeast *TRR1* specific primers, 5'-AGCCCATATGGTTTACAACAAGTTAC-3' and 5'-ACGAAGCTTATTCTAGGGAAGTAAAGT-3' (NdeI and HindIII sites are underlined, respectively). The PCR reaction mixture consisted of TaqTM DNA polymerase (0.625 U), reaction buffer (1X), a dNTP mix (0.2 mM), the forward and reverse primers (250 nM each) and DNA (0.01-1 µg) in 25 µl. The following PCR cycling conditions were used: 94°C, 1 min (initial denaturation); 94°C, 30 sec; 46°C,

30 sec; 72°C, 1 min (35 cycles) and a final extension at 72°C, 5 min. For all PCR experiments a no template control was included in order to check for contamination and the PCR products were analyzed by gel electrophoresis (90 V).

2.7.2 Induction and expression

Protein expression of the pET28a clones (pMPTRRA, B, C, D) was induced as described in Section 2.6.13. Optimization of protein expression was conducted with samples being taken every 60 minutes for 6 hours and an OD₆₀₀ being measured. These samples were centrifuged (12,000 × g, 10 min, 4°C) and re-suspended in water to a final OD₆₀₀ of 10. An equal volume of 2 × sample buffer (125 mM Tris-HCl, 4% (m/v) SDS, 20% (v/v) glycerol, 10% (v/v) mercaptoethanol, 0.01% (m/v) bromophenol blue, pH 6.8) was added to 20 µl of the re-suspended samples and the samples were analyzed by SDS-PAGE (Section 2.3). The cells were then sonicated, centrifuged (15,000 × g, 20 min, 4°C) and thereafter the supernatant was subjected to the DTNB activity assay (Section 2.5.1) (Lim and Lim, 1995). The activity of each sample was calculated and this was used to determine the optimal expression time for purification.

2.8 Recombinant purification of Trx and thioredoxin reductase

2.8.1 Preparation of Trx and thioredoxin reductase crude extract for purification

To purify recombinant proteins, transformed *E. coli* (DE3) cells containing the appropriate plasmid were cultured in LB media (30 µg/ml of kanamycin) until an OD₆₀₀ (0.6-0.7) was reached. Protein expression was induced by adding IPTG (final concentration 0.5 mM) and thereafter the Trx cultures were incubated at 37°C in a shaking water bath for 6 hours whilst the thioredoxin reductase cultures were incubated for 1 hour. Cells were harvested by centrifugation (12,000 × g, 10 min, 4°C), resuspended in 10 volumes of extraction buffer (20 mM Tris-HCl (pH 7.5), 10 mM NaCl, 1 mM EDTA, 0.2 mM AEBSF and 5 mM DTT) and thereafter disrupted by sonication for 5 min. The samples were then centrifuged (12,000 × g, 30 min, 4°C) and the Trx containing supernatant was heat-treated (75°C, 30 min) followed by centrifugation (12,000 × g, 30 min, 4°C). The heat treatment step was omitted for thioredoxin reductase as this protein was not heat stable. The final supernatant of each protein was used as crude extract in Ni-NTA affinity purification.

2.8.2 Ni-NTA affinity purification

Ni-NTA agarose beads (2 ml) were packed into a column (2 ml bed volume, 0.8 x 4 cm), equilibrated with 5 volumes equilibration buffer (0.02 M imidazole, 0.5 M NaCl, 0.001 M mercaptoethanol, 0.02 M Tris-HCl (pH 8.0)) and thereafter incubated with the appropriate crude extract (4°C, 16 hours) in a Revolver™ 360° Sample Mixer. The unbound fraction was eluted by gravity and the resin was washed with 10 volumes of wash buffer (0.5 M NaCl, 0.02 M Tris-HCl (pH 8.0)). Two volumes of elution buffer (0.25 M imidazole, 0.5 M NaCl, 0.02 M Tris-HCl (pH 8.0)) was incubated with the resin (4°C, 30 min) and thereafter the bound protein was eluted. All fractions were analyzed by SDS-PAGE (Section 2.6.14) and the concentration of the purified proteins were determined using the extinction coefficients for thioredoxin and thioredoxin reductase ($10,095 \text{ M}^{-1} \text{ cm}^{-1}$ and $49,320 \text{ M}^{-1} \text{ cm}^{-1}$, respectively). The resin was then washed with 0.5 M NaOH for 30 min and stored in 30% (v/v) ethanol at 4°C. When the resin changed from light-blue to brownish grey, it was regenerated according to the manufacturer's instructions.

2.8.3 Concentration of protein samples

Dilute protein samples were concentrated prior to kinetic analysis by dialysis. Trx and thioredoxin reductase samples were placed in dialysis tubing with a cut-off of 3.5 kDa and 14 kDa, respectively and dialyzed against PEG 20,000.

2.9 Results

2.9.1 Developing a cheaper and faster Trx activity assay

The development of an inexpensive and rapid assay for Trx activity was necessary for the screening of crude fractions during the purification procedure. To develop this assay, various assay conditions were tested as shown below (Table 2.2), using the same source of crude extract.

Assays 1-3 showed no activity for Trx and changes in the reagent concentrations had no effect on the rates observed in these 3 assays (Table 2.2). An unexpected result observed was the lack of activity when using potassium phosphate buffer at pH 6.5 as this pH was expected to increase the sensitivity of the assay due to the lower solubility of reduced insulin at this pH

value (Arnér and Holmgren, 2000a). In fact, it was evident that the DTT-dependent reduction of insulin in the control reaction occurred at a faster rate (Section 2.4.1) and these assay conditions were not suitable for the purpose of this study.

Assay 4 involved a 20 min incubation of all the components of the assay prior to absorbance readings being taken and the reduction of insulin was observed (Sigma-Aldrich, 1994). It was unclear whether the rate obtained was due to a change in the pH of the potassium phosphate buffer (pH 6.5 to pH 7.0) (Table 2.2) or the extended incubation period prior to readings being taken. While a rate was observed, the longer assay posed a problem as this was time consuming for a preparative assay. To minimize the time needed to complete the assay, Trx was reduced by preincubation with DTT for 10 min at 25°C prior to the start of the reaction (Table 2.2, Assay 5) and the rate observed when using this assay was the highest of all the assays. Thus, the inclusion of a simple preincubation step, allowed for an assay that was relatively cheap and faster than published assays for Trx.

2.9.2 The development of the thioredoxin reductase assay

The reduction of DTNB, a generic disulfide substrate, was used to measure thioredoxin reductase activity by the change in absorbance at 412 nm. Various published methods were attempted to obtain a feasible assay (Table 2.3) and all the assays were performed in duplicate with the same crude extract source. It was evident that while both Assay 1 and 2 could be used to determine the activity of thioredoxin reductase based on the reduction of DTNB (Table 2.3), the inclusion of NaCl in the assay dramatically increased the rate of DTNB reduction and therefore Assay 3 was chosen as the activity assay for thioredoxin reductase.

Table 2.2 Comparison of the rates obtained by the modification of two Trx activity assays.

Assay	Reference ^a	Assay Reagents				Total time (min) ^b	Rate (OD ₆₅₀ /min) x 10 ⁻² ± SE (n=2) ^c	
		Buffer (pH 6.5) (mM)	Buffer (pH 7.0) (mM)	EDTA(mM)	Insulin(mM)			DTT(mM)
1	(Holmgren, 1979b)	100	-	2	0.13	0.33	20	0
2	(Arnér and Holmgren, 2000a)	100	-	2	0.13	1	20	0
3	(Holmgren, 1979b)	100	-	2	0.01	1	20	0
4	(Sigma-Aldrich, 1994)	-	63	2	0.01	1	22	1.01 ± 0.0024
5	This study	-	63	2	0.01	1	10	2.26 ± 0.0048

^a The assays used in this study were modified versions of the assays obtained from the references given.

^b Total time required before measurement could begin.

^c The same crude extract was used for all the assays tested. Assays were performed in duplicate.

Table 2.3 Comparison of the rates obtained by utilizing various thioredoxin reductase activity assays.

Assay	Reference ^a	Assay Reagents					Rate (OD ₄₁₂ /min) x 10 ⁻² ± SE (n=2) ^b
		Univalent cations: NaCl (mM)	Potassium phosphate buffer (pH 7.0) (mM)	Potassium phosphate buffer (pH 7.2) (mM)	DTNB (mM)	NADPH (mM)	
1	(Arnér and Holmgren, 2000a)	-	58	-	5	0.3	0.128 ± 0
2	(Štefanková <i>et al.</i> , 2006)	-	-	100	1	0.5	0.0622 ± 0
3	(Lim and Lim, 1995)	500	^c -	-	0.5	0.24	2.89 ± 0.006235

^a The assays used in this study were modified versions of the assays obtained from the references given.

^b The same crude extract was used for all the assays tested.

^c The buffer used in Assay 3 was Tris-HCl (pH 8.0).

2.9.3 The successful cloning and expression of *TRX1*

Genomic DNA was successfully isolated from *S. cerevisiae* using the Bust 'N Grab method (Figure 2.1 A) (Harju *et al.*, 2004) and PCR amplification of the *TRX1* gene was performed using this DNA as a template with *TRX1* specific primers (Figure 2.1 B). Upon completion of the PCR reaction, the amplicons were gel purified (Figure 2.1 C), ligated to the pTZ57R/T vector using the InsTAcloneTM PCR cloning kit and transformed into *E. coli* JM109 cells to yield three clones. Plasmid DNA from these clones, pTrxA, pTrxB and pTrxC, was isolated using a mini-prep procedure and linear, nicked and closed coiled circular plasmid forms were obtained (Figure 2.2 A). The identities of the clones were confirmed by performing a single restriction digestion with BamHI to linearize the plasmid DNA (Figure 2.2 B). The size of the bands obtained was 3162 bp which was close to the expected size of 3211 bp. To further confirm that the pTrxA-C clones contained the *TRX1* fragment, a PCR was performed using the plasmid DNA as a template. The amplicons (316 bp) obtained clearly showed that *TRX1* was present in the pTrxA-C vectors (Figure 2.2 C). Bands appearing higher up are due to the plasmid template in the reaction. A final confirmation was achieved by digesting the pTrxA-C vectors with HindIII and NdeI to liberate the *TRX1* fragment (Figure 2.2 D). Both Molecular weight marker XIV and Molecular weight marker III were loaded so as to size the *TRX1* fragments and the restricted vectors, respectively.

pET28a was isolated from *E. coli* BL21 (DE3) cells using the standard mini-prep procedure (Figure 2.3 A) and a double digestion with NdeI and HindIII was performed (Figure 2.3 B) so that the equivalently cut *TRX1* fragment could be ligated into the expression vector.

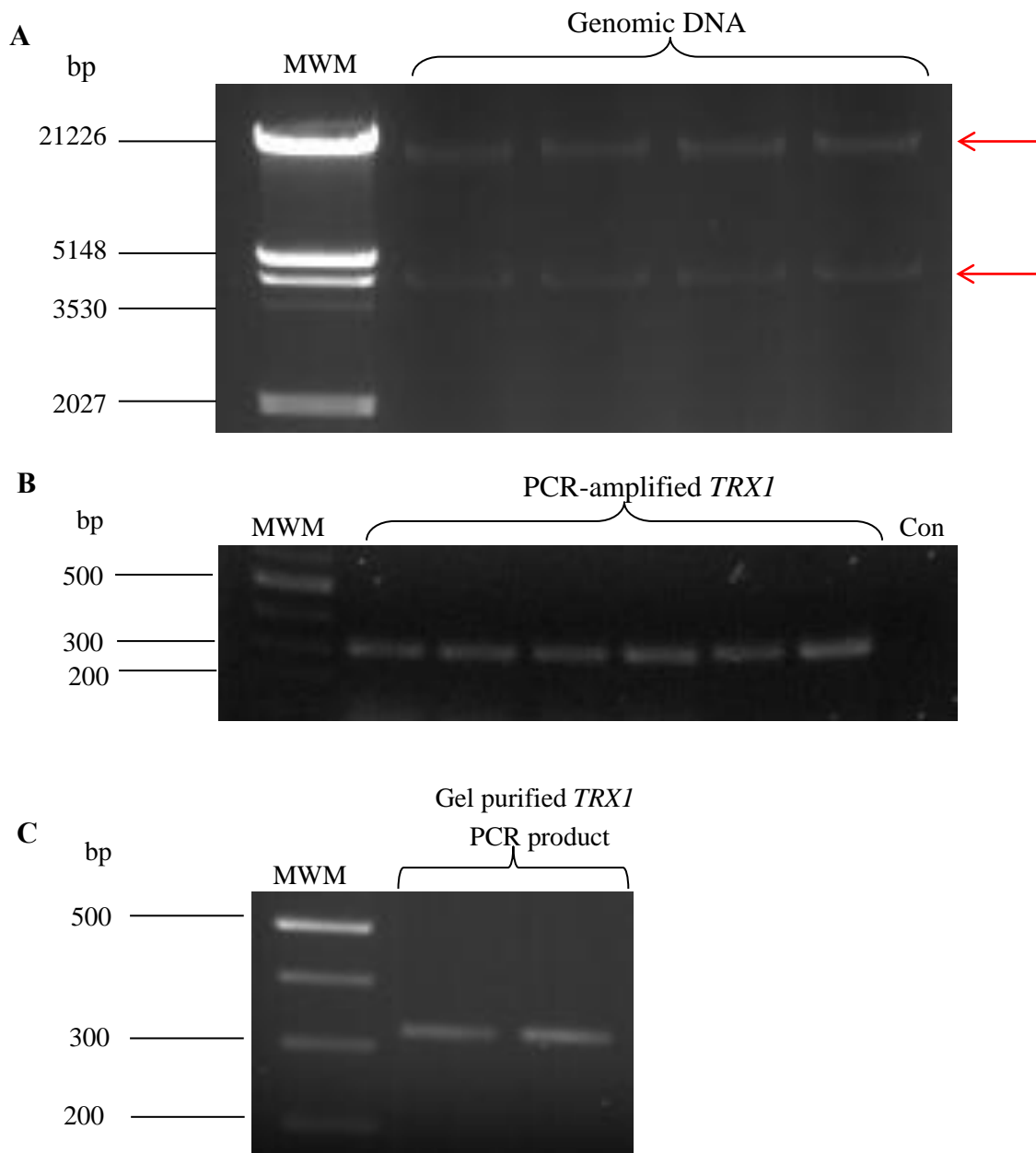


Figure 2.1 Genomic DNA isolation and PCR amplification of the *TRX1* gene. Genomic DNA was isolated from *S. cerevisiae* using the Bust ‘n Grab procedure (Harju *et al.*, 2004) (A). PCR of the DNA was undertaken using *TRX1*-specific primers (B). The PCR product was gel purified using the Fermentas gel purification kit (C). The gels have been cropped to fit the figures into this thesis but no other bands were observed in the non-MWM lanes.

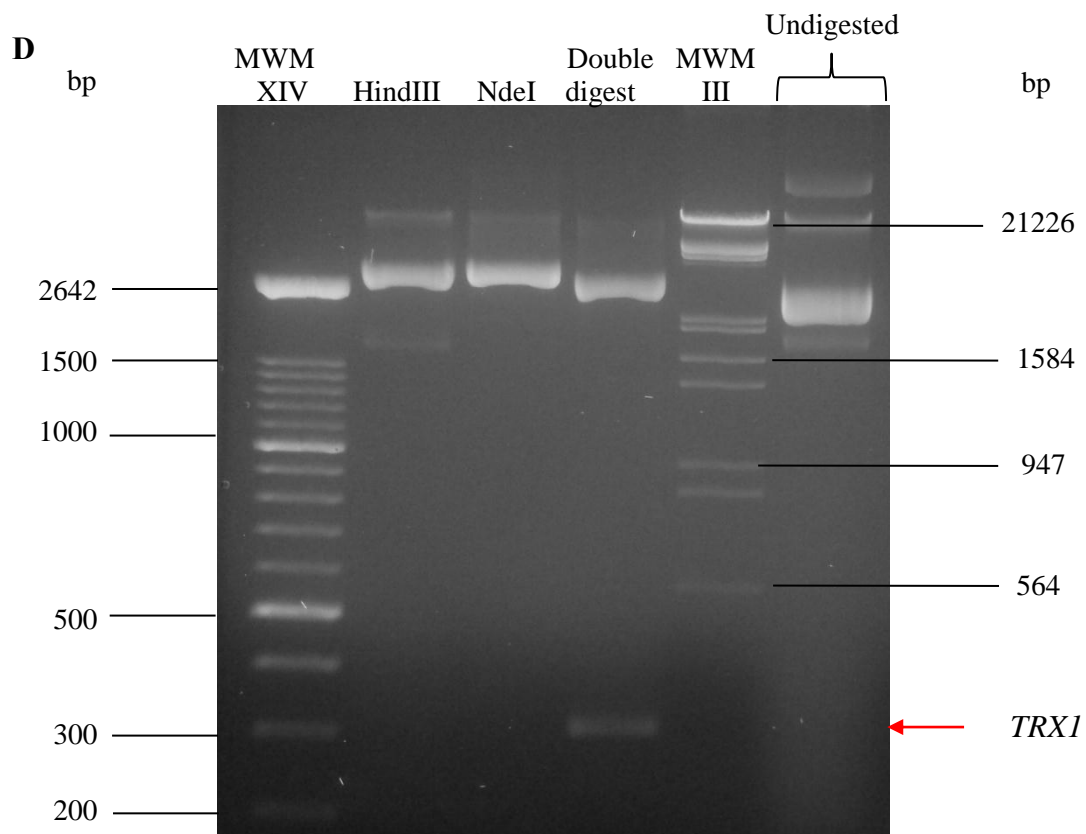
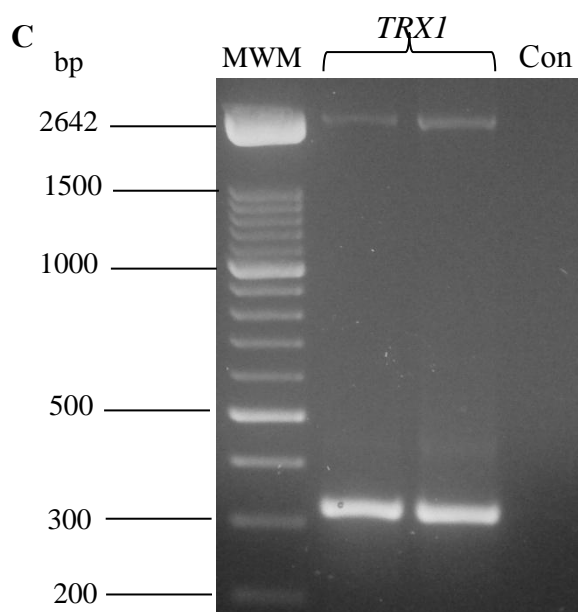
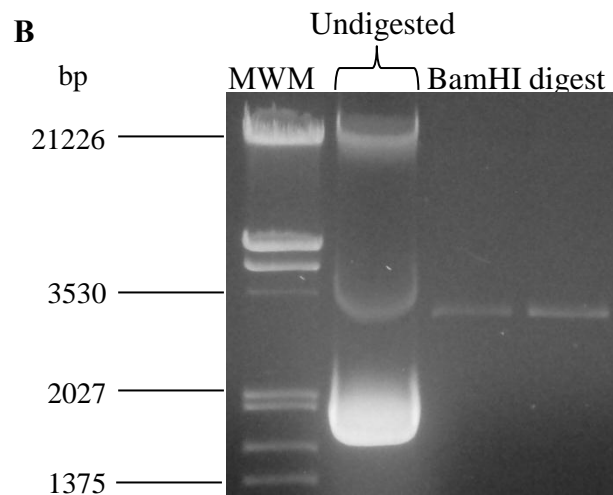
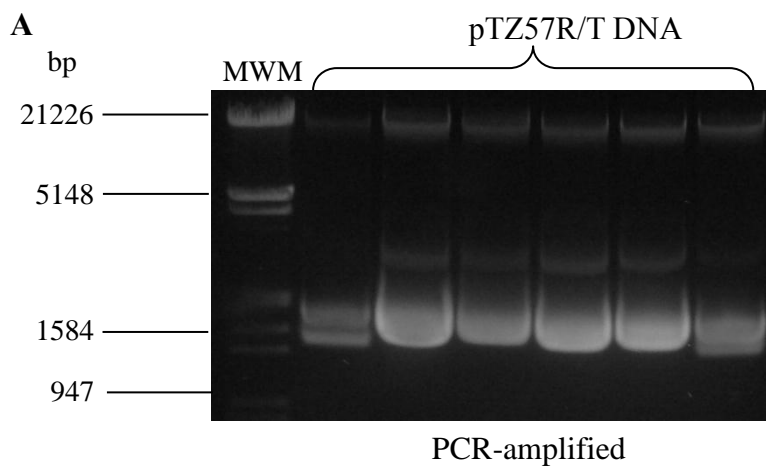


Figure 2.2 Confirming that the pTZ57R/T clones contained *TRX1*. pTZ57R/T DNA was isolated from *E. coli* JM109 cells using a standard mini-prep procedure and was restricted with BamHI to linearize the plasmid (B). In addition, PCR of the plasmid DNA was undertaken using *TRX1*-specific primers to confirm the presence of the insert (C). Restriction digestion of the cloning vector pTZ57R/T-*TRX1* showing the release of the *TRX1* fragment (D). Some gels have been cropped to fit the figures into this thesis but no other bands were observed in the non-MWM lanes.

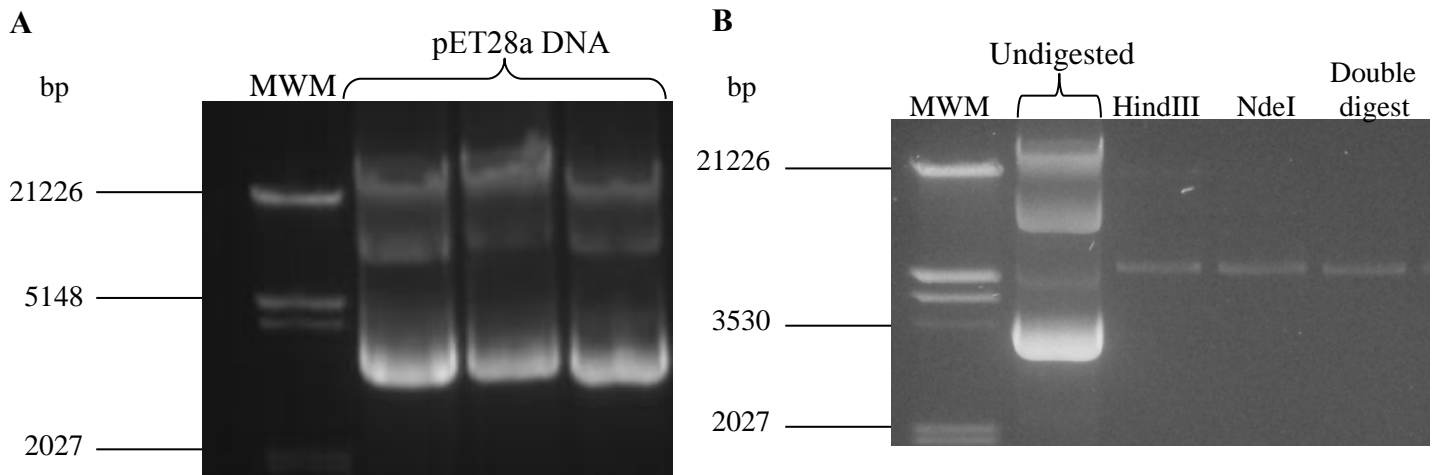


Figure 2.3 pET28a expression vector isolation and restriction endonuclease digestion. pET28a was isolated from *E. coli* BL21 (DE3) cells using a standard mini-prep procedure (A). Restriction digestion of the expression vector (B). The gels have been cropped to fit the figures into this thesis but no other bands were observed in the non-MWM lanes.

The restriction digested pET28a and the liberated *TRX1* fragment were both gel purified using a ThermoScientific Gel Extraction Kit. The gel-extracted *TRX1* fragment and restricted pET28a expression vector were subsequently ligated, transformed into *E. coli* BL21 (DE3) cells and a mini-prep was performed to isolate the plasmid DNA (Figure 2.4 A). A PCR was performed on the mini-prep to verify the success of the transformation (Figure 2.4 B). The band sizes of the mini-prep PCR (316 bp) indicated that *TRX1* was successfully cloned into the pET28a expression vector. A single restriction digest was performed on the pLPTrxA/B/C clones using HindIII and the resulting band size (5623 bp), which was very close to the expected band size (5,620 bp), indicated that the transformation was successful (Figure 2.4 C). To further confirm a successful transformation the pLPTrxA/B/C clones were double digested with HindIII and NdeI to liberate the *TRX1* fragment (Figure 2.4 D).

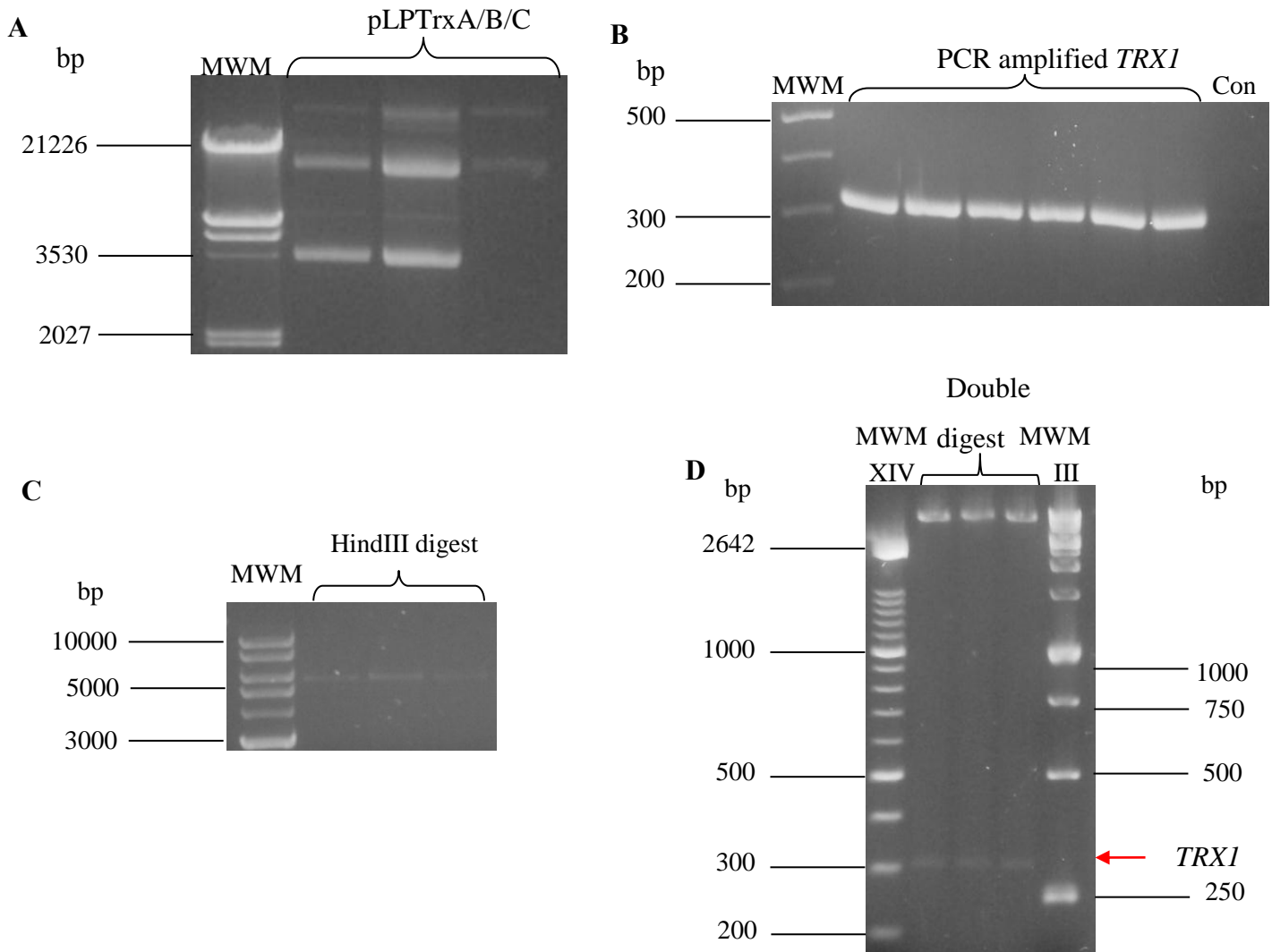


Figure 2.4 Transformation of *E. coli* BL21 (DE3) with pLPTrxA/B/C. pLPTrxA/B/C DNA was isolated from *E. coli* BL21 (DE3) cells using a standard mini-prep procedure (A). PCR performed on pLPTrxA/B/C clones to verify success of transformation (B). Single restriction digestion of pLPTrxA/B/C clones was undertaken with HindIII to size the clones (C) and double digestion with HindIII and NdeI was undertaken to release the *TRX1* gene (D). The gels have been cropped to fit the figures into this thesis but no other bands were observed in the non-MWM lanes.

The pLPTrxA/B/C clones were subsequently sequenced (Central Analytical Facilities, Stellenbosch University) in both directions and the sequencing traces were also manually evaluated. The sequences were aligned to the *TRX1* sequence from the SGD (<http://www.yeastgenome.org>) using ClustalW2 (<http://www.ebi.ac.uk/Tools/msa/clustalw2/>).

A

```

gi | 330443681_c232013-231702      ATGGTTACTCAATTCAAAACAGCCAGCAATTCGACTCTGCAATTGCTCA 50
F06_pET_28a_LPTrxA_T7_promoter    ATGGTTACTCAATTCAAAACAGCCAGCAATTCGACTCTGCAATTGCTCA 50
H10_pET_28a_LPTrxC_T7_promoter     ATGGTTACTCAATTCAAAACAGCCAGCAATTCGACTCTGCAATTGCTCA 50
G10_pET_28a_LPTrxB_T7_promoter      ATGGTTACTCAATTCAAAACAGCCAGCAATTCGACTCTGCAATTGCTCA 50
*****

gi | 330443681_c232013-231702      AGACAAGCTAGTTGTCGTAGATTCTACGCCACTTGGTGGTCCATGTA 100
F06_pET_28a_LPTrxA_T7_promoter     AGACAAGCTAGTTGTCGTAGATTCTACGCCACTTGGTGGTCCATGTA 100
H10_pET_28a_LPTrxC_T7_promoter      AGACAAGCTAGTTGTCGTAGATTCTACGCCACTTGGTGGTCCATGTA 100
G10_pET_28a_LPTrxB_T7_promoter      AGACAAGCTAGTTGTCGTAGATTCTACGCCACTTGGTGGTCCATGTA 100
*****

gi | 330443681_c232013-231702      AAATGATTGCTCCAAATGATTGAAAAATTCCTGAACAATACCCACAAGCT 150
F06_pET_28a_LPTrxA_T7_promoter     AAATGATTGCTCCAAATGATTGAAAAATTCCTGAACAATACCCACAAGCT 150
H10_pET_28a_LPTrxC_T7_promoter      AAATGATTGCTCCAAATGATTGAAAAATTCCTGAACAATACCCACAAGCT 150
G10_pET_28a_LPTrxB_T7_promoter      AAATGATTGCTCCAAATGATTGAAAAATTCCTGAACAATACCCACAAGCT 150
*****

gi | 330443681_c232013-231702      GATTTCTATAAATGGATGTCGATGAATGGGTGATGTTGCACAAAAGAA 200
F06_pET_28a_LPTrxA_T7_promoter     GATTTCTATAAATGGATGTCGATGAATGGGTGATGTTGCACAAAAGAA 200
H10_pET_28a_LPTrxC_T7_promoter      GATTTCTATAAATGGATGTCGATGAATGGGTGATGTTGCACAAAAGAA 200
G10_pET_28a_LPTrxB_T7_promoter      GATTTCTATAAATGGATGTCGATGAATGGGTGATGTTGCACAAAAGAA 200
*****

gi | 330443681_c232013-231702      TGAAGTTTCCGCTATGCCAATTTGCTTCATTCAAGAACGGTAAGGAAG 250
F06_pET_28a_LPTrxA_T7_promoter     TGAAGTTTCCGCTATGCCAATTTGCTTCATTCAAGAACGGTAAGGAAG 250
H10_pET_28a_LPTrxC_T7_promoter      TGAAGTTTCCGCTATGCCAATTTGCTTCATTCAAGAACGGTAAGGAAG 250
G10_pET_28a_LPTrxB_T7_promoter      TGAAGTTTCCGCTATGCCAATTTGCTTCATTCAAGAACGGTAAGGAAG 250
*****

gi | 330443681_c232013-231702      TTGCAAAGGTTGTTGGTGCCAACCCAGCGGCTATTAAGCAAGCCATTGCT 300
F06_pET_28a_LPTrxA_T7_promoter     TTGCAAAGGTTGTTGGTGCCAACCCAGCGGCTATTAAGCAAGCCATTGCT 300
H10_pET_28a_LPTrxC_T7_promoter      TTGCAAAGGTTGTTGGTGCCAACCCAGCGGCTATTAAGCAAGCCATTGCT 300
G10_pET_28a_LPTrxB_T7_promoter      TTGCAAAGGTTGTTGGTGCCAACCCAGCGGCTATTAAGCAAGCCATTGCT 300
*****

gi | 330443681_c232013-231702      GCTAATGCTTAA 312
F06_pET_28a_LPTrxA_T7_promoter     GCTAATGCTTAA 312
H10_pET_28a_LPTrxC_T7_promoter      GCTAATGCTTAA 312
G10_pET_28a_LPTrxB_T7_promoter      GCTAATGCTTAA 312
*****

B

gi | 330443681_231702-232013      TTAAGCATTAGCAGCAATGGCTTCTTAATAGCCGCTGGGTTGGCACCAA 50
G12_pET_28a_LPTrxC_T7_terminat    TTAAGCATTAGCAGCAATGGCTTCTTAATAGCCGCTGGGTTGGCACCAA 50
G11_pET_28a_LPTrxA_T7_terminat     TTAAGCATTAGCAGCAATGGCTTCTTAATAGCCGCTGGGTTGGCACCAA 50
H11_pET_28a_LPTrxB_T7_terminat     TTAAGCATTAGCAGCAATGGCTTCTTAATAGCCGCTGGGTTGGCACCAA 50
*****

gi | 330443681_231702-232013      CAACCTTTGCAACTTCCCTTACCCTTCTGAATAGAAGCAAAGTTGGCATA 100
G12_pET_28a_LPTrxC_T7_terminat    CAACCTTTGCAACTTCCCTTACCCTTCTGAATAGAAGCAAAGTTGGCATA 100
G11_pET_28a_LPTrxA_T7_terminat     CAACCTTTGCAACTTCCCTTACCCTTCTGAATAGAAGCAAAGTTGGCATA 100
H11_pET_28a_LPTrxB_T7_terminat     CAACCTTTGCAACTTCCCTTACCCTTCTGAATAGAAGCAAAGTTGGCATA 100
*****

gi | 330443681_231702-232013      GCGGAAACTTCATTCTTTTGTGCAACATCACCCAATTCATCGACATCCAA 150
G12_pET_28a_LPTrxC_T7_terminat    GCGGAAACTTCATTCTTTTGTGCAACATCACCCAATTCATCGACATCCAA 150
G11_pET_28a_LPTrxA_T7_terminat     GCGGAAACTTCATTCTTTTGTGCAACATCACCCAATTCATCGACATCCAA 150
H11_pET_28a_LPTrxB_T7_terminat     GCGGAAACTTCATTCTTTTGTGCAACATCACCCAATTCATCGACATCCAA 150
*****

gi | 330443681_231702-232013      TTTATAGAATCAGCTTGGGTATTGTTTCAGAGAATTTTCAATCATTG 200
G12_pET_28a_LPTrxC_T7_terminat    TTTATAGAATCAGCTTGGGTATTGTTTCAGAGAATTTTCAATCATTG 200
G11_pET_28a_LPTrxA_T7_terminat     TTTATAGAATCAGCTTGGGTATTGTTTCAGAGAATTTTCAATCATTG 200
H11_pET_28a_LPTrxB_T7_terminat     TTTATAGAATCAGCTTGGGTATTGTTTCAGAGAATTTTCAATCATTG 200
*****

gi | 330443681_231702-232013      GAGCAATCATTTTACATGGACCGCACCAAGTGGCGTAGAAATCTACGACA 250
G12_pET_28a_LPTrxC_T7_terminat    GAGCAATCATTTTACATGGACCGCACCAAGTGGCGTAGAAATCTACGACA 250
G11_pET_28a_LPTrxA_T7_terminat     GAGCAATCATTTTACATGGACCGCACCAAGTGGCGTAGAAATCTACGACA 250
H11_pET_28a_LPTrxB_T7_terminat     GAGCAATCATTTTACATGGACCGCACCAAGTGGCGTAGAAATCTACGACA 250
*****

gi | 330443681_231702-232013      ACTAGCTTGTCTTGAGCAATTCAGAGTCAATTCGCTGGCAGTTTTGAA 300
G12_pET_28a_LPTrxC_T7_terminat    ACTAGCTTGTCTTGAGCAATTCAGAGTCAATTCGCTGGCAGTTTTGAA 300
G11_pET_28a_LPTrxA_T7_terminat     ACTAGCTTGTCTTGAGCAATTCAGAGTCAATTCGCTGGCAGTTTTGAA 300
H11_pET_28a_LPTrxB_T7_terminat     ACTAGCTTGTCTTGAGCAATTCAGAGTCAATTCGCTGGCAGTTTTGAA 300
*****

gi | 330443681_231702-232013      TTGAGTAACCAT 312
G12_pET_28a_LPTrxC_T7_terminat    TTGAGTAACCAT 312
G11_pET_28a_LPTrxA_T7_terminat     TTGAGTAACCAT 312
H11_pET_28a_LPTrxB_T7_terminat     TTGAGTAACCAT 312
*****

```

Figure 2.5 Alignment of the pLPTrxA/B/C (A) promoter sequences and (B) terminator sequences with the *TRX1* sequence and reverse complement of the *TRX1* sequence from *S. cerevisiae* (NCBI Reference Sequence: NC_001144.5), respectively. Identical residues are denoted with an asterisk. The overall percentage identity between each promoter and reference sequence as well as each terminator and reference sequence was 100 %.

Sequence analysis revealed that the *TRX1* gene was a successfully cloned (Figure 2.5) and these clones could be used for expression. To determine whether Trx could be successfully expressed by the pLPTrxA/B/C clones as well as to determine the optimal induction time for harvesting Trx, the clones were induced for a number of time points (2-19 hours) and analyzed by SDS-PAGE (Figure 2.6 A) and activity assays (Figure 2.6 B) at each time point was performed. The protein was successfully expressed as the calculated band size was 12 kDa for Trx. Optimum expression (Figure 2.6 A) and maximum specific activity (Figure 2.6 B) was observed after inducing the cells for 6 hours and this time point was therefore used in the purification of Trx.

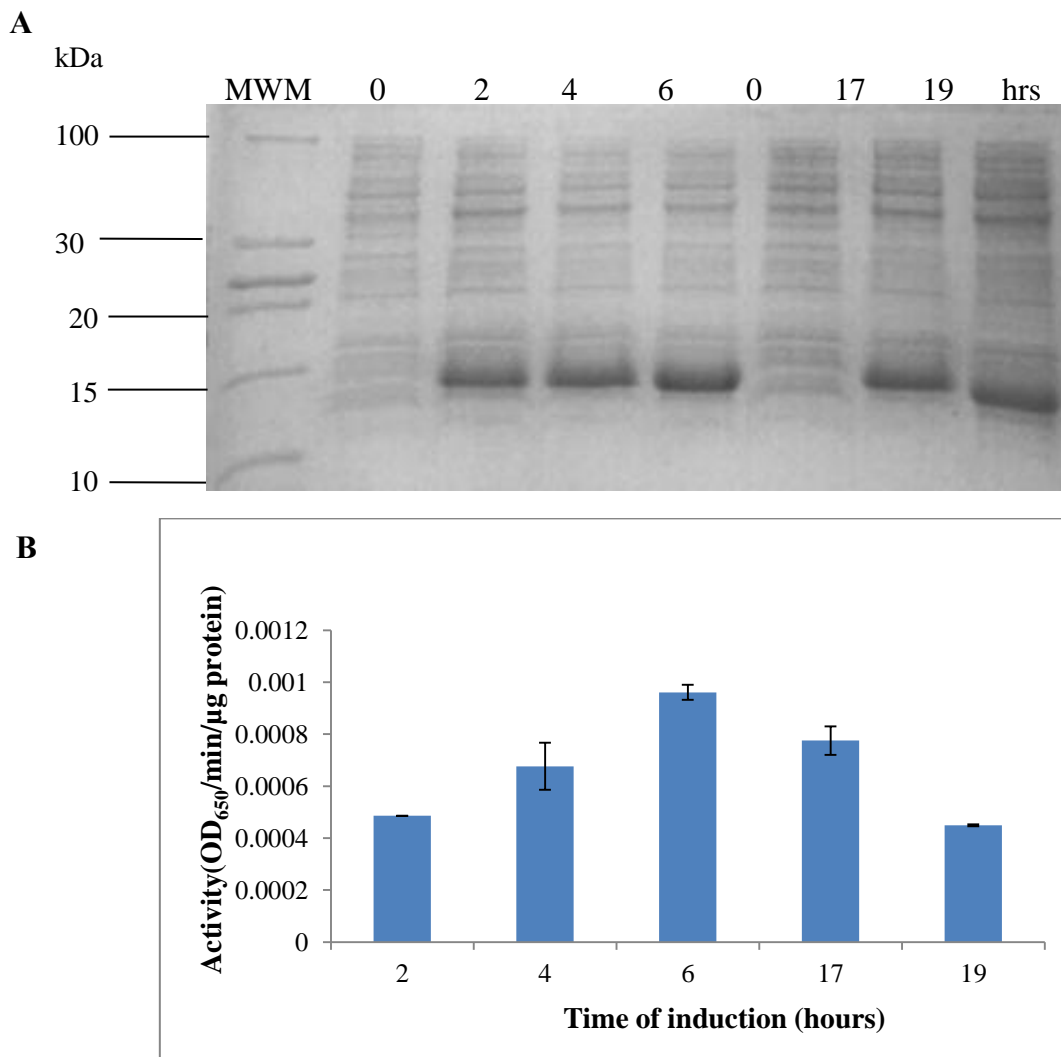


Figure 2.6 Expression and specific activity of *TRX1* at various time points (2-19 hours). Recombinant *TRX1* expression was induced with 0.5 mM IPTG for 0-19 hours and analyzed by SDS-PAGE (A). The specific activity of induced fractions (B) was also determined. Duplicate biological samples were assayed at a given time point and the standard error is indicated.

2.9.4 The purification of recombinant thioredoxin reductase and Trx by affinity chromatography

The pMPTRRA/B/C/D clones were obtained from Miss M.M Photolo (Genetics, UKZN) and were evaluated by colony PCR to ensure that the *TRRI* gene was present. Upon confirmation (data not shown), these clones were IPTG-induced at different time intervals in order to confirm that this protein could be expressed by these clones. The protein was expressed successfully with an induced band at a calculated size of 36 kDa which was very close to the expected size of 35 kDa (Figure 2.7 A). Once successful induction was observed, it was necessary to determine the optimal induction time for harvesting thioredoxin reductase. Cultures were IPTG-induced for a number of time points (1-6 hours) (Figure 2.7 A) and assayed for activity (Figure 2.7 B). Over the time points tested, optimum expression (Figure 2.7 A) and maximum specific activity (Figure 2.7 B) were observed after inducing the cells for 1 hour and this time point was used for the purification of thioredoxin reductase. The gel has been cropped to fit the figure into this thesis but no other bands were observed in the non-MWM lanes.

To purify the recombinant proteins, transformed *E. coli* (DE3) cells containing the appropriate plasmid were cultured and induced with IPTG for the appropriate time. These fractions were then treated as described above (Section 2.8.1) and used as crude extract for nickel affinity purification. The presence of single bands in the latter lanes indicated a successful purification of Trx and thioredoxin reductase with sizes of 12 kDa and 35 kDa respectively (Figure 2.8).

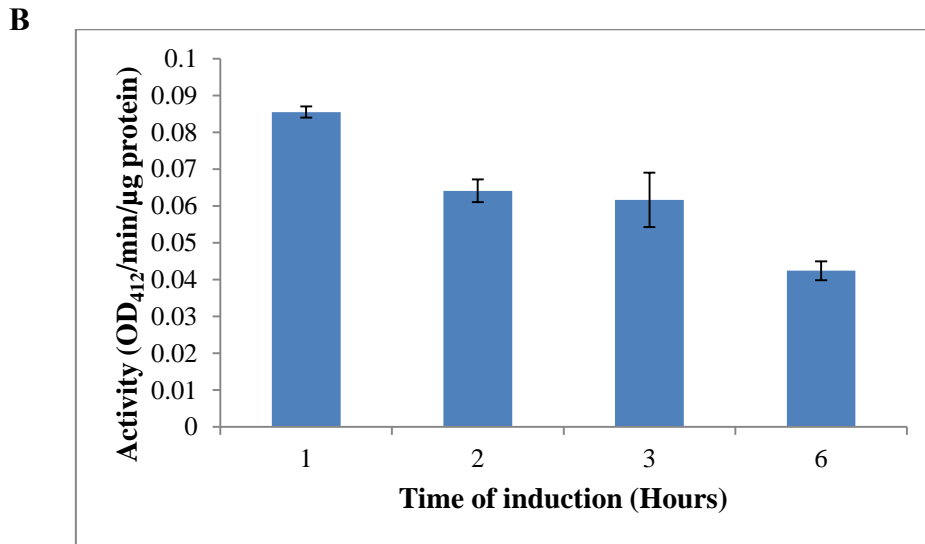
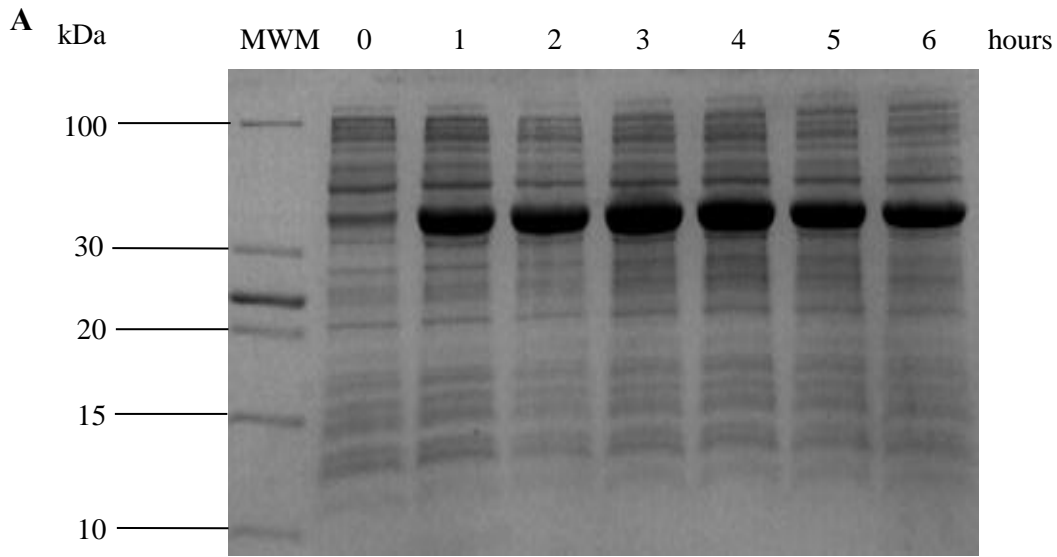


Figure 2.7 Induction of *TRR1*. Recombinant *TRR1* expression was induced with 0.5 mM isopropyl β -D-1-thiogalactopyranoside (IPTG) for various time intervals (0-6 hours) and analyzed by SDS-PAGE (A) and the DTNB reduction assay (B). Duplicate biological samples were assayed at each time point and the standard error is indicated.

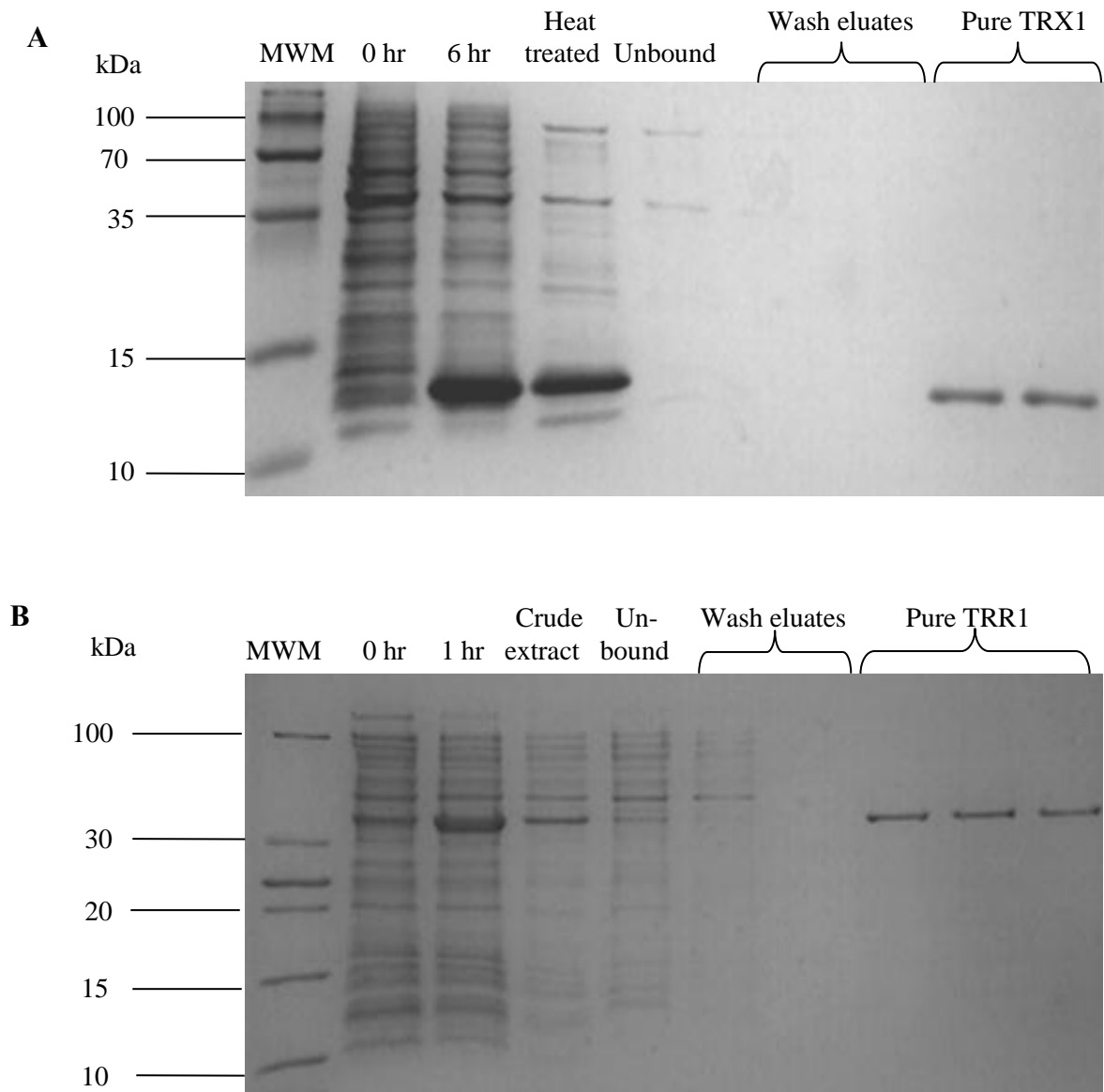


Figure 2.8 Ni-NTA affinity purification of recombinant TRX1 (A) and TRR1 (B). *TRX1* expression was induced for 6 hours and the cells processed as described in Section 2.8.1 to yield pure TRX1 (A). *TRR1* was induced for 1 hour and the cells processed as described in Section 2.8.1 to yield pure TRR1 (B). The gels were stained with Coomassie blue.

2.10 Discussion

To purify Trx and thioredoxin reductase, a number of hurdles had to be overcome. Firstly, a major problem with assaying coupled systems is that at least one of the components must be readily available. Both Trx and thioredoxin reductase are extremely expensive and therefore purchasing these proteins was not an option. For this reason, it was necessary to develop assays for each protein that did not require its counterpart.

The standard insulin assay (Arnér and Holmgren, 2000a) for determining the activity of thioredoxin is both time-consuming and costly which makes it impractical for protein isolations. We developed an assay based on the DTT-dependent reduction of insulin by Trx (Holmgren, 1979b) and found that DTT could indeed be used instead of thioredoxin reductase which provided a considerable saving. Further, the inclusion of a preincubation step with DTT increased the rate of reduction and the assay could be completed in a shorter time interval (10 min) (Table 2.2). This assay was used for the subsequent purification steps.

Thioredoxin, the natural substrate of thioredoxin reductase is also very expensive and difficult to obtain so the activity of thioredoxin reductase is usually assayed using 5,5'-dithiobis-2-nitrobenzoic acid (DTNB). For this study, assays described by Arner and Holmgren (2000a) as well as Štefanková *et al.* (2006) were attempted. These assays enabled the detection of thioredoxin reductase present in crude extracts in the absence of Trx, thereby greatly reducing the cost associated with the native assay. However, the rates obtained through both methods were not satisfactory (Table 2.3) and could have been caused by the NADPH-dependent inactivation of thioredoxin reductase (Štefanková *et al.*, 2006). However, by including univalent cations (Lim and Lim, 1995), the sensitivity of the assay was significantly increased compared to the assays that lacked these cations (Table 2.3).

Once activity assays for both Trx and thioredoxin reductase were developed, the next step involved the recombinant expression and purification of both proteins. Genomic DNA from *S. cerevisiae* was isolated and the *TRX1* gene was amplified and cloned into the pTZ57R/T cloning vector and then subcloned into the pET28a expression vector. The successful induction of Trx expression (Figure 2.6) and the 100% similarity observed with the sequence data alignments (Figure 2.5) showed that *TRX1* was successfully cloned and expressed.

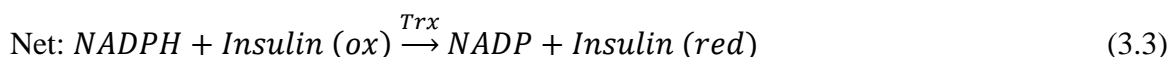
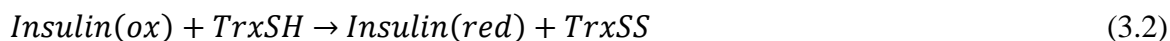
To obtain thioredoxin reductase, clones were tested and found to contain the *TRR1* gene. Thioredoxin reductase expression was induced (Figure 2.7) and both thioredoxin and thioredoxin reductase were successfully purified by nickel affinity chromatography (Figure 2.8). The purified thioredoxin system was then concentrated as described in Section 2.8.3 and was thereafter available for kinetic analysis experiments.

Chapter 3: The thioredoxin system and not the Michaelis-Menten equation should be fitted to substrate saturation datasets from the thioredoxin insulin assay¹

3.1 Introduction

Several substrates such as 5,5'-dithiobis (2-nitrobenzoic acid) (DTNB) (Akif *et al.*, 2008, Mark and Richardson, 1976) and fluorescently labelled proteins (Heuck and Wolosiuk, 1997b) have been used to measure thioredoxin activity but insulin with a single intrachain and two interchain disulfide bonds (Li *et al.*, 2012) still remains the most popular substrate for characterizing thioredoxin activity *in vitro* (Holmgren, 1979a). This assay involves either turbidimetrically monitoring the aggregation of the free B-chain resulting from the reduction of insulin by thioredoxin (Holmgren, 1979b) or by coupling the reaction to NADPH oxidation (Scheme I) (Holmgren, 1979a).

Scheme I: Thioredoxin enzyme model



where *TrxSS* and *TrxSH* represent reduced and oxidized thioredoxin respectively and *TR* represents thioredoxin reductase.

Increases in the insulin concentration result in a classical substrate saturation profile and Michaelis-Menten parameters have consequently been assigned to thioredoxin (Holmgren, 1979a, Obiero *et al.*, 2010, Maeda *et al.*, 2010, Bao *et al.*, 2009, Chen *et al.*, 2014, Juttner *et al.*, 2000). Despite mammalian insulin not being the physiological substrate for all the thioredoxins characterized with this assay, it is readily reduced by most thioredoxins. This common substrate therefore allows for semi-quantitative kinetic comparisons between different thioredoxins. However, in many of these studies it was not always clear whether

¹Padayachee, L. & Pillay, C. S. 2016. The thioredoxin system and not the Michaelis–Menten equation should be fitted to substrate saturation datasets from the thioredoxin insulin assay. *Redox Report*, 21, 170-179.

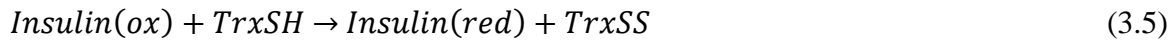
thioredoxin reduction or thioredoxin oxidation was the rate-limiting step in the assay (Scheme I). The activities of other redoxins (glutaredoxins and peroxiredoxins) have also been described using Michaelis–Menten kinetic parameters (see for example (Akerman and Müller, 2003, Akerman and Müller, 2005, Peltoniemi *et al.*, 2006)).

There have been a number of conflicting reports on the interpretation of the plots generated in these experiments (Mashamaite *et al.*, 2015). For example, unlike most enzymes, thioredoxin is inactivated by its substrate and requires thioredoxin reductase to regenerate it. Further, in the original description of the thioredoxin insulin assay, it appeared that varying concentrations of thioredoxin reductase in the assay led to changes in the observed turnover number for thioredoxin activity (Holmgren, 1979a). Moreover, in other studies, oxidized and reduced thioredoxins have been detected *in vivo* (Trotter and Grant, 2003, Watson *et al.*, 2004), suggesting that the thioredoxin redox couple's activity should be characterized by redox potentials and not enzyme kinetic parameters. For computational systems biology studies, in particular, these discrepancies posed a serious limitation as it was not clear whether thioredoxin should appear in the stoichiometric matrix or rate vector of the equation describing the kinetic model of the system (Pillay *et al.*, 2013).

Using a computational model, it was suggested that these disparate observations could be reconciled by proposing that the saturation observed in the insulin assay was due to a limitation in the thioredoxin redox cycle (Pillay *et al.*, 2009). As the insulin concentration was increased, thioredoxin oxidation increased and the activity of the thioredoxin reduction reaction correspondingly increased until it was limited by the availability of oxidized thioredoxin or by saturation of the thioredoxin reductase, or both. This in turn limited the reduced thioredoxin available for insulin reduction and the flux through the system saturated (Pillay *et al.*, 2009). It was further proposed that mass-action kinetics appeared to be sufficient to describe insulin reduction by thioredoxin. Substrate reduction by thioredoxin proceeds via the formation of a mixed-disulfide complex between the redoxin and its substrate (Wynn *et al.*, 1995). Once formed, the breakdown of these redoxin–substrate complexes is highly favorable and therefore the intermediate steps involving the mixed-disulfide complex were not explicitly modeled but were instead combined into a single second-order rate constant (Pillay *et al.*, 2009). The validity of this simplification was tested by fitting a computational model of the *E. coli* thioredoxin system to a published *in vitro* dataset (Holmgren, 1979a). Collectively, these findings suggested that the kinetic parameters

for thioredoxin should be obtained by fitting a kinetic model of the entire thioredoxin system (Scheme II) to a given substrate saturation dataset and that mass-action kinetics could adequately describe insulin reduction.

Scheme II: Thioredoxin redox couple model



A number of systems biology studies have since used this approach to describe thioredoxin activity in large-scale kinetic models (Pillay *et al.*, 2011, Adimora *et al.*, 2010, Benfeitas *et al.*, 2014). However, Lin (2010) found a discrepancy between the model output and the insulin reduction profile obtained when using a minimal model (Pillay *et al.*, 2009) of the yeast thioredoxin system (equation 3.6):

$$v = \frac{(k_1 \cdot NADPH \cdot Trx_{tot}) Insulin}{\frac{k_1}{k_2} NADPH + Insulin} \quad (3.6)$$

In this minimal description of the entire thioredoxin system (Scheme II), the thioredoxin reductase reaction was described by mass-action kinetics with a second-order rate constant (k_1), Trx_{tot} refers to the total thioredoxin concentration and insulin reduction was also described by a second-order rate constant (k_2). Note that equation (3.6) has the same form as the Michaelis-Menten equation with a V_{max} described by $k_1 \cdot NADPH \cdot trx_{tot}$, an apparent k_{cat} described by $k_1 \cdot NADPH$ and an apparent K_m described by $k_1 \cdot NADPH / k_2$; therefore the ratio k_{cat} / K_m is equal to k_2 , the true rate constant for insulin reduction (Pillay *et al.*, 2009).

As thioredoxin reductase is fully saturated by NADPH in the insulin assay, the flux through the system is effectively zero-order with respect to the NADPH concentration and therefore equation (3.6) has limited value for fitting datasets under these conditions. Lin (2010) nonetheless proposed that thioredoxin was indeed an enzyme whose activity could presumably be described with Michaelis-Menten parameters. Thus, it is not clear whether substrate saturation datasets from the thioredoxin insulin assay should be fitted with the Michaelis-Menten equation or whether they should be fitted with the entire thioredoxin system (Scheme II). Therefore computational modeling and *in vitro* kinetic assays of the

thioredoxin insulin system were employed to determine which of these approaches should be used to characterize thioredoxin activity.

3.2 Materials

Trichloroacetic acid (TCA) and methoxypolyethylene glycol maleimide (PEG-maleimide M_n 5,000) were obtained from Sigma (Capital Labs, Johannesburg, South Africa) and all other common chemicals were from Saarchem/Merck (Johannesburg, South Africa) and were of the highest purity available.

3.3 Methods

3.3.1 Kinetic modeling

Kinetic modeling experiments were carried out using the open source Python Simulator for Cellular Systems (PySCeS) modeling software (Olivier *et al.*, 2005) (<http://pysces.sourceforge.net>) as described previously (Pillay *et al.*, 2011). Detailed models were created to analyze the *E. coli* and *S. cerevisiae* thioredoxin systems and were parameterized with realistic parameter sets (Table 3.1) which were obtained from either primary literature sources, the BRENDA kinetic parameter database (Chang *et al.*, 2009) (<http://www.brenda-enzymes.info>), or from the *in vitro* kinetic assays performed. In these models, thioredoxin reductase was modeled with a two-substrate Michaelis-Menten kinetic expression and insulin reduction was modeled with mass-action kinetics as described previously (Pillay *et al.*, 2009). Kinetic models of the entire thioredoxin system or the Michaelis-Menten equation were fitted to *in vitro* datasets using non-linear least squares regression with the Levenberg–Marquardt algorithm (Pillay *et al.*, 2009). The PySCeS versions of the kinetic models are available in the appendix section.

Table 3.1 Kinetic parameters and species concentrations used for building computational models of the *E. coli* and baker's yeast thioredoxin systems.

Species	<i>E. coli</i>	<i>S. cerevisiae</i>	Reference
	(μM)	(μM)	
NADPH	400	400	Holmgren (1979a), this study
NADP	1.0	1.0	Holmgren (1979a), this study
TrxSS	0.05	0.75	Holmgren (1979a), this study
TrxSH	0.05	0.75	Holmgren (1979a), this study
Insulin (oxidized)	30	20	Holmgren (1979a), this study
Insulin (reduced)	1.0	1.0	
Kinetic Parameters	Thioredoxin Reductase	Thioredoxin Reductase	
[TR]	0.1 μM	0.05 - 0.25 μM	Holmgren (1979a), this study
k_{cat}	22.8 s^{-1}	66.6 s^{-1}	Gleason <i>et al.</i> , (1990), Chang <i>et al.</i> , (2009)
K_{nadph}	1.2 μM	1.2 μM	Williams (1976)
K_{trxss}	2.8 μM	4.4 μM	Williams (1976), Speranza <i>et al.</i> , (1973)
Insulin reduction			
k_2	0.064 $\mu\text{M} \cdot \text{s}^{-1}$	0.003 $\mu\text{M} \cdot \text{s}^{-1}$	Pillay <i>et al.</i> , (2009), this study

3.3.2 Thioredoxin insulin reduction assay

A number of variations of coupled redoxin assays have been presented in the literature. In some assays, NADPH oxidation was monitored by a decrease in absorbance at 340 nm starting at a positive value (Baker *et al.*, 2001, Si *et al.*, 2014), typically 0.9 for an NADPH concentration of 150 μM (Nelson and Parsonage, 2011), while in other assays, a decrease in absorbance from the blank was monitored (Arnér and Holmgren, 2000a). To compare these methods, insulin reduction was undertaken at 25°C in a final volume of 1 ml in a 100 mM potassium phosphate (pH 7.0) buffer containing EDTA (2 mM), NADPH (0.15 or 0.4 mM), insulin (20-160 μM), thioredoxin (1.5 μM) and thioredoxin reductase (0.05 μM). NADPH oxidation was monitored at 340 nm in a UV-1800 Shimadzu Spectrophotometer and depending on the assay being tested, a sample without the addition of either NADPH or thioredoxin reductase was used as the reference cuvette. To determine the effect of

thioredoxin reductase on the rate of insulin reduction, the assay was undertaken as described above with NADPH (0.4 mM), insulin (20-200 μM) and varying thioredoxin reductase concentrations (0.05-0.25 μM). Insulin reduction activity was defined as the concentration of NADPH oxidized per min using a molar extinction coefficient (Arnér and Holmgren, 2000a) of $6,200 \text{ M}^{-1}\text{cm}^{-1}$. Absorbance measurements were taken for at least five minutes, although initial studies showed that the system remained in steady state well beyond this assay period during which no significant insulin precipitation occurred. All assays were undertaken in triplicate and the data obtained were plotted as a mean \pm standard error.

3.3.3 Determination of the redox state of Trx

The redox state of thioredoxin was determined using the method described by Hugo *et al.* (2014). The steady state insulin reduction assay components were added directly into 100% (w/v) ice-cold TCA (100 μl) and incubated on ice for 30 min. The TCA-treated samples were then transferred to an Amicon® Ultra 2 ml centrifugal filter (10,000 NMWL) and centrifuged (7,500 $\times g$, 20 min, 4°C) to remove the insulin. As a control to ensure that no protein was lost during centrifugation, the eluate was assayed for thioredoxin and thioredoxin reductase activity and was also tested by SDS-PAGE. The remaining concentrate was transferred and centrifuged (22,065 $\times g$, 40 min, 4°C). The resulting pellet was washed with ice-cold acetone (100 μl), dried at 37°C and resuspended in 50 μl of alkylation buffer (3 mM PEG-maleimide, 50 mM Tris (pH 7.5), 10 mM EDTA (pH 8.0), 0.1% (m/v) SDS). After a 45 min incubation period at 45°C, the alkylated samples were mixed with an equal volume of $2 \times$ non-reducing sample buffer (125 mM Tris-HCl, 4% (m/v) SDS, 20% (v/v) glycerol, 0.01% (m/v) bromophenol blue, pH 6.8), and then separated by electrophoresis on a 15% acrylamide Tris-Tricine gel, which was subsequently stained with Coomassie blue. All assays were undertaken in triplicate and representative gel images are shown below. As migration controls, reduced thioredoxin was obtained by incubating thioredoxin (1.5 μM) with DTT (1 mM) at 37°C for 1 hour, while purified thioredoxin served as the oxidized control. The control samples were processed for electrophoresis as described above, and as expected, the reduced form of thioredoxin migrated higher on these gels. The intensity ratio of the bands was determined with ImageJ (<http://imagej.nih.gov/ij/>) using the reduced control as the standard.

3.4 Results

3.4.1 Computational models with thioredoxin described either as an enzyme, or as a redox couple, have contrasting kinetic properties.

To determine whether it really mattered if thioredoxin activity was described with Michaelis-Menten parameters or with mass-action kinetics, two distinct kinetic models in which thioredoxin acts as an enzyme (equation 3.3, Scheme I) or as a redox couple (Scheme II) were both fitted to a previously published *in vitro* insulin reduction dataset (Holmgren, 1979a). As mammalian insulin contains three disulfide bonds and reduction was followed by NADPH oxidation, it was also important to determine whether it made a difference to the fitting results if the insulin or the disulfide bond concentration was considered as the ‘substrate’ in these experiments. In addition, the computational models were used to highlight the key differences between the thioredoxin enzyme and redox couple fitting approaches.

Both the Michaelis-Menten equation and the redox couple model showed excellent fits ($r^2 \geq 0.996$) to the insulin saturation profile (Figure 3.1 A), suggesting that both models were apparently consistent with the dataset (Table 3.2). As the redox couple model predicted that substrate saturation was due to a limitation in thioredoxin reductase activity, the effect of increasing the thioredoxin reductase concentration on the rates within the system was also tested. Increasing the thioredoxin reductase concentration increased the insulin reduction rate in the thioredoxin redox couple model (Figure 3.1 A), confirming that its activity was limiting in this system. Note that in the kinetic model, thioredoxin reductase was described with Michaelis-Menten kinetics, which would not be accurate at thioredoxin and thioredoxin reductase concentrations of 1.5 and 0.1 μM respectively, as the thioredoxin concentration was only fifteen-fold larger than the thioredoxin reductase concentration. Nonetheless, the fitted second-order rate constant obtained over a range of thioredoxin reductase concentrations showed very little variation (Table 3.2), suggesting that this method is robust in obtaining kinetic parameters.

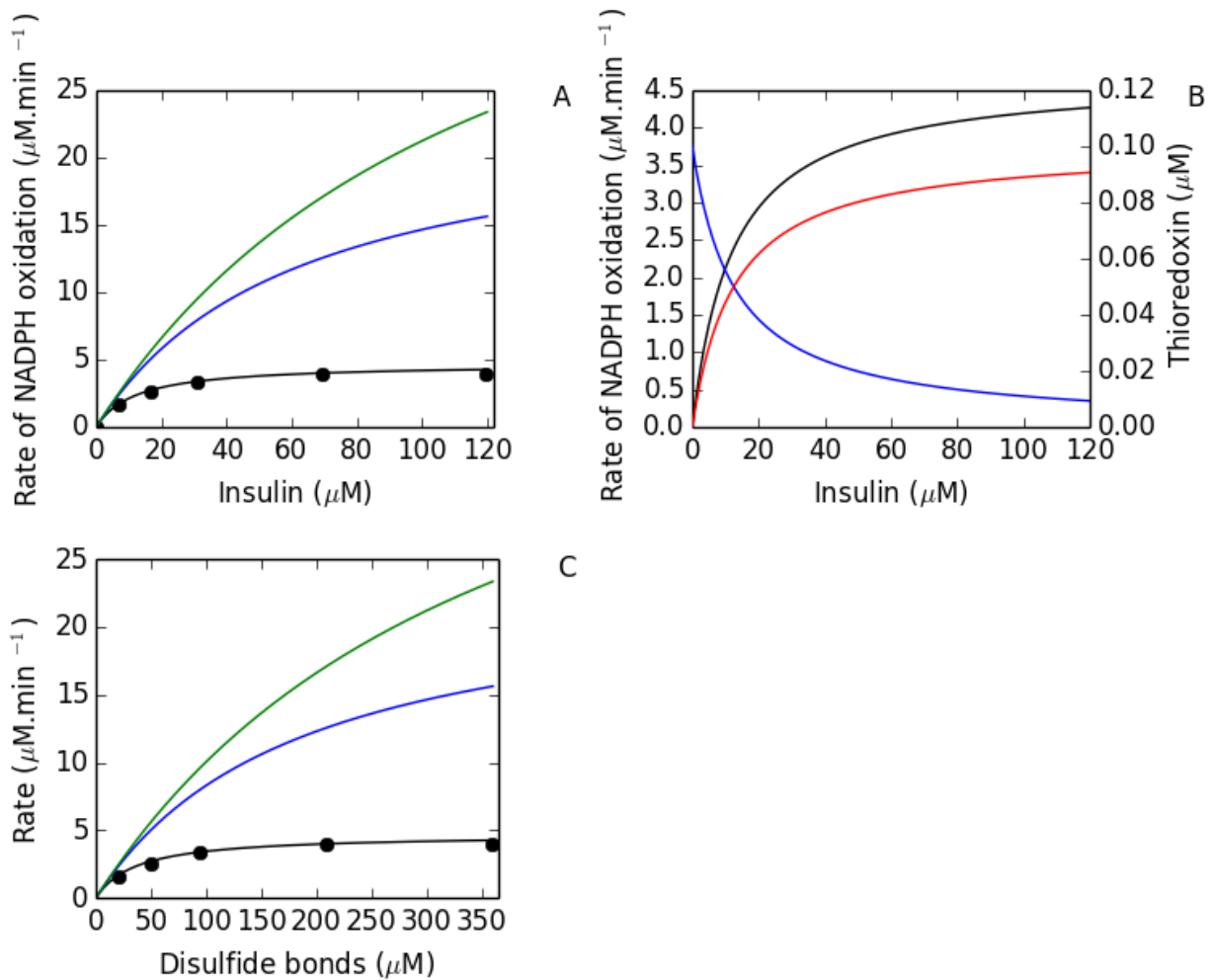


Figure 3.1 The Michaelis-Menten equation and the thioresoxin redox couple model both fit an *in vitro* insulin reduction dataset (Holmgren, 1979a) but the resulting kinetic models show distinct responses to thioresoxin reductase concentration and substrate saturation. In (A) the Michaelis-Menten equation and the thioresoxin redox couple kinetic model (black line) both showed excellent fits ($r^2 \geq 0.996$) to an insulin substrate saturation dataset (\bullet). Increasing the thioresoxin reductase concentration (0.05 μM) in the thioresoxin redox couple model to 0.15 (blue) or 0.25 μM (green) increased the flux within the system at a given insulin concentration. Substrate saturation (black) within a fitted thioresoxin redox couple model (0.05 μM thioresoxin reductase) was accompanied by the redistribution of thioresoxin from its reduced (blue) to oxidized (red) form (B). In (C) disulfide bond rather than insulin concentration was used to determine the kinetic parameters for thioresoxin-dependent insulin reduction.

In contrast, the apparent Michaelis-Menten parameters of the system varied significantly at different thioredoxin reductase concentrations, although the k_{cat}/K_m compared favorably to the second-order rate constant obtained by fitting the redox couple model (Table 3.2, cf. equation 3.6). Thus, if correct, the redox couple model (Scheme II) predicted that the apparent Michaelis-Menten parameters for the system would vary depending on the thioredoxin reductase concentration used in the experiment, while fitting of the entire system should yield a consistent second-order rate constant over a range of thioredoxin reductase concentrations. Conversely, if thioredoxin was indeed limiting in the system and responsible for the substrate saturation profile, increasing thioredoxin reductase should have negligible effects on the insulin reduction rate and the Michaelis-Menten parameters obtained (Holmgren, 1979a). An additional distinguishing prediction made by these simulations was that substrate saturation in the redox couple model was accompanied by the progressive redistribution of the thioredoxin moiety into its oxidized form (Figure 3.1 B). In contrast, if thioredoxin was described as an enzyme, there should be no net change in the steady-state redox state of thioredoxin (equation 3.3, Scheme I).

Models using the disulfide bond concentration as the ‘substrate’ were also developed and analyzed (Figure 3.1 C) to determine if it made a difference to the kinetic rate parameters obtained in the fitting experiments. Not surprisingly, it was found that the mass-action rate constants (k_2) obtained for the disulfide bond reduction were lower than the rate constants for insulin reduction but again showed a good correlation with the k_{cat}/K_m values obtained when using this substrate (Table S1). A limitation with such an analysis is that it assumes that all three disulfide bonds in insulin are equally accessible. However, data from insulin aggregation studies have shown that the porcine insulin intrachain A6-A11 and interchain A7-B7 disulfide bonds were more accessible to reduction than the buried A20-B19 disulfide bond (Li *et al.*, 2012). Thus, the second-order rate constant obtained from this analysis and indeed the analysis with insulin as the substrate (above) describes a complex set of reduction events within a single aggregated parameter. As a final control, the redox couple model was modified to determine if another rate expression could be used for the insulin reduction reaction (equation 3.5) in these fitting experiments. This reaction was therefore described with reversible mass-action, Hill and Michaelis-Menten kinetics, but appreciably poorer fits of the data (data not shown) were obtained, suggesting that irreversible mass-action kinetics were apparently sufficient to describe the reduction of insulin for the concentrations of thioredoxin reductase tested. As these computational modeling observations could be directly

tested *in vitro*, the thioredoxin system was isolated from *S. cerevisiae* and analyzed using the insulin reduction assay.

Table 3.2 The Michaelis-Menten parameters and second-order rate constants (k_2) for insulin reduction from computational modeling of the *E. coli* thioredoxin system at varying thioredoxin reductase (TR) concentrations.

Substrate		Apparent Michaelis-Menten parameters				Redox couple model	
Varying insulin concentrations	TR	$K_m \pm SE^*$	$k_{cat} \pm SE^*$	k_{cat}/K_m	r^2	$k_2 \pm SE$	r^2
	(μM)	(μM)	(s^{-1})	($\mu\text{M}^{-1}.\text{s}^{-1}$)		($\mu\text{M}^{-1}.\text{s}^{-1}$)	
	0.1	11.52 ± 1.12	0.75 ± 0.02	0.06	0.996	0.06 ± 0.005	0.997
	0.5	57.37 ± 1.41	3.88 ± 0.04	0.06	0.999	0.07 ± 0.001	0.999
1.0	110.09 ± 4.27	7.53 ± 0.17	0.06	0.999	0.07 ± 0.001	0.999	

* As the standard errors for the k_{cat} and K_m values were less than 5% of the total, the standard errors for the k_{cat}/K_m values were not considered.

Table 3.3 The Michaelis-Menten parameters and second-order rate constants (k_2) for insulin reduction by the baker's yeast thioredoxin system at varying thioredoxin reductase (TR) concentrations.

Substrate		Apparent Michaelis-Menten parameters				Redox couple model	
Varying insulin concentrations	TR	$K_m \pm SE^*$	$k_{cat} \pm SE^*$	k_{cat}/K_m	r^2	$k_2 \pm SE$	r^2
	(μM)	(μM)	(s^{-1})	($\mu\text{M}^{-1}.\text{s}^{-1}$)		($\mu\text{M}^{-1}.\text{s}^{-1}$)	
	0.05	38.21 ± 5.85	0.11 ± 0.01	0.003	0.97	0.003 ± 0.0003	0.97
	0.15	25.81 ± 6.74	0.15 ± 0.01	0.006	0.92	0.005 ± 0.0008	0.94
0.25	29.27 ± 3.97	0.18 ± 0.01	0.006	0.98	0.005 ± 0.0004	0.98	

* As the standard errors for the k_{cat} and K_m values were less than 5% of the total, the standard errors for the k_{cat}/K_m values were not considered.

3.4.2 Assay of the yeast thioredoxin system

The insulin reduction assay with the oxidation of NADPH was used to determine the kinetic parameters for the reaction schemes (I and II). Two variations of the coupling assay to NADPH have been presented in the literature, where NADPH oxidation was monitored by a

decrease in absorbance at 340 nm starting at a positive absorbance value (Baker *et al.*, 2001, Si *et al.*, 2014) or by a decrease in absorbance from the blank (Arnér and Holmgren, 2000a). Both these methods (Figure 3.2) were compared and no differences in the rates obtained over a range of NADPH concentrations (0.15-0.4 mM) were found. However, the former assay was used as it appeared less noisy over the range of insulin concentrations tested in the experiments.

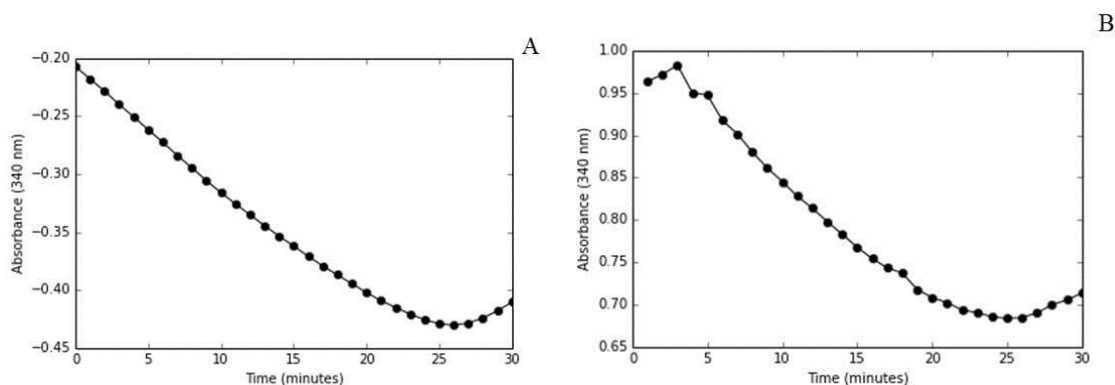


Figure 3.2 Similar rates were obtained when the thioredoxin insulin assay was initiated with thioredoxin reductase or NADPH. Insulin reduction by the thioredoxin system was initiated with either thioredoxin reductase (A) or NADPH (B) and a decrease in absorbance was monitored over negative and positive scales, respectively. The assay contained insulin (80 μM), thioredoxin reductase (0.05 μM), thioredoxin (1.5 μM) and NADPH (150 μM) and was performed in duplicate.

3.4.3 Thioredoxin reductase activity is limiting in the insulin reduction assay

According to the thioredoxin redox couple model, increases in the thioredoxin reductase concentration should increase the flux through the system (Figure 3.1 A). To test this prediction, the rate of NADPH oxidation was measured at varying concentrations of insulin (20-200 μM) and yeast thioredoxin reductase (0.05-0.25 μM). As the concentration of thioredoxin reductase was increased, there was a corresponding increase in the flux through the system (Figure 3.3) supporting the thioredoxin redox couple model (Scheme II) and showing that the saturation observed in this assay was due to an apparent limitation in thioredoxin reductase activity.

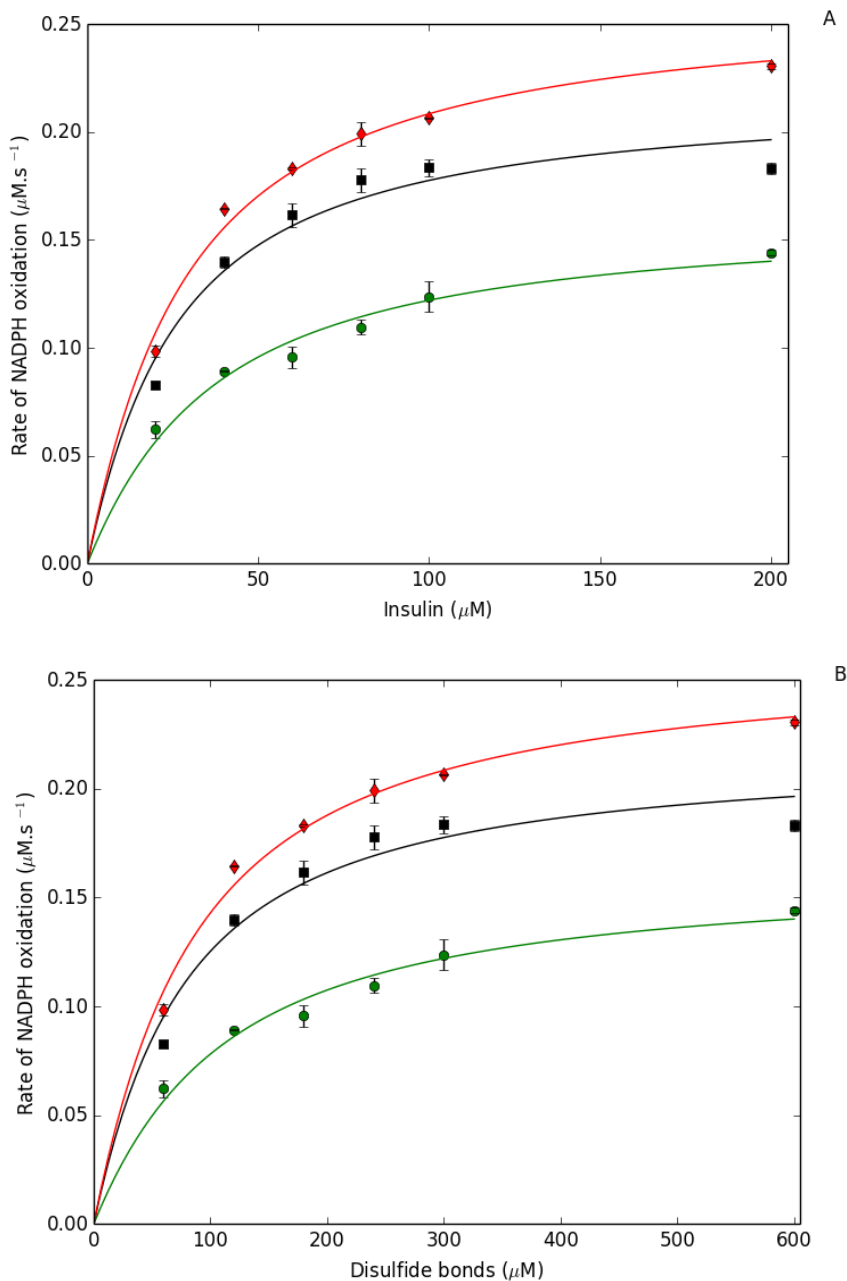


Figure 3.3 Changing the thioredoxin reductase concentration altered the kinetic profile and parameters obtained with the yeast thioredoxin insulin reduction assay. The flux obtained for a given insulin concentration increased as the thioredoxin reductase concentration was increased over the range 0.05 (\bullet), 0.15 (\blacksquare) and 0.25 μM (\blacklozenge). The Michaelis-Menten equation and the redox couple model were both fitted to these datasets using either insulin concentration (A) or the disulfide bond concentration (B). All assays were performed in triplicate with standard errors shown.

The computational modeling also predicted that changes in the thioredoxin reductase concentration would cause changes in the Michaelis-Menten parameters if its activity was limiting in the assay (Table 3.1). Therefore the effect of changing the thioredoxin reductase concentration on the Michaelis-Menten parameters (Scheme I) and on the second-order rate constant for insulin reduction obtained by fitting the entire thioredoxin system to the saturation datasets (Scheme II) was determined. While the K_m values remained relatively constant, changes in the thioredoxin reductase concentration resulted in changes to the apparent k_{cat} values, which was also noted in a previous study (Holmgren, 1979a). In contrast, the second-order rate constant for insulin reduction (k_2 , obtained by fitting the complete system) remained relatively constant and, as expected (Table 3.2), showed a good correlation with the k_{cat}/K_m Michaelis-Menten parameters (Table 3.3). Fitting experiments performed with the disulfide bond concentrations rather than the insulin concentrations also resulted in different Michaelis-Menten and second-order rate constant parameter values. As with the computational modeling studies, there was a good correlation between the k_2 and the k_{cat}/K_m values obtained (Table S1). However, a satisfactory global fit of all the experimental data was unobtainable, suggesting that the kinetic model could not completely describe the complex set of reduction and aggregation events associated with insulin reduction (Li *et al.*, 2012, Zako *et al.*, 2009).

3.4.4 Saturation of the redox cycle and redistribution of the thioredoxin moiety

Over the complete range of thioredoxin reductase concentrations tested, increases in the insulin concentration resulted in observed substrate saturation. According to the redox couple model (Pillay *et al.*, 2009), this would be due to the saturation of the thioredoxin redox cycle as thioredoxin reductase activity became limiting and the thioredoxin moiety distributed into its oxidized form (Figure 3.1 B). To experimentally verify whether there indeed was a redistribution of the oxidized and reduced forms of the thioredoxin moiety, the thioredoxin redox state was preserved by rapidly treating the steady-state insulin reduction reactions with TCA and alkylating the extracts with PEG-maleimide (Hansen and Winther, 2009). Increases in the insulin concentration resulted in the progressive redistribution of the thioredoxin moiety into its oxidized form (Figure 3.4), which was consistent with the computational model (Figure 3.1 B).

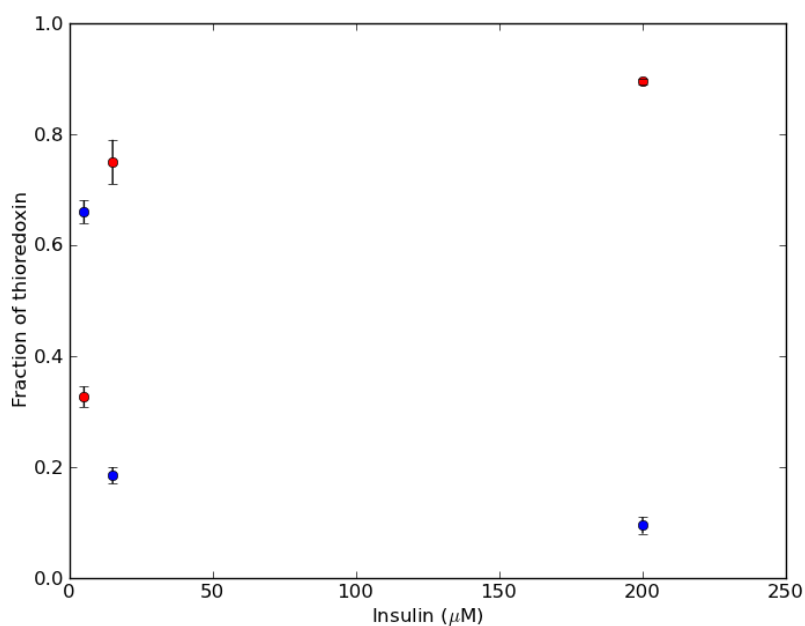
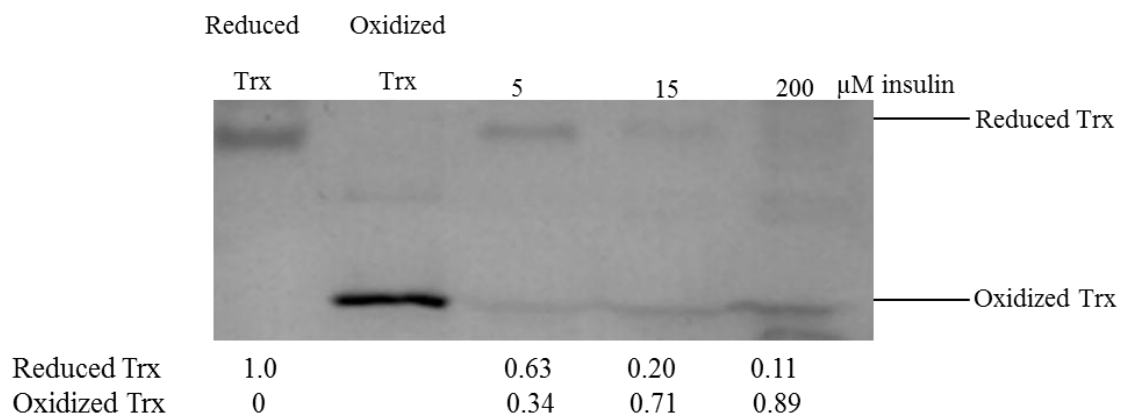


Figure 3.4 Substrate saturation is associated with redistribution of the thioredoxin moiety into its oxidized form in the insulin reduction assay. Reduced thioredoxin in the insulin reduction assay was alkylated with PEG-maleimide. As migration controls, reduced thioredoxin was obtained by incubating thioredoxin (1.5 μM) with DTT (1 mM), while purified thioredoxin served as the oxidized control. Equal concentrations of the thioredoxin test samples were loaded onto the gel and the relative concentration of the oxidized and reduced forms of thioredoxin were quantified using ImageJ with the reduced thioredoxin control acting as a loading standard (A). The experiment was performed in triplicate over a range of thioredoxin reductase concentrations (0.05-0.25 μM) and a representative gel image is shown here. To illustrate the reproducibility of the experiment, the mean and the standard error values of the oxidized (●) and reduced (●) thioredoxin fractions retrieved from triplicate gel images was also determined (B).

3.5 Discussion

The insulin reduction assay is one of the most commonly used methods to determine thioredoxin activity *in vitro*, but the classical substrate saturation profile generated with increasing insulin concentrations has usually been fitted to the Michaelis-Menten equation (Scheme I) (Holmgren, 1979a, Obiero *et al.*, 2010, Maeda *et al.*, 2010, Bao *et al.*, 2009, Juttner *et al.*, 2000, Chen *et al.*, 2014), although it was recently proposed that these datasets should be fitted to a model of the entire system of reactions (i.e. the redox couple model approach, cf. Scheme II) (Pillay *et al.*, 2009). To distinguish between these approaches, a computational model of an *E. coli* thioredoxin system was used which yielded three key predictions. If the redox couple model fitting approach were correct, a) the second-order rate constant for insulin reduction (k_2) would remain constant but the apparent Michaelis-Menten parameters would change with varying thioredoxin reductase concentrations (Table 3.2), b) thioredoxin reductase activity would be limiting in the system (Figure 3.1 A), and c) the thioredoxin moiety would redistribute into its oxidized form with increasing substrate concentration (Figure 3.1 B). On the other hand, if fitting with the Michaelis-Menten equation (Scheme I) were correct, the thioredoxin reductase concentration would have a negligible effect on the rate and Michaelis-Menten parameters for insulin reduction, and thioredoxin should remain in its reduced, active enzymatic form with increasing substrate concentration.

To test the predictions *in vitro* the classical insulin reduction assay for thioredoxin activity was used (Holmgren, 1979a). The data showed that increasing the thioredoxin reductase concentration resulted in an increased flux through the system (Figure 3.3) and also caused a significant change to the k_{cat} values while the second-order rate constant for insulin reduction (k_2) obtained from fitting the redox couple model remained relatively constant over a range of thioredoxin reductase concentrations. Further, using an alkylation assay, the steady-state oxidation of the thioredoxin moiety was observed with increasing insulin concentrations (Figure 3.4). Collectively, the data obtained from the *in vitro* analysis support the redox couple model for saturation in the thioredoxin system and suggest that fitting experiments on insulin reduction assay datasets should use models of the entire system of reactions under study. A potential limitation of the combined experimental and modeling approach is that it might be possible that other kinetic models may also fit these datasets. Therefore a number of other rate expressions for insulin reduction (equation 3.5, Scheme II) were tested, but these

fitting experiments were unsuccessful. Irreversible mass-action kinetics for thioredoxin-dependent insulin reduction appeared to be sufficient to describe the data for each concentration of thioredoxin reductase used in the experiments. While several studies have shown that fitting of other redoxin systems to substrate saturation datasets does indeed yield consistent and reproducible parameter sets (Benfeitas *et al.*, 2014, Mashamaite *et al.*, 2015), a satisfactory global fit with all the datasets was unobtainable. This result suggests that the differences in the kinetic profiles obtained for different thioredoxin reductase concentrations could not be completely explained by the computational models, which was not surprising given the complex reduction and aggregation kinetics of insulin (Li *et al.*, 2012, Zako *et al.*, 2009).

The results presented here make two important contributions to our understanding of redoxin kinetics and analysis. First, consistent second-order rate constants for thioredoxin-dependent insulin reduction should be obtainable regardless of the thioredoxin reductase concentration used in the assay. A good correlation was noted between the k_{cat}/K_m values and the second-order rate constant obtained by direct fitting of the entire system (Tables 3.2-3.3). Thus, specifically the k_{cat}/K_m values (but not all the Michaelis-Menten parameters in general) reported for thioredoxin in previous studies (see for example (Holmgren, 1979a, Lin, 2010)) could still be used in modeling thioredoxin-dependent networks or in the kinetic analysis of related reactions such as peroxiredoxin reduction. A second contribution from this study is that it provides the first experimental support for the computational and theoretical modeling studies that have already used the redox couple approach to develop kinetic models of the thioredoxin system in *E. coli* (Pillay *et al.*, 2011), *Schizosaccharomyces pombe* (Tomalin *et al.*, 2016) as well as the Jurkat-T (Adimora *et al.*, 2010) and red blood cells (Benfeitas *et al.*, 2014). Further, validation of the approach to characterize thioredoxin activity allowed us to confidently use computational models of the thioredoxin system to identify the minimum, experimentally tractable, parameter set needed to quantitatively describe the behaviour of this system under reductive supply and oxidative demand conditions.

Chapter 4: The thioredoxin redox charge as a surrogate measure for flux

4.1 Introduction

The thioredoxin system plays a central role in redox regulation by providing reducing equivalents for a diverse range of metabolic, signaling and antioxidant targets (Chapter 1). The activity of the thioredoxin system is a function of both the reductive electron supply (NADPH, thioredoxin reductase and thioredoxin concentrations) as well as the oxidative demand for thioredoxin by its target reactions (Pigiet and Conley, 1977, Das and Das, 2000, Mukherjee and Martin, 2008, Holmgren and Lu, 2010, Sengupta and Holmgren, 2012). This connectivity within the thioredoxin system allows for a number of important emergent properties such as ultrasensitivity and adaptability (Pillay *et al.*, 2011) but poses a significant challenge for quantification and several measures have been used to estimate the activity of the system *in vivo* including the thioredoxin and thioredoxin reductase specific activities (Lovell *et al.*, 2000) thioredoxin redox potentials (Watson *et al.*, 2003) and redox ratios (Nkabyo *et al.*, 2002, Trotter and Grant, 2003, Watson and Jones, 2003). Although these measures may be readily obtained through activity assays or redox western blotting (Trotter and Grant, 2003, Halvey *et al.*, 2005, Sobhakumari *et al.*, 2012, Ungerstedt *et al.*, 2012), it is arguable whether any of these measures provides an accurate quantitative measure of the activity of the *system*. A combination of these measures has consequently been reported for thioredoxin/thioredoxin reductase inhibitor studies *in vivo* (Du *et al.*, 2012, Lu *et al.*, 2013, Jortzik *et al.*, 2014).

A system's flux represents an integrated outcome of transcript, metabolite and protein levels as well as post-translation modifications (Nielsen, 2003) and for the Trx system specifically, the flux is also a direct measure of the reductive supply and oxidative demand activities on the system (Figure 4.1). While the thioredoxin system flux can be readily obtained through spectrophotometry *in vitro* (Holmgren, 1979a, Arnér and Holmgren, 2000a), measuring this flux *in vivo* is significantly challenging although the development of redox systems biology approaches has allowed for flux estimation using computational models and data-fitting (Sauer, 2006, Adimora *et al.*, 2010, Benfeitas *et al.*, 2014, Tomalin *et al.*, 2016). However, even this approach has its limitations as the choice of kinetic

expressions for redoxins in these models has been ambiguous which can affect the models' properties and outputs (Mashamaite *et al.*, 2015, Padayachee and Pillay, 2016, Pillay *et al.*, 2016). An experimentally tractable surrogate measure for flux would therefore represent a useful advance in analyzing these systems.

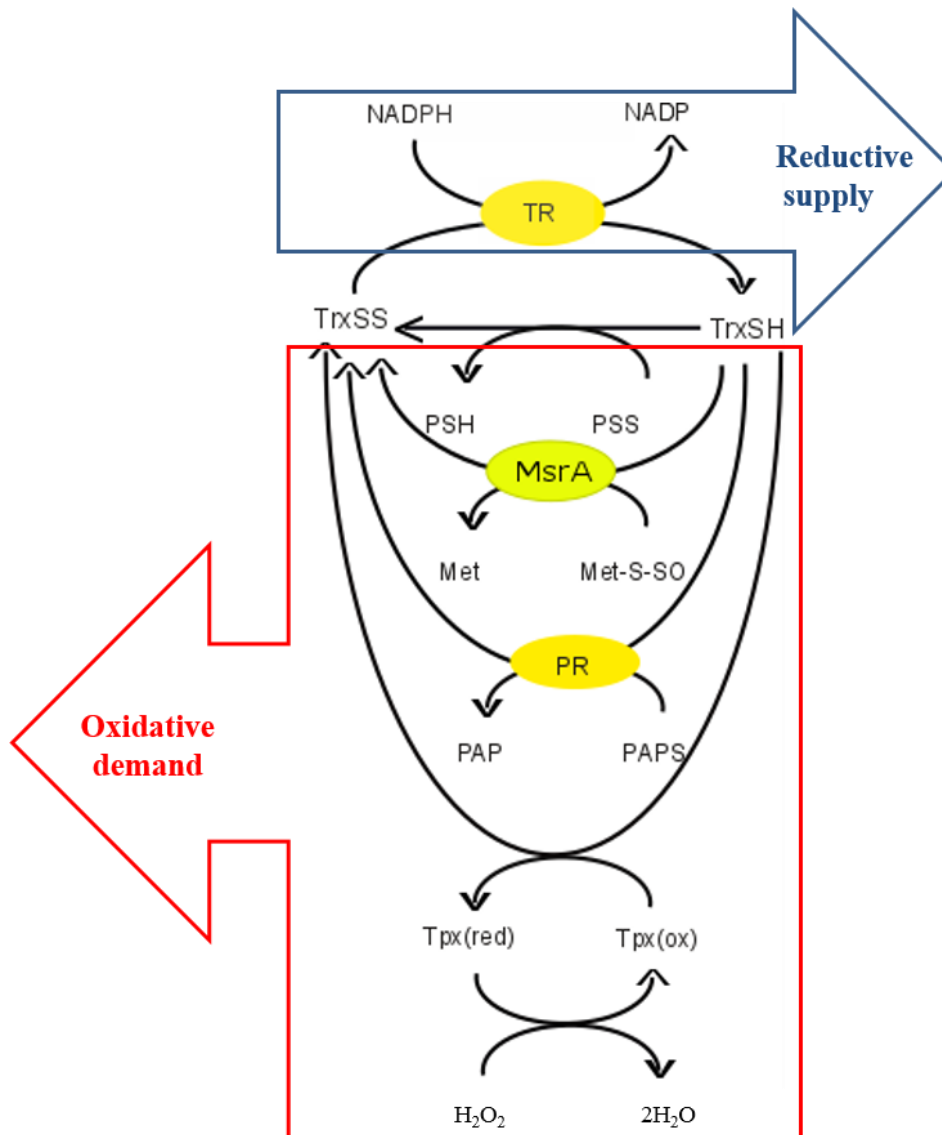


Figure 4.1 A model of the *E. coli* thioredoxin system illustrating the reductive supply and oxidative demand activities on the system. The reduction of oxidized thioredoxin (TrxSS) is catalyzed by thioredoxin reductase (TR) and NADPH, and in turn reduced thioredoxin (TrxSH) serves as an electron donor for the reduction of methionine sulfoxide (MetSO) and 3'-phosphoadenosine-5'-phosphosulfate (PAPS) by methionine sulfoxide and PAPS reductase respectively. Also included is the reduction of the peroxiredoxin (Tpx) by thioredoxin and its oxidation by hydrogen peroxide (H_2O_2) as well as the reduction of protein disulfides (PSS) (Adapted from Pillay *et al.*, 2011).

The mechanism of saturation in the thioredoxin system was previously confirmed which revealed that increases in thioredoxin substrate concentration leads to an increased flux and the concomitant distribution of thioredoxin into its oxidized state (Chapter 3). Changes in the thioredoxin redox state therefore correspond to changes in the flux of the thioredoxin system and we propose that the thioredoxin redox charge, analogous to the adenylate energy charge index (Atkinson and Walton, 1967), could be used as a surrogate measure for flux in the thioredoxin system. This charge could be described in terms of either thioredoxin moiety, with the oxidative thioredoxin redox charge (TrxSS/Trx Total) or the reductive thioredoxin redox charge (TrxSH/Trx Total) measuring perturbations in oxidative demand and reductive supply respectively. Note that normalization against the total thioredoxin concentration ensures that the redox charge is bounded between zero and one allowing for comparative analyses between systems. In this chapter, computational modelling using a basic model of the *E. coli* thioredoxin system and comprehensive, *in vivo* computational models of hydrogen peroxide metabolism in the red blood cell (Benfeitas et al., 2014) and in the fission yeast, *S. pombe* (Tomalin et al., 2016) as well as *in vitro* assays were performed to test the utility of the thioredoxin redox charge as a surrogate measure for flux in the thioredoxin system under conditions of perturbed oxidative demand and reductive supply.

4.2 Materials

The Thrombin CleanCleave™ Kit, Freund's complete and incomplete adjuvants were purchased from Capital Labs (Johannesburg, South Africa). The Pierce AminoLink™ coupling resin was obtained from Separations (Johannesburg, South Africa) while the Clarity western ECL substrate, nitrocellulose membrane, Precision Plus Protein™ WesternC™ standards and the Precision Protein™ StrepTactin-HRP Conjugate was obtained from Bio-Rad, South Africa. The PageRuler™ unstained protein ladder was purchased from Thermo Scientific (Johannesburg, South Africa). A HRP conjugated rabbit anti-chicken secondary antibody and all other common chemicals were from Merck/Saarchem (Johannesburg, South Africa) and were of the highest purity available.

4.3 Methods

4.3.1 Kinetic modeling

Kinetic modeling experiments were carried out using the PySCeS modeling software (Olivier *et al.*, 2005) (<http://pysces.sourceforge.net>) or the complex pathway simulator

(COPASI) software (<http://copasi.org/>). Simulations were carried out using a core model of the *E. coli* thioredoxin system (Pillay *et al.*, 2011) and realistic models of the red blood cell (Benfeitás *et al.*, 2014) and hydrogen peroxide-induced peroxiredoxin oxidation in *S. pombe* (Tomalin *et al.*, 2016). The red blood cell and fission yeast COPASI models were generously supplied by Prof. Armindo Salvador (University of Coimbra) and Dr Elizabeth Veal (Newcastle University) respectively. The model files are all available in the appendix.

4.3.2 Antibody preparation

4.3.2.1 Chicken immunization

Recombinant Trx protein (50 µg/ml, 1.5 ml) was added to an equal volume of Freund's complete adjuvant and triturated to form a stable water-in-oil emulsion which was used to immunize two chickens intramuscularly, sterilized with 70% (v/v) ethanol on either side of the breast bone followed by booster injections with Freund's incomplete adjuvant at weeks 2, 4 and 6. Eggs collected prior to immunization served as the pre-immune control, and those collected throughout the 16 week immunization schedule were stored at 4°C until the IgY isolation was performed. Ethics permission was obtained from the UKZN animal ethics committee (ethics number: 037/15/Animal) for all animal experiments described in the chapter.

4.3.2.2 IgY isolation

Chicken immunoglobulin (IgY) was isolated from the eggs collected at each week following the protocol of Goldring and Coetzer (2003). Briefly, the yolk was separated from the egg white and carefully rinsed under running water to remove all the albumin. The yolk sac was punctured and discarded and the yolk volume determined. Two volumes of 100 mM phosphate buffer (pH 7.6) containing 0.02% (w/v) sodium azide were added to the yolk and mixed thoroughly using a glass rod. A sample was removed and PEG 6,000 (3.5% (w/v)) was added and stirred gently until the PEG completely dissolved. The solution was then centrifuged (4,420 x g, 20 min, room temperature) and the resulting supernatant was filtered through absorbent cotton wool which was placed at the base of a funnel. The filtrate volume was recorded and another sample (50 µl) was removed. PEG 6,000 was then added to the filtrate to a concentration of 12% (w/v) and stirred gently until completely dissolved. The resulting mixture was centrifuged (12,000 × g, 10 min, room temperature) and a further sample (50 µl) was taken from the supernatant. The remaining supernatant was discarded and the pellet was dissolved in a volume of phosphate buffer equal

to the original egg yolk volume. PEG 6,000 was added to a final concentration of 12% (w/v) and allowed to dissolve completely with gentle stirring. This mixture was then centrifuged ($12,000 \times g$, 10 min, room temperature) and a sample (50 μ l) was taken from the supernatant before discarding. The pellet was resuspended in $\frac{1}{6}$ of the original egg yolk volume in 100 mM phosphate buffer (pH 7.6) containing 0.1% NaN_3 and a sample removed for SDS-PAGE analysis (data not shown). The isolated IgY was then stored at 4 °C.

4.3.2.3 Preparation of AminoLink™ matrix for antibody purification

Purified Trx was coupled to the AminoLink™ coupling resin for the affinity purification of antibodies produced against this recombinant protein. The resin (1 ml) was equilibrated with 6 column volumes of coupling buffer (100 mM NaH_2PO_4 , 0.05% (w/v) NaN_3 , pH 7.2) in a mini-column. Recombinant Trx (5 mg) dialysed against the coupling buffer was added to the resin with cyanoborohydride solution (40 μ l 5M NaCNBH_3 in 1M NaOH) and mixed overnight at 4°C using a Revolver™ 360° Sample Mixer (Whitehead Scientific, Cape Town, South Africa). The unbound fraction was collected and the protein concentration was compared to fractions retained prior to coupling. The column was washed with coupling buffer (4 ml) and thereafter with an equal volume of quenching buffer (1 M Tris-HCl buffer, pH 7.4). Cyanoborohydride solution (40 μ l) and quenching buffer (2 ml) were added to the resin and mixed using a Revolver™ 360° Sample Mixer (30 min at RT). The column was then drained and washed with 1 M NaCl (10 ml) and 10 ml wash buffer (100mM NaH_2PO_4 , 0.2% (w/v) NaN_3 , pH 6.5) and thereafter stored upright at 4 °C until required.

4.3.2.4 Purification of polyclonal anti-Trx 1 antibodies

The AminoLink™ affinity column was equilibrated with 6 column volumes of 1 x PBS (137 mM NaCl, 3 mM KCl, 7 mM Na_2HPO_4 and 1.5 mM KH_2PO_4 , pH 7.4) and the isolated IgY (4.3.2.2) was pooled, diluted with an equal volume of 1 x PBS and circulated over the column overnight at room temperature. The unbound IgY was collected and the resin was subsequently washed with 10 column volumes of 1 x PBS. The bound IgY, specific to the Trx on the column, was then eluted with a change in pH by adding elution buffer (8 ml, 100 mM glycine-HCl, 0.02% (w/v) NaN_3 , pH 2.8) and 950 μ l fractions were collected into microcentrifuge tubes containing 50 μ l neutralisation buffer (1 M NaH_2PO_4 , 0.02% (w/v) NaN_3 , pH 8.5). The IgY concentration was then determined by measuring the A_{280} values of the samples and calculated using the extinction coefficient of IgY ($\epsilon_{280 \text{ nm}}^{1 \text{ mg/ml}}$

= 1.25) (Goldring and Coetzer, 2003). The affinity purified IgY-containing fractions were pooled and NaN_3 was added to a final concentration of 0.1% (w/v) before storing at 4°C. The affinity columns were washed with 12 column volumes of 1 x PBS buffer, equilibrated with 12 column volumes of 1 x PBS buffer containing 0.05% NaN_3 and thereafter stored at 4°C.

4.3.3 Recombinant purification of TSA

A pET28a expression plasmid containing TSA1 was obtained from Miss B.D Eagling (Genetics, UKZN) and the identity of this clone was confirmed by DNA sequencing. TSA1 expression was induced by using a high cell density culture method (Sivashanmugam *et al.*, 2009). Briefly, *E. coli* BL21 cells transformed with the TSA1 expression plasmid were grown at 37°C (overnight, 150 rpm) in 2 x YT media (1.6% (w/v) tryptone, 1% (w/v) yeast extract, 0.5% (w/v) NaCl, pH 7.0) containing kanamycin (30 µg/ml), centrifuged (1,500 x g, 10 min, RT) and resuspended in high cell density media (2 x YT, 50 mM Na_2HPO_4 , 25 mM KH_2PO_4 , 5 mM MgSO_4 , 0.2 mM CaCl_2 , 0.1% (w/v) NH_4Cl , 1% (v/v) glucose, pH 8.2). The cells were grown at 37°C until the OD_{600} had increased by one unit (1-1.5 hours, 150 rpm). IPTG (0.5 mM) was then added to the cultures and induction of the recombinant protein expression proceeded at 30°C (2 hours, 150 rpm). Cells were centrifuged at room temperature (12,000 x g, 10 min) and the crude extract containing TSA1 was prepared as described previously (section 2.8.1). Thereafter recombinant TSA1 was purified using Ni-NTA affinity chromatography (section 2.8.2) while purified Trx and thioredoxin reductase were obtained as described previously (section 2.8).

The activity of purified peroxiredoxin was determined using a DTT peroxidase assay in which DTT oxidation was monitored at 310 nm (Tairum *et al.*, 2012) in the presence of hydrogen peroxide. The final reaction mixture contained 25 mM potassium phosphate (pH 7.0), 1 mM EDTA, 100 mM ammonium sulfate, 30 µM hydrogen peroxide, freshly prepared DTT (10 mM) and varying concentrations of TSA1 (1 µM, 2 µM) in a final volume of 1 ml. The reaction was initiated by the addition of the TSA1 and proceeded at 30°C for 10 min with the change in absorbance at 310 nm being directly monitored using a sample without TSA1 as the reference cuvette. Absorbance measurements were made with a UV-1800 Shimadzu Spectrophotometer.

4.3.4 His-tag cleavage of recombinant thioredoxin reductase and peroxiredoxin

The Thrombin CleanCleave™ Kit from Sigma was used for the cleavage of TRR1 and TSA1 His-tags. Both recombinant proteins were dialysed with 1 x cleavage buffer (50 mM Tris-HCl, 10 mM CaCl₂, pH 8.0) to remove any residual salts present from the affinity purification process which could inhibit cleavage. Thrombin resin (100 µl) was centrifuged (500 x g, 3 min, RT) and the supernatant was discarded. The resin was twice washed with 1 x cleavage buffer (500 µl) and thereafter resuspended in 100 µl of 10 x cleavage buffer (500 mM Tris-HCl, 100 mM CaCl₂, pH 8.0). Approximately 1 mg of recombinant protein was added to the mixture and made up to a final volume of 1 ml with distilled water. The reaction was incubated overnight at room temperature using the Revolver™ 360° Sample Mixer. The thrombin resin was removed from the sample (500 x g, 3 min, RT) and the supernatant was treated with AEBSF (final concentration, 0.5 mM) to inhibit any further thrombin activity. Samples were pooled and incubated on a Ni-NTA column as described above (section 2.8.2) to separate the cleaved proteins from the uncleaved proteins which was confirmed by SDS-PAGE. The cleaved proteins, no longer containing the His-tag, eluted as the unbound fraction whilst the His-tagged proteins bound to the column. The thrombin resin was regenerated by washing with an equal volume of 50 mM Tris-HCl (pH 8.0) containing 500 mM NaCl and thereafter washing twice with an equal volume of 50 mM Tris-HCl (pH 8.0). The regenerated resin was then resuspended in storage buffer (50% glycerol, 20 mM Tris-HCl, pH 8.0) and stored at 4°C.

4.3.5 Kinetic assays

The concentration of freshly prepared NADPH was verified at A₃₄₀ using the extinction co-efficient of 6,220 M⁻¹ cm⁻¹. The initial assay contained 150 µM NADPH, 1 µM thioredoxin, thioredoxin reductase (0-700 nM) and reaction buffer (25 mM potassium phosphate, 1 mM EDTA, 100 mM ammonium sulfate, pH 7.0) in a 1 ml UV cuvette which was equilibrated at 25°C for 15 minutes before the assay was initiated by the addition of peroxiredoxin. The consumption of NADPH was monitored as a decrease in absorbance at 340 nm. Absorbance measurements were collected over 6 min and initial studies showed that the system remained in steady state beyond this period. A series of assays were performed with varying thioredoxin reductase (0-700 nM) and peroxiredoxin concentrations (0-4000 nM) and a sample omitting the variable protein in the reaction was used as the reference cuvette.

The steady state assay components were alkylated as described previously (Section 3.3.3) with minor modifications. Firstly, the TCA concentration was increased from 10% to a final concentration of 20% according to the manufacturer's instructions as higher TCA concentrations were recommended for proteins smaller than 20 kDa. Although no quantifiable differences in the protein yield were obtained between the two concentrations tested, a final concentration of 20% TCA was used for all the alkylation experiments described in this chapter. Additionally, the centrifugation of the TCA-treated samples in an Amicon® Ultra 2 ml centrifugal filter (10,000 NMWL) which was previously used to remove insulin (Section 3.3.3) was omitted in this experiment and the excess TCA was removed by an additional acetone (200 µl) wash step. The pellets were treated as described previously (Section 3.3.3) and the alkylated fractions were then separated by electrophoresis on a 12.5% acrylamide SDS gel. All assays were undertaken in triplicate and as assay migration controls, reduced thioredoxin was obtained by incubating thioredoxin (1 µM) with thioredoxin reductase (0.1 µM), NADPH (150 µM) and reaction buffer at 25°C for 15 minutes, while purified thioredoxin (1 µM) served as the oxidized control.

4.3.6 Western blot

Upon completion of the SDS-PAGE, the gel was sandwiched between a nitrocellulose membrane (0.2 µm) and two stacks of filter paper that had been presoaked in transfer buffer for 5 min to allow for the transfer of the proteins from the gel to membrane. Electrophoretic transfer was then carried out for 7 min at 25 V using the Trans-Blot® Turbo™ transfer system (Bio-Rad). Total proteins on the membrane were detected with ponceau S staining while the gel was stained with Coomassie brilliant blue to confirm that complete transfer had occurred. All western blotting procedures were carried out at room temperature with agitation unless stated otherwise. The nitrocellulose membrane was blocked with 10% (w/v) BSA in TBST (20 mM Tris; 137 mM NaCl, 0.1% Tween-20, pH 7.6) for 30 min. Thereafter, the blocking buffer was removed and the blot was incubated overnight at 4°C with the chicken anti-thioredoxin polyclonal primary antibody solution (1:3,000) prepared in 5% (w/v) BSA-TBST (Section 4.3.2.4). Removal of excess primary antibodies was carried out by washing the membrane in TBST six times for 2 min each. A HRP conjugated rabbit anti-chicken secondary antibody solution (1:3,000) prepared in 5% (w/v) BSA-TBST was then incubated with the membrane for 1 hour. The blot was washed again with TBST as described above and thereafter the membrane was incubated with the Clarity western ECL substrate for 3 min at room temperature and visualized using the G:BOX Chemi-XR5 GENESys imaging system.

4.4 Results

4.4.1 Comparative analysis of the thioredoxin redox charge and the existing *in vivo* measures of the Trx system.

Several measures have been used to quantitatively describe the activity of the Trx system *in vitro* and *in vivo* including specific activities, redox potentials (Watson *et al.*, 2003) and redox ratios (Nkabyo *et al.*, 2002, Trotter and Grant, 2003, Watson and Jones, 2003). To determine if any of these existing measures correlate with the flux through the system, a core model of the *E. coli* Trx system was analyzed (Pillay *et al.*, 2011) which included reactions for the reduction of oxidized thioredoxin (TrxSS) by thioredoxin reductase, the thioredoxin-dependent reductions of methionine sulfoxide (Met-S-SO) by methionine sulfoxide reductase (MsrA) and 3'-phosphoadenosine-5'-phosphosulfate (PAPS) by PAPS reductase (PR), the non-specific reduction of cytosolic protein disulfides (PSS) as well as the peroxiredoxin (Tpx)-dependent reduction of hydrogen peroxide (Figure 4.1, Table 4.1). As a control, the model was simulated and the model's steady-state behavior corresponded with published results (Pillay *et al.*, 2011). Further and consistent with published results (Pillay *et al.*, 2011), varying the concentrations of other oxidative demands such as PSS, PAPS and MetSO did not result in major flux changes (data not shown) and were therefore not analyzed further.

Simulations with varying concentrations of the reductive supplies, NADPH and thioredoxin reductase (TR) as well as the oxidative demands, hydrogen peroxide and peroxiredoxin (Tpx) were performed and the effect on flux, redox potentials, redox ratios (TrxSH/TrxSS), the oxidative thioredoxin redox charge (TrxSS/Trx Total) and the reductive thioredoxin redox charge (TrxSH/Trx Total) were determined. Although varying NADPH and TR or hydrogen peroxide and Tpx effectively represented a Trx supply or demand perturbation respectively (Figure 4.1), each parameter was tested to account for any saturation effects within the respective subsystems.

Table 4.1 Kinetic parameters and species concentrations used in the core model of the *E. coli* thioredoxin system (Adapted from Pillay *et al.*, 2011)

Reaction	Parameter	Value
NADPH + TrxSS \rightarrow NADP + TrxSH	k_{cat1}	22.75 s ⁻¹
	K_{nadph}	1.2 μ M
	K_{1trxss}	2.8 μ M
	Thioredoxin reductase	4.74 μ M
TrxSH + PSS \rightarrow TrxSS + PSH	k_2	0.064 μ M ⁻¹ s ⁻¹
MetSO + TrxSH \rightarrow Met + TrxSS	k_{cat3}	3.7 s ⁻¹
	K_{metso}	1900.0 μ M
	K_{3trxsh}	10.0 μ M
	Methionine sulfoxide reductase	2.35 μ M
PAPS + TrxSH \rightarrow SO ₃ + PAP + TrxSS	k_{cat4}	3.5 s ⁻¹
	K_{paps}	22.5 μ M
	K_{4trxsh}	13.7 μ M
	PAPS reductase	0.345 μ M
H ₂ O ₂ + TpxSH \rightarrow H ₂ O + TpxSS	k_5	44.0 μ M ⁻¹ s ⁻¹
TrxSH + TpxSS \rightarrow TrxSS + TpxSH	k_6	3000.0 μ M ⁻¹ s ⁻¹
Species	Concentration (μ M)	
NADPH	137.0	
NADP	1.0	
TrxSH	1.0	
TrxSS	1.0	
PSS	4.23	
PSH	1.0	
MetSO	970.0	
Met	4.83 $\times 10^4$	
PAPS	0.07	
PAP	1.0	
SO ₃	1.0	
H ₂ O ₂	0.02	
H ₂ O	1.0	
TpxSH	4.88	
TpxSS	1.0	

As the system's flux was perturbed by varying the NADPH or thioredoxin reductase concentration, the redox potential (Figure 4.2 A and E), redox ratio (Figure 4.2 B and F) as well as the oxidative thioredoxin redox charge (Figure 4.2 C and G) showed poor correlations with the flux. However, as these perturbations would be expected to distribute the thioredoxin redox couple into its reduced moiety, the reductive thioredoxin redox charge correspondingly appeared to follow changes in the flux (Figure 4.2 D and H).

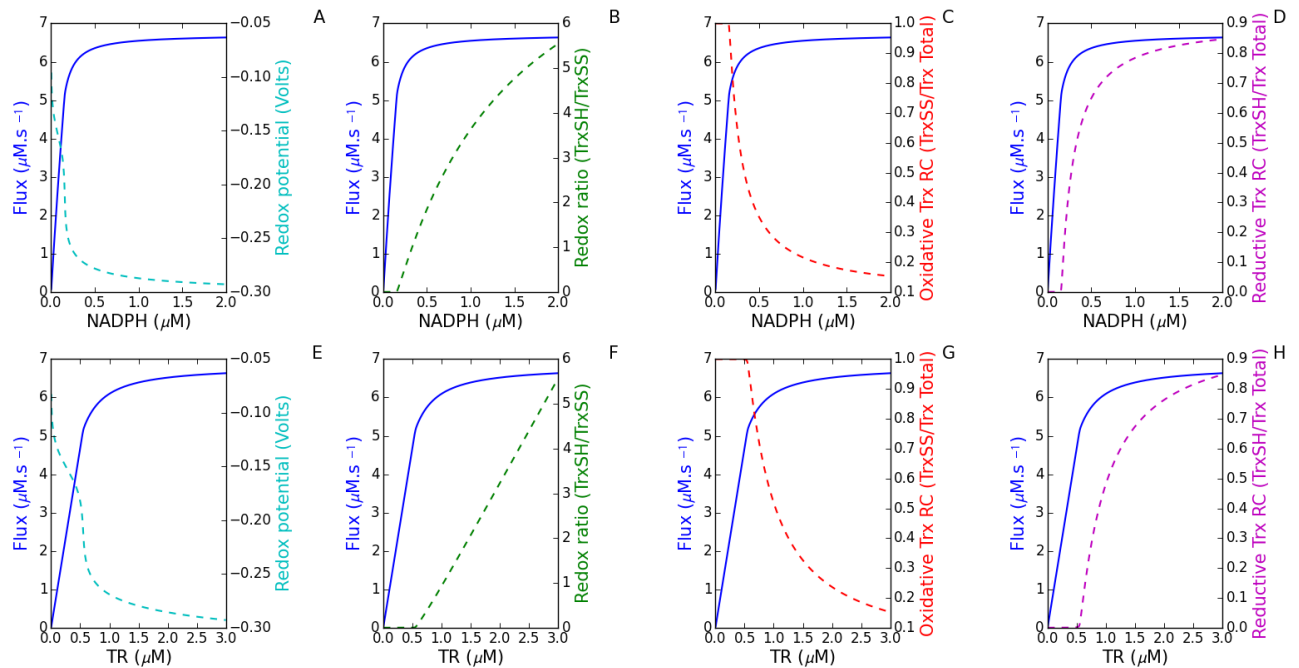


Figure 4.2 The reductive thioredoxin redox charge correlated with the flux as the reductive supply from NADPH and thioredoxin reductase increased. Varying concentrations of NADPH and thioredoxin reductase (TR) were used to determine the relationship between the flux (blue) and redox potential (cyan, A and E), redox ratio (TrxSH/TrxSS) (green, B and F), oxidative thioredoxin redox charge (TrxSS/Trx Total) (red, C and G) and reductive thioredoxin redox charge (TrxSH/Trx Total) (magenta, D and H).

To simulate oxidative demand conditions, the hydrogen peroxide and Tpx concentrations were increased (Figure 4.3) which would be expected to trigger the oxidation of the thioredoxin redox couple. Under these conditions, the redox ratio which has commonly been used to measure the thioredoxin system (Nkabyo *et al.*, 2002, Trotter and Grant, 2003, Watson and Jones, 2003) and the reductive redox charge did not correlate with the flux (Figure 4.3 B, F, D, H) while the oxidative thioredoxin redox charge most closely tracked changes in the flux (Figure 4.3 C and G).

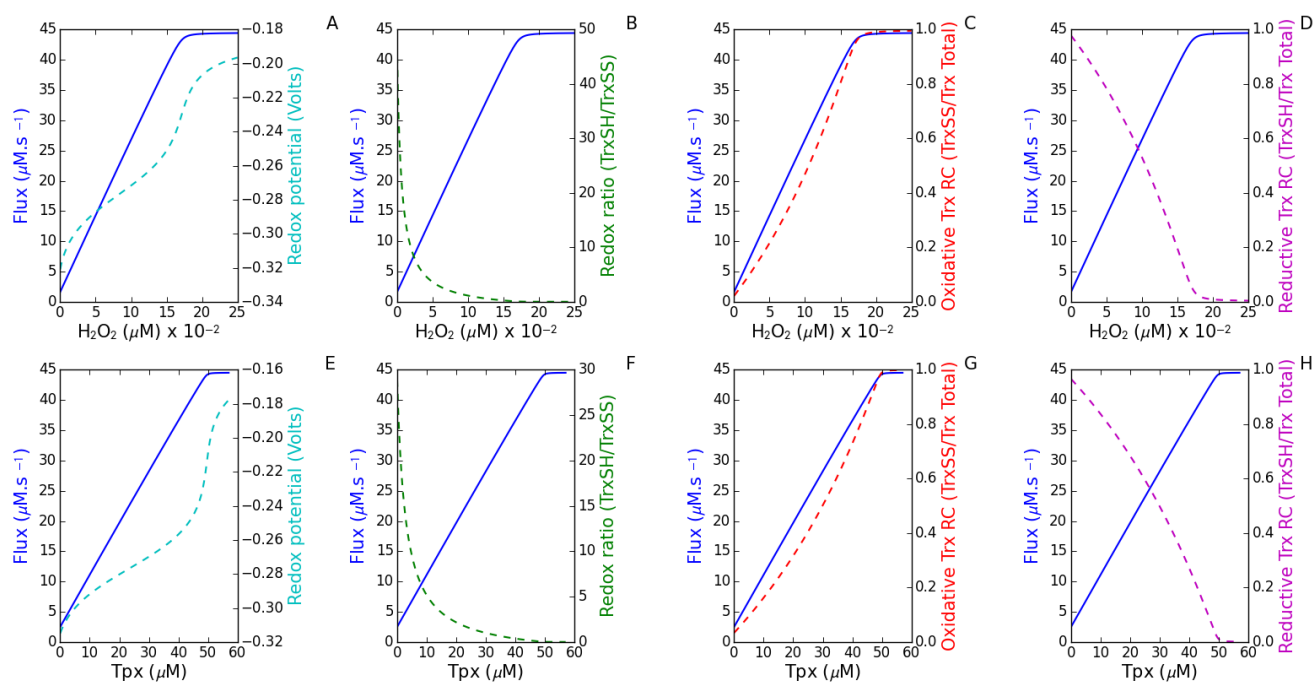


Figure 4.3 The oxidative thioredoxin redox charge corresponded with the flux as the oxidative demand increased. The relationship between the flux (blue) and existing measures of the thioredoxin system including the redox potential (cyan, A and E), redox ratio (TrxSH/TrxSS) (green, B and F), oxidative thioredoxin redox charge (TrxSS/Trx Total) (red, C and G) and reductive thioredoxin redox charge (TrxSH/Trx Total) (magenta, D and H) were evaluated with varying concentrations of H_2O_2 and Tpx, respectively.

The redox potential which has been used as an endpoint quantitative measure in several studies (Jones, 2006, Kranner *et al.*, 2006) showed a surprising correlation to oxidatively-induced changes in the flux (Figure 4.3 A and E). A number of studies have highlighted the limitations associated with this measure (Flohé, 2010, Pillay *et al.*, 2013) and it was therefore hypothesised that the log function within the Nernst equation (Chapter 1) was normalising the thioredoxin redox ratio (Feng *et al.*, 2014). To test this hypothesis, the flux, redox ratio and the log transformed redox ratio data were plotted simultaneously with NADPH and hydrogen peroxide perturbations. Rather than revealing a true correlation with electrochemical potential, logarithmic transformation of the thioredoxin redox ratio data was indeed normalizing the data which consequently approximated the redox charge (Figure 4.4).

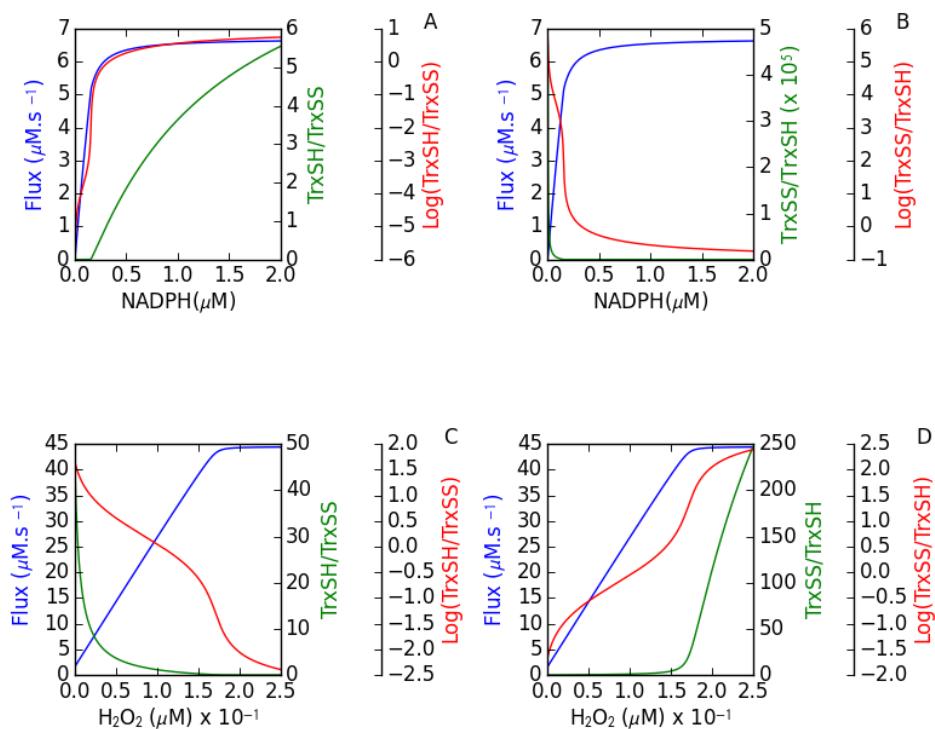


Figure 4.4 The flux through the thioredoxin system correlated with the log transformation of the thioredoxin redox ratio. Models with varying concentrations of NADPH (A-B) and H_2O_2 (C-D) were simulated and the effect on the flux (blue) and the thioredoxin redox ratio, (TrxSH/TrxSS) (A and C, green) or (TrxSS/TrxSH) (B and D, green) was investigated. The log transformation of the respective redox ratio (red) was simultaneously plotted.

Once a qualitative relationship between each of the measures of the thioredoxin system and the flux was established, co-response plots were generated to determine the quantitative relationship with varying concentrations of hydrogen peroxide, peroxiredoxin, NADPH and thioredoxin reductase (Figure 4.5). Co-response plots allow for quantitative analysis of how perturbations of supply and demand determine the behaviour and control of the flux of a system (Hofmeyr and Cornish-Bowden, 2000). The plots were generated in double log-space as the use of logarithmic rather than linear scales offers several advantages; the most important being that it allows direct comparison of the magnitude of steady-state responses to perturbations even with different fluxes and concentrations (Hofmeyr, 1995).

As the reductive supply from NADPH and thioredoxin reductase increased, the oxidative redox charge (Figure 4.5 C) showed no correlation with the flux while the redox potential (Figure 4.5 A), the redox ratio (Figure 4.5 B) and the reductive thioredoxin redox charge

(Figure 4.5 D) appeared to correspond with the flux within limits. Notably at very high reductive supply conditions, the relationship between the reductive thioredoxin redox charge and the flux was non-linear (Figure 4.5 D) which reflected a limitation in this computational model. As the reductive supply was increased, the Tpx redox cycle became saturated and therefore further increases in the reduced thioredoxin concentration did not result in corresponding changes to the flux. Increasing the concentration of hydrogen peroxide would therefore result in an increased demand for reduced Tpx and a linear relationship between the reductive thioredoxin redox charge and the flux was subsequently obtained (Figure S1). The co-response plots also revealed that with perturbations in both oxidative demands, the oxidative thioredoxin redox charge showed a quasi-linear relationship to the flux over a 1000-fold change in the flux (Figure 4.5 G) while the other measures showed a non-linear response. In these simulations, the reductive supply was not limiting and therefore the redox charge tracked the flux over a large range. Collectively these results strongly argued that the thioredoxin reductive and oxidative redox charges may be surrogate measures for flux within limits that are determined by the kinetics of reductive supplies and oxidative demands respectively.

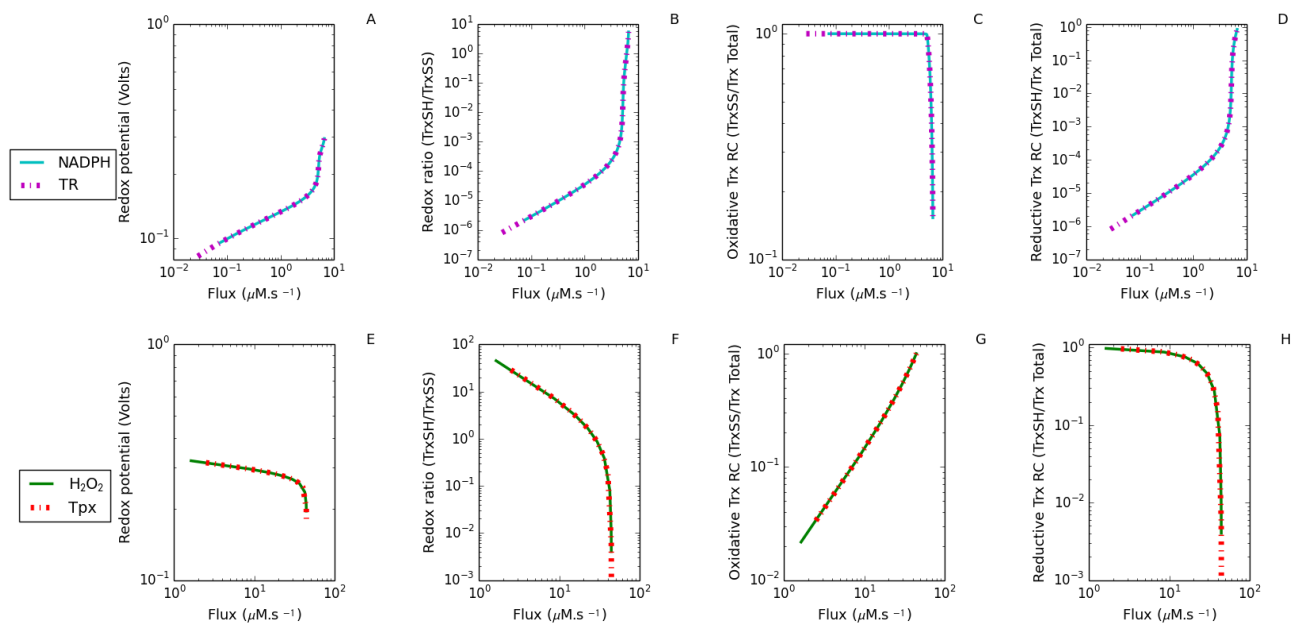


Figure 4.5 Co-response analysis confirms that the reductive and oxidative thioredoxin redox charge correlated with the flux under reductive supply and oxidative demand conditions, respectively. Co-response plots were generated for NADPH (-) and thioredoxin reductase (-.-) (A-D) as well as H_2O_2 (-) and peroxiredoxin (-.-) (E-H) perturbations and the relationship with the redox potential (A and E), redox ratio (TrxSH/TrxSS) (B and F), oxidative thioredoxin redox charge (TrxSS/Trx Total) (C and G) and reductive thioredoxin

redox charge (TrxSH/Trx Total) (D and H) was determined. Each y-axis was scaled according to the range of output values for each measure.

The applicability of the surrogate measure in drug design studies was also tested as the Trx system represents an attractive target for drug therapy (Welsh *et al.*, 2003, Jones *et al.*, 2006, Urig and Becker, 2006, Cai *et al.*, 2012, Fan *et al.*, 2014, Saccoccia *et al.*, 2014, Ahrens *et al.*, 2015). As a first step, Ebselen, a competitive inhibitor which reacts with the active site dithiol of the *E. coli* thioredoxin reductase enzyme (Lu *et al.*, 2013), was incorporated into the *E. coli* thioredoxin system core model. The effect of varying concentrations of the inhibitor on each of the thioredoxin measures was then tested. As Ebselen inhibits the activity of thioredoxin reductase, it was expected that increasing inhibitor concentrations would decrease both the flux through the system as well as the concentration of reduced thioredoxin available. The computational modeling results supported these expectations (Figure 4.6) and corroborated published *in vitro* data where the fast oxidation of thioredoxin by ebselen was shown through alkylation and western blotting analysis (Lu *et al.*, 2013). In addition treatment of a cell with thioredoxin reductase specific inhibitors also causes a decrease in the amount of reduced Trx present (Lu *et al.*, 2006, Du *et al.*, 2012).

The modeling results revealed that the redox potential (Figure 4.6 A), redox ratio (Figure 4.6 B) and the oxidative thioredoxin redox charge (Figure 4.6 C) showed a weak or no correlation with the flux. Not surprisingly, the reductive thioredoxin redox charge corresponded with the flux with increasing inhibitor concentrations (0-5 μM) as this inhibitor affects the reductive supply of the system (Figure 4.6 D). The thioredoxin redox charge could therefore serve as a useful measure for analyzing therapeutics that target the reductive thioredoxin supply *in vivo*.

As the *S. cerevisiae* clones for thioredoxin reductase, Trx (Chapter 3) and peroxiredoxin were readily available, these computational modeling results were tested using *in vitro* kinetic assays and western blot analysis.

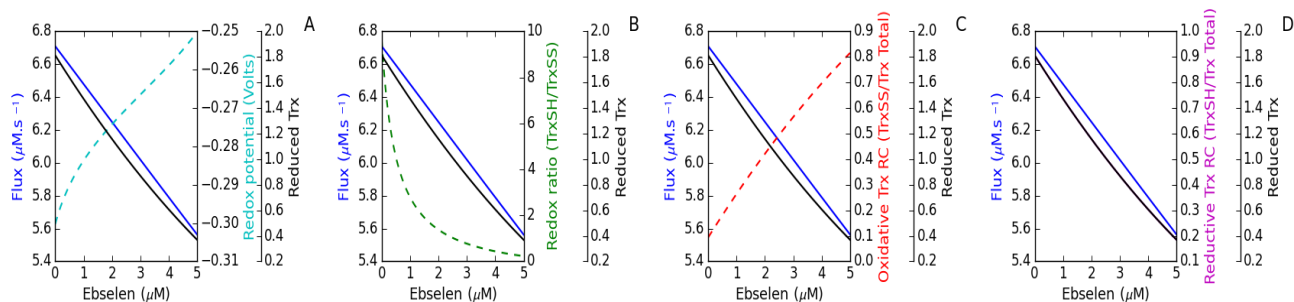


Figure 4.6 The reductive thioredoxin redox charge correlated with the flux with varying concentrations of a competitive inhibitor. Simulations were performed with varying concentrations of Ebselen and the relationship between the flux (blue) and redox potential (cyan, A), redox ratio (TrxSH/TrxSS) (green, B), oxidative thioredoxin redox charge (TrxSS/Trx Total) (red, C) and reductive thioredoxin redox charge (TrxSH/Trx Total) (magenta, D) was tested. The effect of the inhibitor on the concentration of reduced thioredoxin (black, A-D) was also determined. It should be noted that the reductive thioredoxin redox charge plot was superimposed on the reduced thioredoxin plot (D).

4.4.2 The thioredoxin redox charge tracks changes in the thioredoxin reductive supply and oxidative demand *in vitro*

To perform the *in vitro* analysis, recombinant thioredoxin reductase, Trx (Chapter 3) and the yeast peroxiredoxin, TSA1 had to be expressed and purified using nickel affinity chromatography. TSA1 was successfully purified with a size of 24 kDa (Figure 4.7) which was close to the expected size of 22 kDa and its activity was confirmed using a DTT peroxidase assay in which the oxidation of DTT was monitored at 310 nm (Tairum *et al.*, 2012) in the presence of hydrogen peroxide (data not shown).

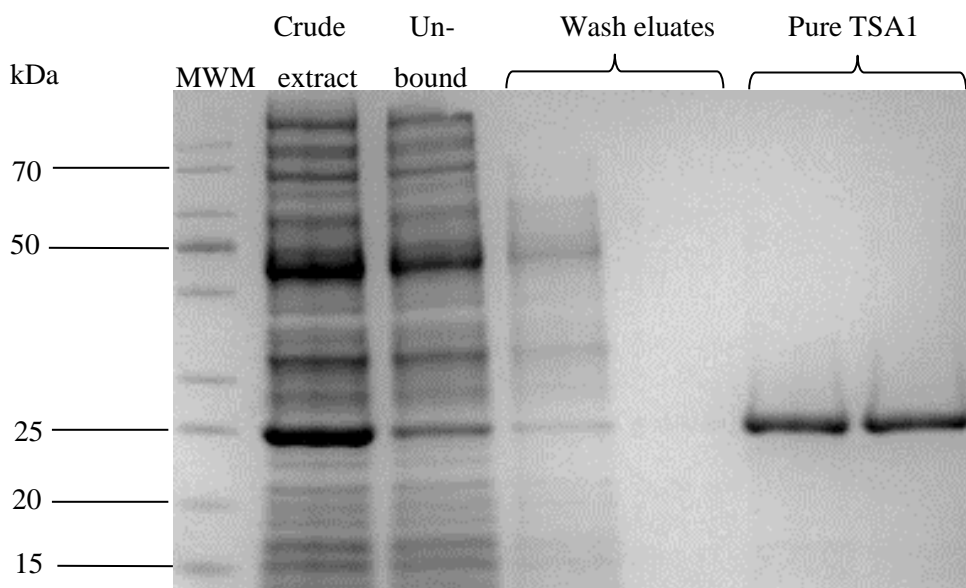


Figure 4.7 Ni-NTA affinity purification of recombinant TSA1. *TSA1* expression was induced for 2 hours and the cells processed as described in Section 2.8.1 to yield pure TSA1. The gel was stained with Coomassie blue.

Previous studies found that the presence of C-terminus His-tags on peroxiredoxins could negatively affect protein activity due to a change in its native structure (Cao *et al.*, 2007, Barranco-Medina *et al.*, 2009). The conformation of the N-terminus tagged TSA1 used in this study was determined by a Blue Native (BN)-PAGE which uses Coomassie blue dye to resolve proteins by supplying a charge to allow them to separate according to size in their native form and omits detergents such as SDS that disrupt protein-protein interactions in typical protein electrophoresis (Manns, 2005). The BN-PAGE of TSA1 revealed that this protein assembled into a high molecular weight decameric structure and the presence or absence of the His-tag did not affect its activity (Eagling, 2015). However, both peroxiredoxin and thioredoxin reductase were recognised by the polyclonal antibodies produced for Trx because the His-tag epitope was present on both proteins. These tags were therefore cleaved and the cleaved proteins were purified using nickel affinity chromatography (Figure 4.8 A).

To confirm if the His-tag cleavage was successful as well as to test the specificity of the antibodies generated against Trx1, a western blot was performed using polyclonal anti-thioredoxin antibodies. Purified thioredoxin which served as the oxidized Trx control (Ox Trx1) in the alkylation studies was also analyzed.

Nickel affinity purification depends on the binding of the histidine residues in the His-tag of the recombinant protein to the immobilized nickel ions in the resin. Upon cleavage of the His-tag, the proteins elute from the resin as the unbound fraction providing an efficient method to separate the cleaved proteins from the uncleaved fractions. The His-tag is approximately 1 kDa in size and therefore cleavage causes a subsequent decrease in the molecular weight of the recombinant protein (Figure 4.8 A). Cleavage of the His-tags from recombinant TRR1 and TSA1 prevented cross-detection by the anti-Trx 1 antibodies (Figure 4.8 B) and the western blot confirmed that the antibodies were able to detect the oxidized Trx control (Ox Trx1) (Figure 4.8 C).

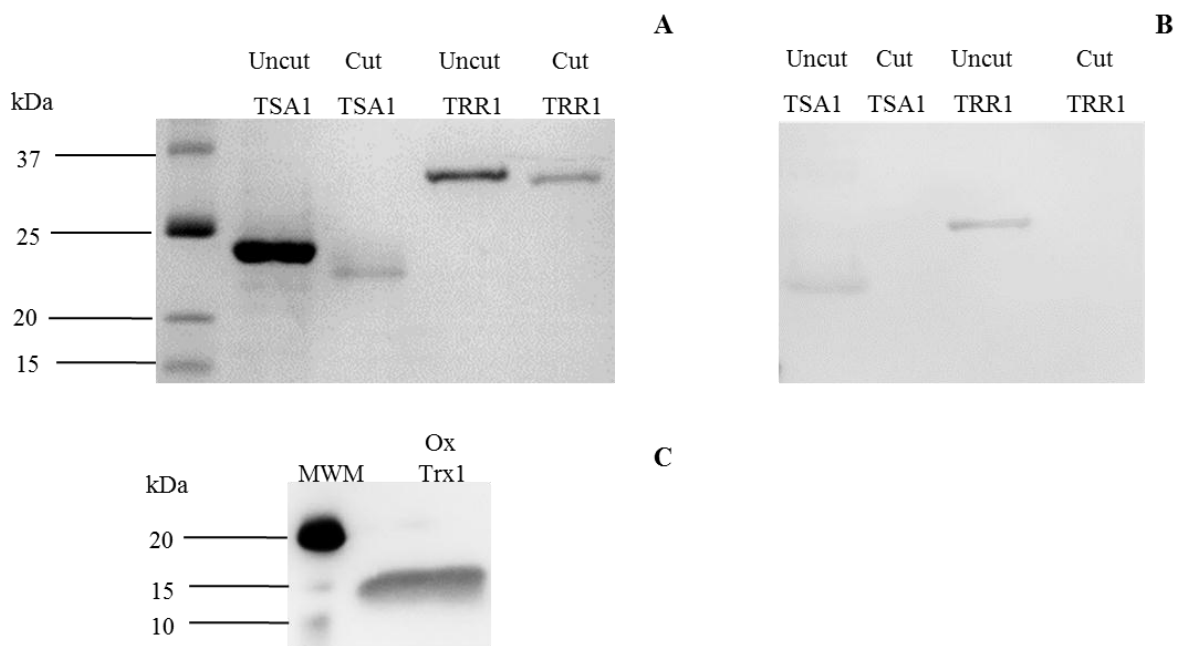


Figure 4.8 Nickel affinity purification of His-tag cleaved recombinant TSA1 and TRR1 (A) and western blot analysis confirming the specificity of the anti-Trx1 antibodies (B and C). His-tags from TSA1 and TRR1 were cleaved using the Thrombin CleanCleave kit and the extract was mixed with Ni-NTA agarose. The proteins cleaved to completion eluted as the unbound fractions and ran at a lower molecular weight when analyzed by SDS-PAGE. The gel in this figure was stained with Coomassie blue (A). Western blotting analysis confirmed that the cleavage removed the His-tag (B) and the polyclonal antibodies specifically recognised thioredoxin (Ox Trx1) (C). The gels have been cropped to fit the figures into this thesis but no other bands were observed in the non-MWM lanes.

Using the His-tag cleaved proteins and Trx, kinetic analysis involving the spectrophotometric monitoring of the flux as the rate of NADPH oxidation with varying thioredoxin reductase (reductive supply) or peroxiredoxin concentrations (oxidative demand) was performed to determine if the thioredoxin redox charge is a surrogate measure for flux *in vitro*. With increasing thioredoxin reductase and TSA concentrations, a corresponding increase in the flux was observed (Figure 4.9). In keeping with computational modeling studies (Pillay *et al.*, 2011, Rohwer *et al.*, 2016), the flux displayed an ultrasensitive response to perturbations of the reductive supply and the oxidative demand showing how the flux was a function of the activity of demand and supply reactions respectively (cf. Figure 4.5). To the best of our knowledge, this study was the first to detect this ultrasensitive response *in vitro*.

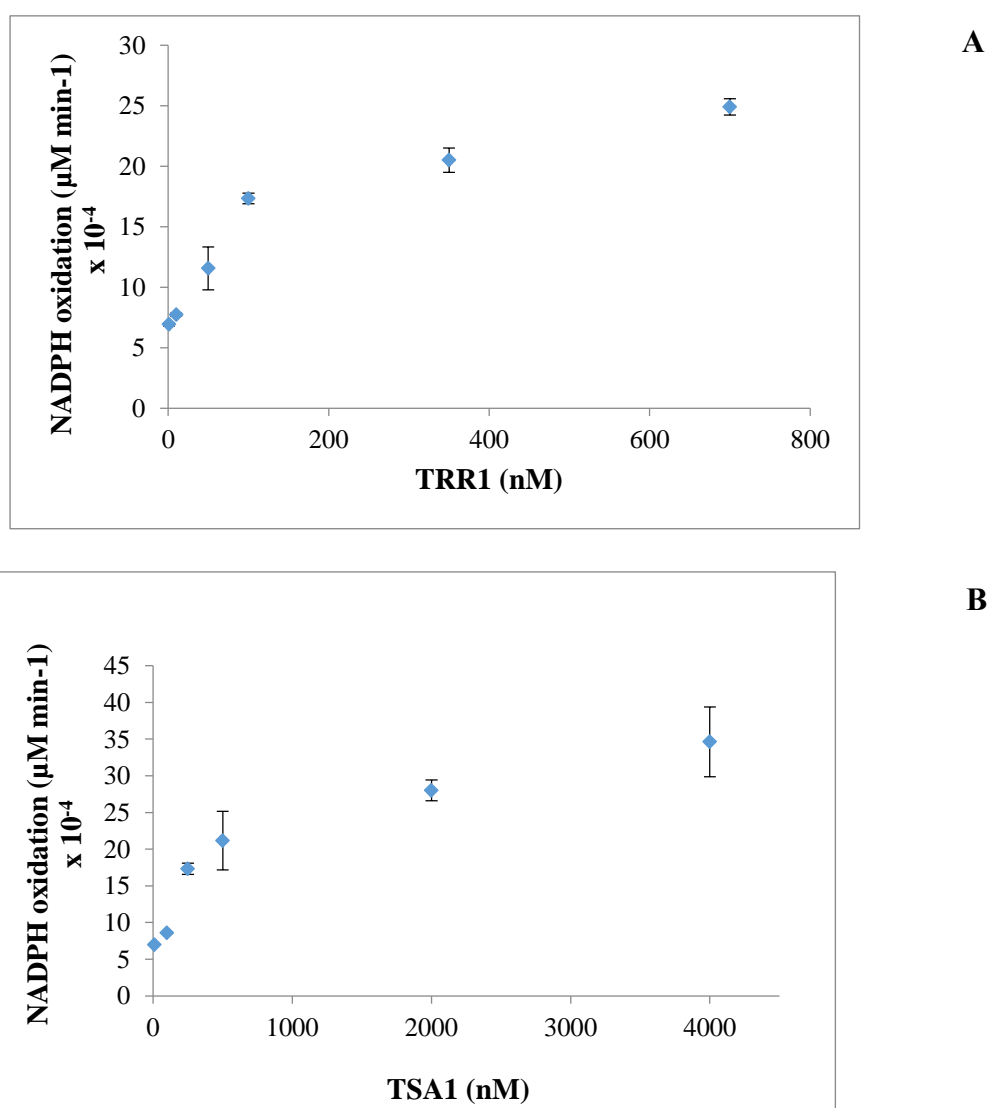


Figure 4.9 The rate of NADPH oxidation was measured at 340 nm at various concentrations of thioredoxin reductase (0-700 nM) (A) and peroxiredoxin (0-4000 nM) (B). The reaction mixture contained in a final volume of 1 ml, 150 μM NADPH, 1 μM Trx,

reaction buffer (25 mM potassium phosphate, 1 mM EDTA, 100 mM ammonium sulfate, pH 7.0), 100 nM TRR1 for varying TSA1 assays (A) and 250 nM TSA1 for varying TRR1 assays (B). Experiments were performed in triplicate and the standard error bars are indicated.

Based on previous data (Chapter 3), it was expected that a reduced/alkylated thioredoxin isoform and lower molecular weight oxidized thioredoxin isoform would be obtained in these experiments. However, in migration control experiments where purified thioredoxin served as an oxidized thioredoxin control (Ox Trx), PEG-maleimide surprisingly appeared to increase the size of this thioredoxin isoform to 26 kDa without prior reduction in the assay (Figure 4.10 A) while a small fraction of the oxidized thioredoxin control remained at 15 kDa which was close to the expected size of 12 kDa. As an assay control to ensure that a functioning system was utilized in the assays, thioredoxin (1 μ M) was reduced with NADPH (150 μ M) and thioredoxin reductase (0.1 μ M) which resulted in a higher molecular weight band (47 kDa) (Figure 4.10 A) corresponding to the alkylation of fully reduced thioredoxin (Chapter 3, Figure 3.4). DTT treatment of the oxidized thioredoxin control prior to alkylation resulted in the near-complete disappearance of the 15 and 26 kDa bands and the appearance of fully reduced thioredoxin at 47 kDa (Figure 4.10 B).

Upon alkylation, PEG-maleimide binds to free thiols in proteins, increasing the molecular mass of the protein by 5 kDa per PEG-maleimide bound. Therefore, a fully oxidized form of thioredoxin should be approximately 12 kDa, a partially oxidized form should be approximately 17 kDa and a fully reduced and alkylated thioredoxin should have a size of 22 kDa. However several studies have found that due to the extensive hydration of PEG, the mobility shift in SDS-PAGE can be much larger than expected, up to 22 kDa per PEG-maleimide bound (Makmura *et al.*, 2001, Chibani *et al.*, 2011, Biran *et al.*, 2014, Nikkanen *et al.*, 2016) which was consistent with our findings. Three thioredoxin isoforms have previously been reported in alkylation studies which include the fully oxidized, partially oxidized and fully reduced forms (Requejo *et al.*, 2010) and two oxidized forms of thioredoxin were also obtained in *Candida albicans* alkylation studies. Consistent with our results, both these forms were lost upon DTT treatment prior to alkylation with 4-acetamido-4'-maleimidyl-stilbene-2,2'-disulfonate (AMS) confirming that the bands represented different oxidized forms of thioredoxin (da Silva Dantas *et al.*, 2010). Thus, in our assays the two bands at 15 and 26 kDa following PEG-maleimide alkylation were assigned as the

oxidized thioredoxin fraction for this analysis, while the 47 kDa band represented the reduced thioredoxin fraction. It should be noted that the samples were not pre-reduced with DTT in these kinetic assays as this would have changed the reductive supply conditions in the assay.

The western blot analysis revealed that an increase in the thioredoxin reductase concentration resulted in a progressive increase in the concentration of the reduced Trx fraction relative to the oxidized fraction (Figure 4.10 C) while increases in peroxiredoxin concentration were accompanied by the conversion of the Trx moiety into its oxidized form (Figure 4.10 D). The intensity ratio of the bands from these western blots obtained with ImageJ (<http://imagej.nih.gov/ij/>) was combined with the *in vitro* assay data (Figure 4.9) to determine the correlation between each of the measures of the Trx system and the flux (Figure 4.11) as well as to generate co-response plots (Figure 4.12) to determine their quantitative relationships. At higher concentrations of the reductive supply or the oxidative demand, the demand or supply cycle saturated and therefore the measures of the Trx system were calculated across the entire dataset (Figure S2-S3) as well as within the initial linear regions.

As the reductive supply from NADPH and thioredoxin reductase increased, the redox potential (Figure 4.11 A) most closely correlated with the flux. The redox ratio (Figure 4.11 B) and the reductive thioredoxin redox charge (Figure 4.11 D) showed a good correlation while the oxidative redox charge (Figure 4.11 C) showed no correlation with the flux. On the other hand, with increasing concentrations of peroxiredoxin, the oxidative redox charge (Figure 4.11 G) most closely correlated with the flux compared to all the measures tested. The co-response analysis revealed non-linear plots for the correlation between the flux and the redox potential (Figure 4.12 A) as well as the oxidative thioredoxin redox charge (Figure 4.12 C) with increasing concentrations of thioredoxin reductase. Consistent with the modeling results obtained above (Figure 4.5), both the redox ratio (Figure 4.12 B) and the reductive thioredoxin redox charge (Figure 4.12 D) correlated with the flux producing quasi-linear plots. Both the redox potential (Figure 4.12 E) and the oxidative thioredoxin redox charge (Figure 4.12 G) displayed good correlations with the flux with perturbations in the peroxiredoxin concentration, while the redox ratio (Figure 4.12 F) and the reductive thioredoxin redox charge (Figure 4.12 H) showed no correlation. In summary, the *in vitro* analyses showed that the thioredoxin redox charge could be used as a surrogate measure for flux. As an additional study to test the applicability of thioredoxin redox charge as a surrogate

measure for flux, realistic models of the Trx system were then analyzed.

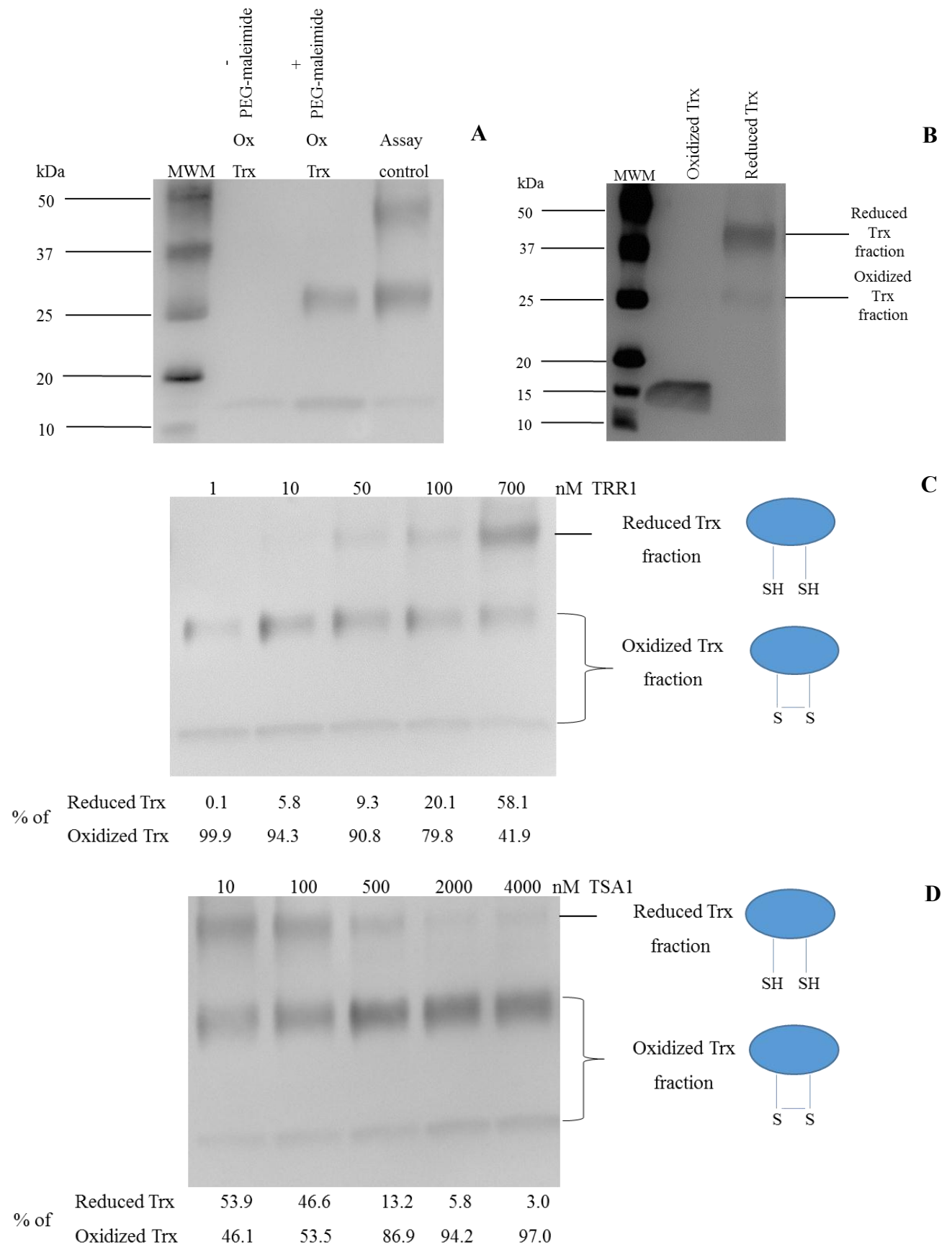


Figure 4.10 The effect of perturbations of the reductive supply and oxidative demand on the thioredoxin redox poise. For the alkylation studies, purified thioredoxin was used as an oxidative control (Ox Trx) and PEG-maleimide treatment increased the molecular weight of this control. In an assay control to ensure the reduction of Trx by thioredoxin reductase, incubation of thioredoxin (1 μM) with thioredoxin reductase (0.1 μM) and NADPH (150 μM) resulted in the appearance of reduced thioredoxin at 47 kDa (A) which was confirmed by DTT-pretreatment of oxidized thioredoxin (B). The kinetic assay samples containing NADPH (150 μM), thioredoxin (1 μM) and varying concentrations of thioredoxin reductase (TRR1) (C) or TSA1 (D) were alkylated with PEG-maleimide and the reduced thioredoxin concentration was detected using polyclonal chicken anti-thioredoxin antibodies. All bands were quantified with Image J. A reduced Trx fraction could not be detected in the 1 nM TRR1 experiment (C) and therefore this fraction was assigned a nominal value of 0.1%. The gels have been cropped to fit the figures into this thesis but no other bands were observed in the non-MWM lane.

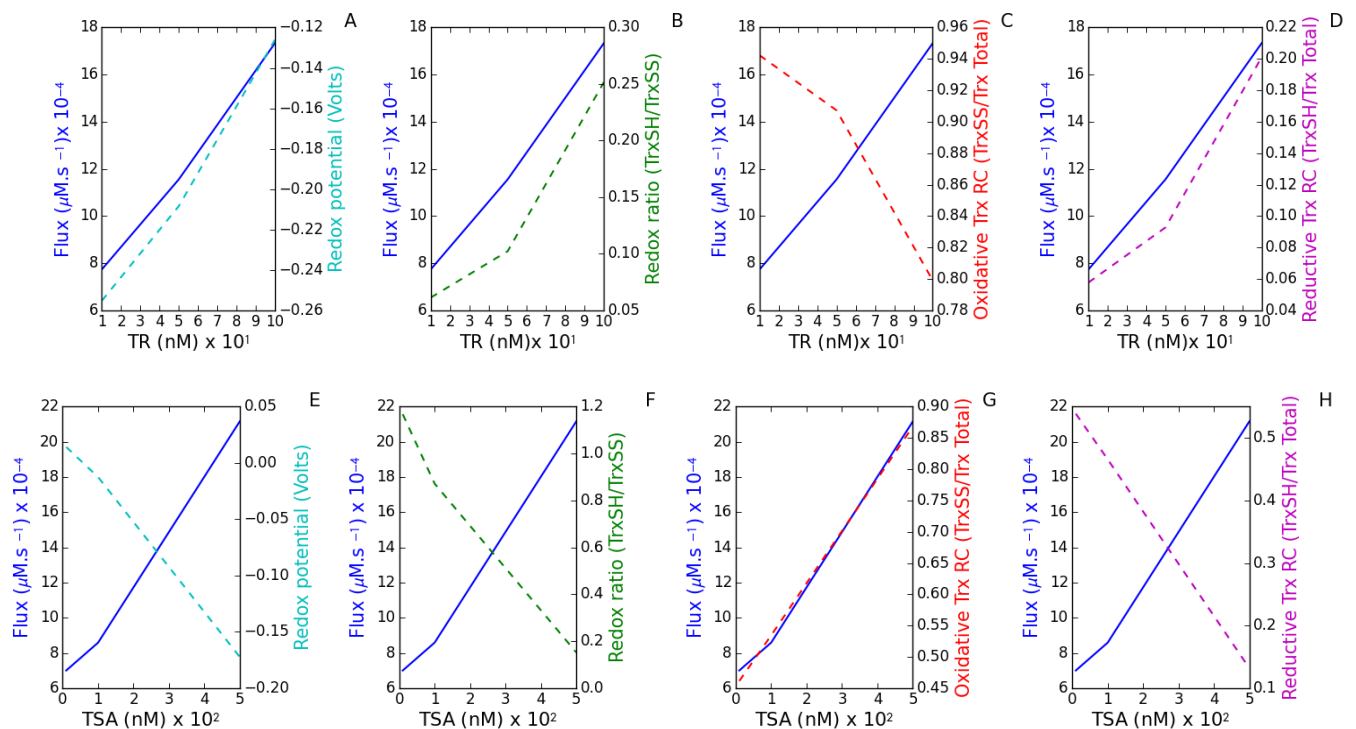


Figure 4.11 The reductive thioredoxin redox charge correlated with the flux as the reductive supply from thioredoxin reductase increased while the oxidative thioredoxin redox charge correlated with the flux with increasing peroxiredoxin concentrations. *In vitro* assays with varying concentrations of thioredoxin reductase and peroxiredoxin were performed to determine the relationship between the flux (blue) and redox potential (cyan, A

and E), redox ratio (TrxSH/TrxSS) (green, B and F), oxidative thioredoxin redox charge (TrxSS/Trx Total) (red, C and G) and reductive thioredoxin redox charge (TrxSH/Trx Total) (magenta, D and H).

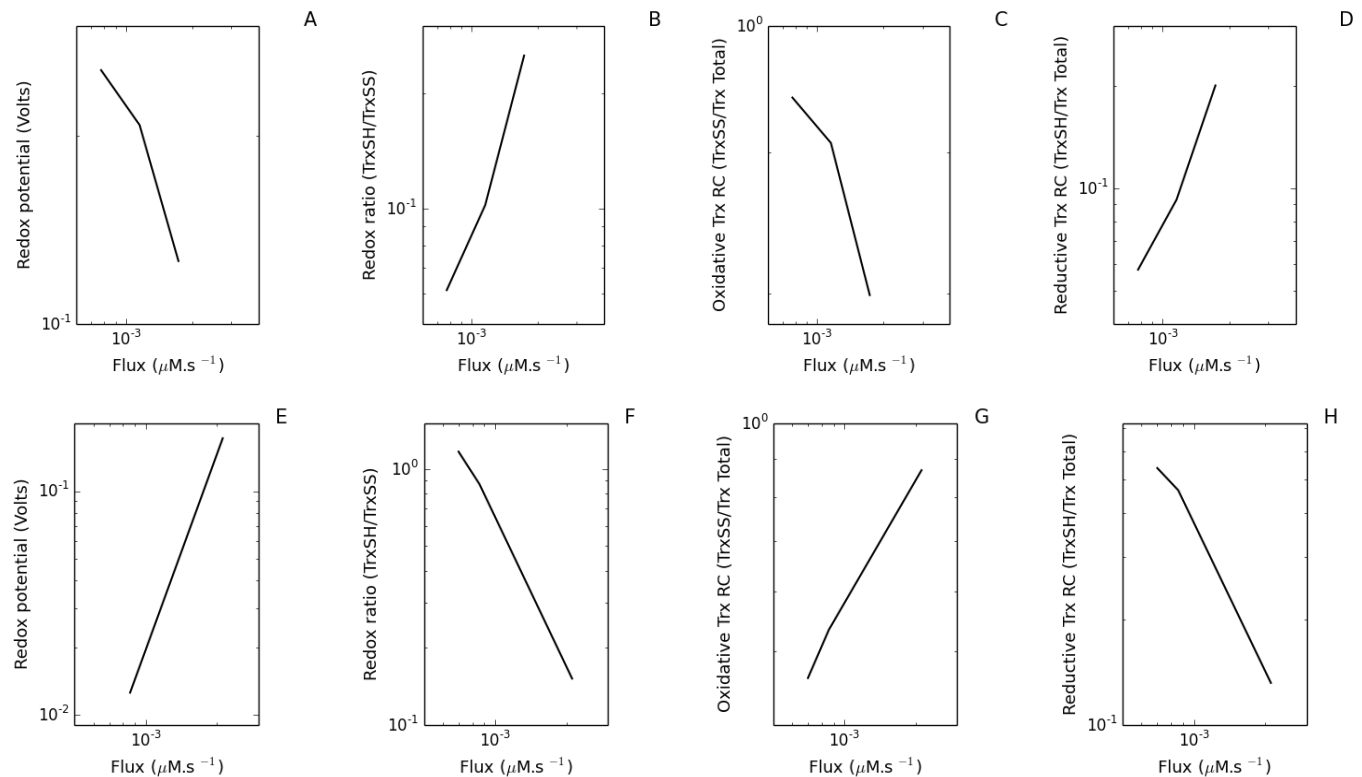


Figure 4.12 Co-response plots generated from *in vitro* assay and western blot data confirmed that the reductive thioredoxin redox charge correlated with the flux with perturbations in reductive supply and the oxidative thioredoxin redox charge correlated with the flux with perturbations in oxidative demand. Co-response plots were generated with varying concentrations of thioredoxin reductase (A-D) and peroxiredoxin (E-H) and the relationship with the redox potential (A and E), redox ratio (TrxSH/TrxSS) (B and F), oxidative thioredoxin redox charge (TrxSS/Trx Total) (C and G) and reductive thioredoxin redox charge (TrxSH/Trx Total) (D and H) was determined.

4.4.3 Realistic models illustrated the general applicability of the thioredoxin redox charge as a surrogate measure for flux

A published model of the red blood cell was used to test the general applicability of the proposed surrogate measure. This comprehensive model was based on hydrogen peroxide metabolism in erythrocytes and included reactions for the (i) generation of intracellular

hydrogen peroxide from both endogenous and exogenous sources; (ii) hydrogen peroxide consumption via catalase, peroxiredoxin 2 and glutathione peroxidase; (iii) peroxiredoxin 2 sulfinylation and reduction of the sulfinic to the sulfenic form; (iv) Trx1 oxidation by peroxiredoxin 2, reduction via thioredoxin reductase and reactions between the active-site dithiol and the regulatory dithiol; (v) glutathione reductase mediated reduction of glutathione disulfide (GSSG); and (vi) NADP⁺ reduction to NADPH by the hexose monophosphate shunt (Benfeitas *et al.*, 2014). A diagrammatic representation of the model (Figure S4) as well as tabulated kinetic parameters and species concentrations are given in the appendix (Table S2).

The model was simulated with increasing hydrogen peroxide concentrations, the effect on each of the measures of the Trx system was determined (Figure 4.13 A-D) and thereafter co-response plots were generated (Figure 4.13 E-H). As the concentration of hydrogen peroxide increased, the redox potential (Figure 4.13 A), redox ratio (Figure 4.13 B) and reductive thioredoxin redox charge (Figure 4.13 D) showed no correlation with the flux. However, this perturbation resulted in an increased demand for peroxiredoxin reduction, leading to greater oxidized thioredoxin concentrations at steady state and the oxidative thioredoxin redox charge consequently correlated with the flux (Figure 4.13 C). The co-response plots confirmed this finding and a linear relationship between the flux and the oxidative thioredoxin redox charge (Figure 4.13 G) was obtained.

An additional realistic computational model monitoring hydrogen peroxide-induced peroxiredoxin oxidation in *S. pombe* was also analyzed to investigate the applicability of the thioredoxin redox charge as a surrogate measure of flux. This model was able to accurately simulate the *in vivo* removal of extracellular hydrogen peroxide and also included the changes in the concentrations of the various peroxiredoxin redox states following exposure to different hydrogen peroxide concentrations. The rates of hydrogen peroxide influx and efflux as well as the removal of hydrogen peroxide from the intracellular compartment were also included in the model. Notably, this model displayed excellent predictive abilities and provided new insights into the underlying causes and function of peroxiredoxin hyperoxidation (Tomalin *et al.*, 2016). A diagrammatic representation of the model (Figure S5) as well as tabulated kinetic parameters and species concentrations are given in the appendix (Table S3).

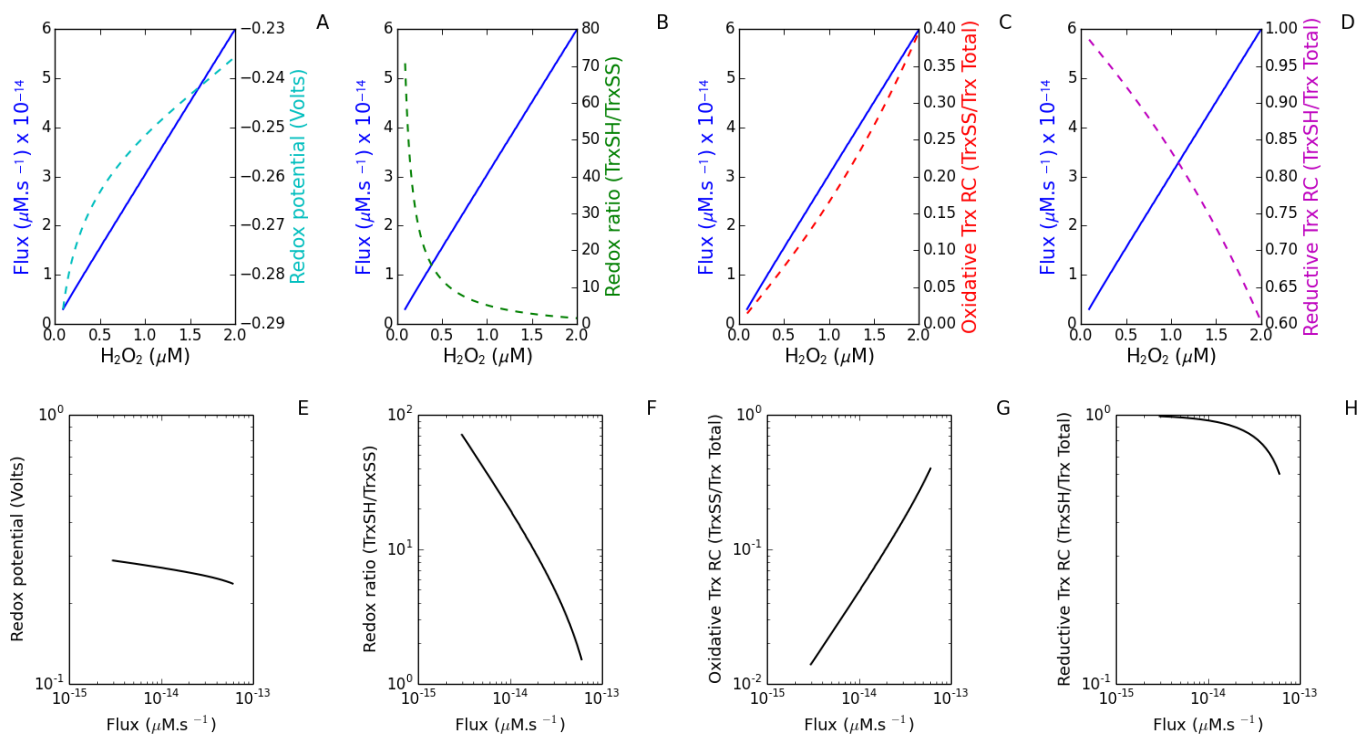


Figure 4.13 A large scale realistic model of the red blood cell supports the use of the thioredoxin redox charge as a surrogate measure for flux. Plots with the flux (blue) and redox potential (cyan, A), redox ratio (TrxSH/TrxSS) (green, B), oxidative thioredoxin redox charge (TrxSS/Trx Total) (red, C) and reductive thioredoxin redox charge (TrxSH/Trx Total) (magenta, D) were generated with varying concentrations of hydrogen peroxide. Using this respective data, co-response plots were then generated (E-H).

The model was simulated with increasing hydrogen peroxide concentrations and the effect on each of the measures of the Trx system including the redox potential, the redox ratio, the oxidative thioredoxin redox charge and the reductive thioredoxin redox charge was determined (Figure 4.14 A-D) and co-response plots were also generated (Figure 4.14 E-H). Of all the measures tested, the oxidative thioredoxin redox charge most closely correlated to the flux (Figure 4.14 C) with perturbations in hydrogen peroxide concentration. A linear curve was also obtained during the co-response analysis confirming a corresponding quantitative relationship between the flux and the oxidative thioredoxin redox charge (Figure 4.14 G).

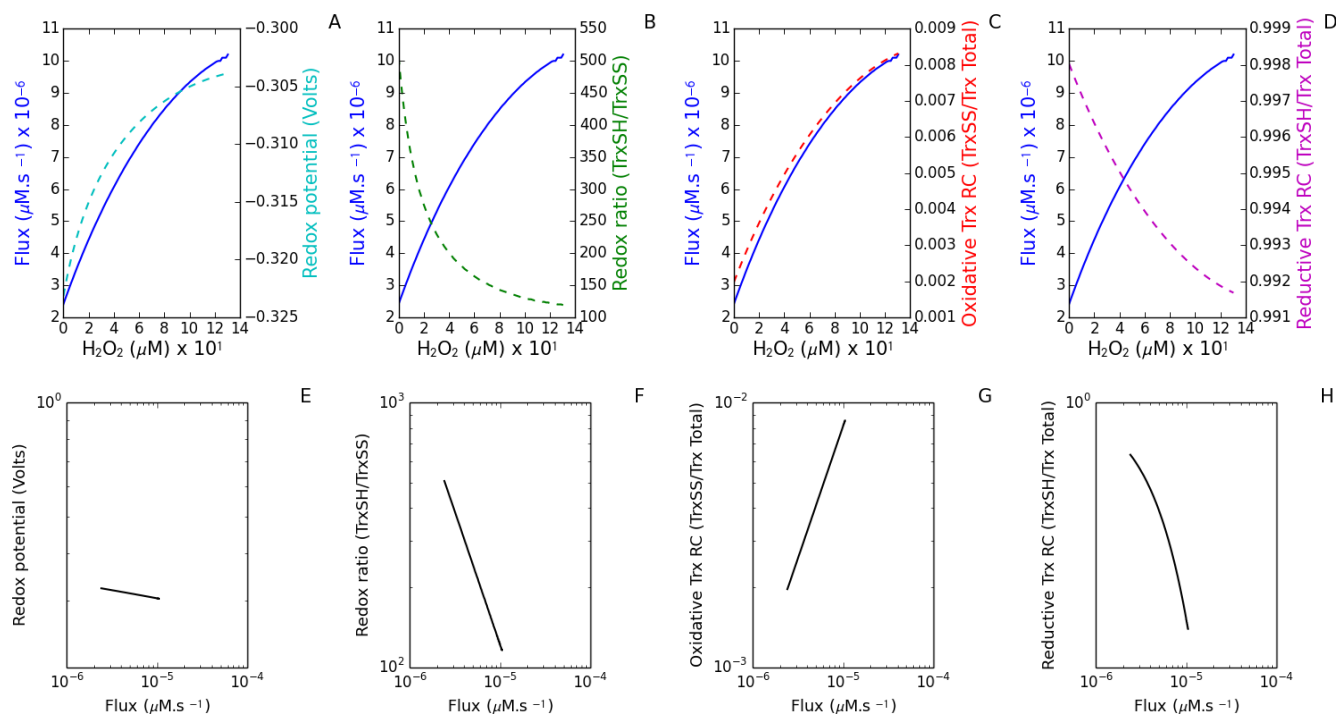


Figure 4.14 A realistic model of the *in vivo* oxidation of *S. pombe* peroxiredoxin supported the use of the thioredoxin redox charge as a surrogate measure for flux. Plots with the flux (blue) and redox potential (cyan, A), redox ratio (TrxSH/TrxSS) (green, B), oxidative thioredoxin redox charge (TrxSS/Trx Total) (red, C) and reductive thioredoxin redox charge (TrxSH/Trx Total) (magenta, D) were generated with varying concentrations of H_2O_2 . Co-response plots were then generated (E-H) using this respective data.

4.5 Discussion

Several measures including Trx and thioredoxin reductase specific activities (Lovell *et al.*, 2000) cellular Trx redox potentials (Watson *et al.*, 2003) and redox ratios (Nkabyo *et al.*, 2002, Trotter and Grant, 2003, Watson and Jones, 2003) have all been used to describe the thioredoxin system *in vitro* and *in vivo*. Although these measures are informative, the connectivity, interactions and ultimately the complexity of the Trx network deem the measurement of individual constituents within the network insufficient as they cannot describe the emergent behaviour of the integrated system. A *system* measure such as flux could provide a comprehensive and integrated measure of the reductive supply and oxidative demand activities on the system.

Currently, *in vitro* assays determine the flux by monitoring the rate of NADPH oxidation (Chapter 3) but this approach is not practical *in vivo* which prompted a search for a surrogate

measure for flux. In addition to the existing measures of the Trx system, a novel measure, the thioredoxin redox charge analogous to the energy charge index (equation 4.1) was tested as a surrogate measure for flux.

$$\text{Energy charge} = \frac{ATP + \frac{1}{2} ADP}{[ATP] + [ADP] + [AMP]} \quad (4.1)$$

where ATP represents adenosine triphosphate, ADP is adenosine diphosphate and AMP is adenosine monophosphate, also known as 5'-adenylic acid.

The energy charge provides a quantitative measure for the energetic state of a biological system (Atkinson and Walton, 1967) and depends on the individual concentrations of ATP, ADP and AMP. This index can have a value ranging from 0 if only AMP is present to 1 if all the AMP is converted to ATP and is mechanistically based on the adenylate kinase equilibrium (Metzler and Metzler, 2001). Similarly, the thioredoxin redox charge, based on the mechanism of saturation in the Trx system, represents a quantitative measure for the flux and can also have a value ranging between 0 and 1.

A core model of the *E. coli* Trx system (Pillay *et al.*, 2011) was analyzed to determine how each of the measures of the Trx system corresponded to the flux under varying reductive supplies (thioredoxin reductase or NADPH) and oxidative demands (peroxiredoxin or hydrogen peroxide) (Figure 4.2-4.3) and revealed that the reductive thioredoxin charge and the oxidative thioredoxin charge corresponded to the flux under these conditions, respectively. A surprising correlation between the redox potential and the flux was also observed. Several studies have questioned the relevance of this measure as it only describes the electrochemical potential of a given reaction but not whether that reaction is kinetically relevant (Flohé, 2010, Flohé, 2013, Pillay *et al.*, 2013). The modeling results showed that this unexpected correlation was due to the logarithmic transformation of redox ratio dataset (Figure 4.4).

To determine the quantitative relationship between each of the measures and the flux through the system, co-response plots were generated (Figure 4.5) which revealed a quasi-linear relationship between the oxidative thioredoxin charge and the flux when the system was experiencing oxidative demand. As the system's flux was perturbed by varying the

NADPH or thioredoxin reductase concentration, the reductive thioredoxin redox charge corresponded to the flux within limits determined by the complete saturation of the Tpx redox cycle. However for most applications, this limit would not be breached for an extended period as it is a consequence of a very high hydrogen peroxide load which would result in cell death. Promisingly, the reductive thioredoxin redox charge could be highly applicable in thioredoxin reductase inhibition studies as it showed a quasi-linear correlation to the flux under conditions that limited the Trx supply (Figure 4.6).

As these modeling results could be tested *in vitro*, oxidative demand and reductive supply assays as well as western blot analysis using Trx specific antibodies (Figure 4.8) were performed and the utility of the thioredoxin redox charge as a surrogate measure for flux was shown (Figure 4.9-4.12). Further, comprehensive realistic models of the red blood cell (Benfeitás *et al.*, 2014) and *S. pombe* (Tomalin *et al.*, 2016) were also simulated with increasing concentrations of hydrogen peroxide (Figure 4.13-4.14) which confirmed the general applicability of the thioredoxin redox charge as a surrogate measure of flux.

However, three limitations with the thioredoxin redox charge have been identified by this analysis. First, using this measure, concurrent perturbations in both the supply and demand cannot be individually tracked as the oxidative thioredoxin redox charge or the reductive thioredoxin charge measures the net overall change in the Trx system. The thioredoxin redox charge can only give a global measure of changes to flux in the Trx system. Second, at the upper limits of the reductive supply or the oxidative demand, the demand or supply cycle respectively can become saturated resulting in changes to the thioredoxin redox charge with no corresponding changes to the flux. However, it is unlikely that the *in vivo* reductive supply would be increased for an extended period as the flux through the pentose phosphate pathway can be dissipated to other reactions to reduce NADPH production. On the other hand, very high oxidative demands cause peroxiredoxin inactivation by hyperoxidation in eukaryotes (Poole and Nelson, 2008, Day *et al.*, 2012, Collins *et al.*, 2016) which preserves the Trx redox poise (Day *et al.*, 2012). Thus, in these cells, the oxidative thioredoxin redox charge can still follow changes in the flux even under oxidative stress conditions which was shown in our modeling results (Figure 4.13-4.14). Third, while the thioredoxin charge cannot give a quantitative value to the thioredoxin system flux *in vivo*, it can be used to track changes in this flux due to supply or demand perturbations.

This work has a number of major applications in the field of redox biology. An advantage of the thioredoxin redox charge, compared to the redox potential and the redox ratio is that the normalization against the total thioredoxin concentration ensures that the redox charge is bounded between zero and one allowing for comparative analyses between systems. This measure therefore provides quantitative information that is directly comparable across laboratories. Further, from a technical standpoint this normalization approach also reduces ‘in gel’ variability as the measure is normalized against the concentration of protein loaded in each lane. In addition, as the thioredoxin redox charge represents a *system* measure, a similar approach could be adopted for the analysis and quantification of other redoxin systems *in vivo* allowing for the role of redoxin networks in pathologies to be quantified. Notably as the thioredoxin redox charge follows changes in the flux through the system, it can be used as an independent method to confirm and validate perturbations in flux obtained through computational model data-fitting experiments. Finally, as this measure represents a surrogate measure for flux, it may be very useful for clinical/therapeutic studies of the Trx system which currently measure a large number of disparate parameters in order to obtain information on the system as a whole (Du *et al.*, 2012, Lu *et al.*, 2013, Jortzik *et al.*, 2014, Raninga *et al.*, 2015, Metcalfe *et al.*, 2016).

Chapter 5: Conclusion

“When you can measure what you are speaking about, and express it in numbers, you know something about it” -Lord Kelvin

5.1 General discussion

The Trx system is the primary electron donor to several biosynthetic enzymes including ribonucleotide reductase, methionine sulfoxide reductase, and sulfate reductases, and reduces inter- and intramolecular disulfide bonds in oxidized proteins. It also serves a critical function in oxidative stress response in many organisms (Lu and Holmgren, 2014) by reducing deleterious disulfide bonds in oxidatively-damaged proteins and by reducing hydrogen peroxide scavengers such as peroxiredoxins. This system also regulates gene expression and cell signalling in bacteria, plants and mammals (Arnér and Holmgren, 2000b) and plays a role in the pathology of HIV and *Mycobacterium tuberculosis* (Akif *et al.*, 2008, Stantchev *et al.*, 2012, Lin *et al.*, 2016).

Given the ubiquitous distribution and importance of Trx, the properties and functions of the system have been intensely investigated using molecular cell biology tools such as gene knockouts, proteomics, redox probes as well as enzyme kinetic approaches (Chapter 1). Although these methods have provided several insights into the biochemical properties and cellular functions of Trx, these methods have been limited at elucidating the emergent or system-dependant properties of the Trx system, and its multiple interactions with several cellular processes (Chapter 1). These limitations stimulated the development of computational modeling as a powerful complementary tool to conventional molecular biology and kinetic studies and several models of the Trx system and related redoxin systems have been developed, providing insights into key processes such as hydrogen peroxide metabolism and sensitivities within these networks (Figure 5.1).

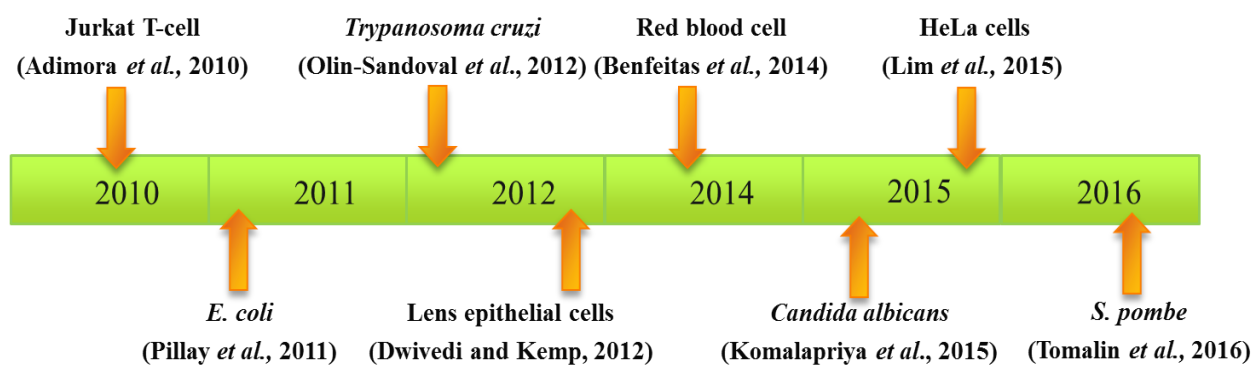


Figure 5.1 A timeline of the computational models of redoxin systems. Several computational models have been developed to elucidate the behavior of redoxin networks in Jurkat T-cells (Adimora *et al.*, 2010), the red blood cell (Benfeitas *et al.*, 2014), HeLa (Lim *et al.*, 2015) and lens epithelial cells (Dwivedi and Kemp, 2012) as well as *E. coli* (Pillay *et al.*, 2011), *Trypanosoma cruzi* (Olin-Sandoval *et al.*, 2012), *Candida albicans* (Komalapriya *et al.*, 2015) and *S. pombe* (Tomalin *et al.*, 2016).

In general, computational modeling is used for hypothesis and behavioural testing, generating new insights, and inspiring new approaches (Brodland, 2015). Modeling also permits tasks that are not experimentally feasible. For example, unlike physical experiments, computational modeling allows for an arbitrary number of experiments to be run from identical starting configurations and also allows for manipulations of arbitrary or user-defined magnitudes which might not be possible in conventional experimental systems. Further, modeling of *in vivo* systems can eliminate cell to cell variation if desired and more importantly for redox biology, modeling enables emergent and system level properties such as flux to be quantified through data fitting experiments. However obtaining this data depends on the generation and use of accurate kinetic models and in this regard, the analyses of redoxin systems (thioredoxin, glutaredoxin and peroxiredoxin) have been limited by the ambiguous descriptions of redoxin activity. For example, the glutaredoxin system is important in the glutathionylation/deglutathionylation process where protein thiols may be glutathionylated under oxidative stress conditions, and glutaredoxin activity is important for restoring the functions of these proteins (Rouhier *et al.*, 2004, Dalle-Donne *et al.*, 2009, Meyer *et al.*, 2009). The kinetic mechanism used by glutaredoxins for deglutathionylation was unclear as a monothiol and a dithiol mechanism have both been proposed for glutaredoxin activity which complicated the modeling of this system (Pillay *et al.*, 2013). Discrepancies on how peroxiredoxins should be described in computational modeling studies have also been identified with peroxiredoxins being characterized as enzymes, with either

ping-pong or mass action kinetics while in other studies peroxiredoxins have been modelled as redox couples (Figure 5.1). This is a central problem for redox systems biology as the choice of kinetic expressions for redoxins in these models can affect the models' properties and outputs for the same set of input parameters (Mashamaite *et al.*, 2015, Padayachee and Pillay, 2016, Pillay *et al.*, 2016).

Similarly Trx has also been ambiguously described as both a redox couple and as an enzyme (Chapter 3). As the Trx system plays a critical role in several processes and is widely used in computational modeling experiments (Figure 5.1), it was essential to confirm the kinetic mechanism of this system for its application in systems biology studies. Using computational modeling and *in vitro* kinetics, it was confirmed that substrate saturation in the thioredoxin system was due to a limitation in the Trx redox cycle and that Michaelis-Menten parameters widely used to describe Trx activity are inappropriate (Chapter 3). This result was significant as it validated the computational and theoretical modeling approaches that have already modeled Trx as a redox couple (Figure 5.1).

These confirmatory experiments also enabled an independent and experimentally tractable surrogate measure for flux to be proposed. Although data fitting experiments used for flux estimation are useful, it has been shown that even dissimilar computational models can fit a dataset. For example, in this study it was shown that the redox couple and enzyme model both showed excellent fits ($r^2 \geq 0.996$) to a previously published *in vitro* insulin reduction dataset (Chapter 3). Therefore having an independent measure could enable confirmation of the flux responses obtained from fitted models and the thioredoxin redox charge represents such an advance. Notably as the thioredoxin redox charge is bounded between zero and one, comparative analyses between conditions or cell types are possible. This may be useful in inhibition studies as this single measure can comparatively test the effect of several inhibitors of the Trx system where a decrease in the reductive thioredoxin redox charge represents a more effective inhibitor. Additionally, given the homology between thioredoxins, glutaredoxins and peroxiredoxins, this measure will encourage further theoretical and experimental systems biology analyses to quantify other redoxin networks *in vivo*.

5.2 Future work

In addition to the thioredoxin redox charge being used to confirm flux perturbations obtained from modeling experiments described above, this measure represents an independent and experimentally tractable approach to derive comparative quantitative information on the Trx system. However, before this measure can be generally accepted, *in vivo* validation is required. Once completed, this will allow for the reanalysis of thioredoxin redox western blotting datasets obtained from previous studies (see for example (Trotter and Grant, 2003, Sobhakumari *et al.*, 2012, Ungerstedt *et al.*, 2012)) which could lead to new insights into these processes.

Although redox western blotting is widely used for quantifying protein redox states, this technique is semi-quantitative as it provides a relative comparison of protein levels, but not an absolute measure of quantity (Mahmood and Yang, 2012). On the other hand, ELISA offers several advantages compared to conventional redox western blotting including reproducibility and efficiency as the need for protein separation by electrophoresis is eliminated. The analysis of a large number of samples within a single run is also possible. The modification of the ELISA method (Potamitou *et al.*, 2002, Lundberg *et al.*, 2014, Fan *et al.*, 2016) to specifically determine the thioredoxin redox charge *in vitro* and *in vivo* would be extremely beneficial as it can be scaled to improve throughput and therefore the role of Trx in pathologies can more readily be explored. However, it should be noted that several limitations have been associated with antibody-based methods. More than 50% of commercially available antibodies are of poor quality and poor validation of these antibodies has shown to compromise experimental results. Additionally, the secondary antibody used affects the signal intensity of the target protein (Gilda *et al.*, 2015). In cases where antibodies cannot be produced, mass spectrometry, which has been used for the identification and characterization of proteins could serve as an alternate method (Clarke *et al.*, 2016).

5.3 Final remarks

The results presented within this thesis represent two important contributions for redox biology. First, the characterization of Trx activity in systems biology applications has been settled and provides a foundation for further systems biology analyses of the Trx network. Second, a novel, independent and experimentally tractable surrogate measure for flux through

the Trx system has been proposed and may play an important role in precisely quantifying changes in this *system* associated with pathological conditions.

References

- Adimora, N. J., Jones, D. P. & Kemp, M. L. 2010. A model of redox kinetics implicates the thiol proteome in cellular hydrogen peroxide responses. *Antioxidants and Redox Signaling*, 13, 731-743.
- Aebersold, R. 2003. A mass spectrometric journey into protein and proteome research. *Journal of the American Society for Mass Spectrometry*, 14, 685-695.
- Aebersold, R., Griffin, T. J. & Donohoe, S. 2007. Isotope-Coded Affinity Tagging of Proteins. *Cold Spring Harbor Protocols*, 2007, pdb.prot4728.
- Ahrens, T. D., Timme, S., Ostendorp, J., Bogatyreva, L., Hoepfner, J., Hopt, U. T., Hauschke, D., Werner, M. & Lassmann, S. 2015. Response of esophageal cancer cells to epigenetic inhibitors is mediated via altered thioredoxin activity. *Lab Invest.*
- Akerman, S. E. & Müller, S. 2003. 2-Cys peroxiredoxin PfTrx-Px1 is involved in the antioxidant defence of *Plasmodium falciparum*. *Molecular and Biochemical Parasitology* 130, 75-81.
- Akerman, S. E. & Müller, S. 2005. Peroxiredoxin-linked Detoxification of Hydroperoxides in *Toxoplasma gondii*. *Journal of Biological Chemistry*, 280, 564-570.
- Akif, M., Khare, G., Tyagi, A. K., Mande, S. C. & Sardesai, A. A. 2008. Functional studies of multiple thioredoxins from *Mycobacterium tuberculosis*. *Journal of Bacteriology*, 190, 7087-7095.
- Alger, H. M., Sayed, A. A., Stadecker, M. J. & Williams, D. L. 2002. Molecular and enzymatic characterisation of *Schistosoma mansoni* thioredoxin. *International Journal for Parasitology*, 32, 1285-1292.
- Arner, E. S. & Holmgren, A. 2006. The thioredoxin system in cancer-introduction to a thematic volume of Seminars in Cancer Biology. *Seminars in Cancer Biology*, 16, 419.
- Arner, E. S. J. & Holmgren, A. 2000a. Measurement of thioredoxin and thioredoxin reductase. *Current Protocols in Toxicology*
- Arner, E. S. J. & Holmgren, A. 2000b. Physiological functions of thioredoxin and thioredoxin reductase. *European Journal of Biochemistry* 267, 6102-6109.
- Arodin, L., Lamparter, H., Karlsson, H., Nennesmo, I., Björnstedt, M., Schröder, J. & Fernandes, A. P. 2014. Alteration of thioredoxin and glutaredoxin in the progression of Alzheimer's disease. *Journal of Alzheimers disease*, 39, 787-797.

- Atkinson, D. E. & Walton, G. M. 1967. Adenosine triphosphate conservation in metabolic regulation: Rat liver citrate cleavage enzyme. *Journal of Biological Chemistry*, 242, 3239-3241.
- Baker, L. M. S., Raudonikiene, A., Hoffman, P. S. & Poole, L. B. 2001. Essential Thioredoxin-Dependent Peroxiredoxin System from *Helicobacter pylori*: Genetic and Kinetic Characterization. *Journal of Bacteriology*, 183, 1961-1973.
- Balmer, Y., Vensel, W. H., Tanaka, C. K., Hurkman, W. J., Gelhaye, E., Rouhier, N., Jacquot, J.-P., Manieri, W., Schürmann, P., Droux, M. & Buchanan, B. B. 2004. Thioredoxin links redox to the regulation of fundamental processes of plant mitochondria. *Proceedings of the National Academy of Sciences of the United States of America*, 101, 2642-2647.
- Bao, R., Zhang, Y., Zhou, C.-Z. & Chen, Y. 2009. Structural and mechanistic analyses of yeast mitochondrial thioredoxin Trx3 reveal putative function of its additional cysteine residues. *Biochimica et Biophysica Acta (BBA) - Proteins & Proteomics*, 1794, 716-721.
- Barranco-Medina, S., Lázaro, J.-J. & Dietz, K.-J. 2009. The oligomeric conformation of peroxiredoxins links redox state to function. *FEBS Letters*, 583, 1809-1816.
- Benfeitas, R., Selvaggio, G., Antunes, F., Coelho, P. M. B. M. & Salvador, A. 2014. Hydrogen peroxide metabolism and sensing in human erythrocytes: A validated kinetic model and reappraisal of the role of peroxiredoxin II. *Free Radical Biology and Medicine*, 74, 35-49.
- Berg, J. M., Tymoczko, J. L. & Stryer, L. 2002. *Biochemistry*, New York, W. H. Freeman and Company.
- Berggren, M., Gallegos, A., Gasdaska, J. R., Gasdaska, P. Y., Warneke, J. & Powis, G. 1996. Thioredoxin and thioredoxin reductase gene expression in human tumors and cell lines, and the effects of serum stimulation and hypoxia. *Anticancer Research*, 16, 3459-3466.
- Biewenga, G. P., Dorstijn, M. A., Verhagen, J. V., Haenen, G. R. M. M. & Bast, A. 1996. Reduction of lipoic acid by lipoamide dehydrogenase. *Biochemical Pharmacology*, 51, 233-238.
- Biran, S., Gat, Y. & Fass, D. 2014. The Eps1p Protein Disulfide Isomerase Conserves Classic Thioredoxin Superfamily Amino Acid Motifs but Not Their Functional Geometries. *PLoS ONE*, 9, e113431.

- Brigelius, R., Muckel, C., Akerboom, T. P. M. & Sies, H. 1983. Identification and quantitation of glutathione in hepatic protein mixed disulfides and its relationship to glutathione disulfide. *Biochemical Pharmacology*, 32, 2529-2534.
- Brodland, G. W. 2015. How computational models can help unlock biological systems. *Seminars in Cell & Developmental Biology*, 47–48, 62-73.
- Brown, Jonathon d., Day, Alison m., Taylor, Sarah r., Tomalin, Lewis e., Morgan, Brian a. & Veal, Elizabeth a. 2013. A Peroxiredoxin Promotes H₂O₂ Signaling and Oxidative Stress Resistance by Oxidizing a Thioredoxin Family Protein. *Cell Reports*, 5, 1425-1435.
- Burke-Gaffney, A., Callister, M. E. J. & Nakamura, H. 2005. Thioredoxin: friend or foe in human disease? *Trends in Pharmacological Sciences*, 26, 398-404.
- Butterfield, D. A., Perluigi, M. & Sultana, R. 2006. Oxidative stress in Alzheimer's disease brain: New insights from redox proteomics. *European Journal of Pharmacology*, 545, 39-50.
- Cai, W., Zhang, L., Song, Y., Wang, B., Zhang, B., Cui, X., Hu, G., Liu, Y., Wu, J. & Fang, J. 2012. Small molecule inhibitors of mammalian thioredoxin reductase. *Free Radical Biology and Medicine*, 52, 257-265.
- Cao, Z., Bhella, D. & Lindsay, J. G. 2007. Reconstitution of the Mitochondrial PrxIII Antioxidant Defence Pathway: General Properties and Factors Affecting PrxIII Activity and Oligomeric State. *Journal of Molecular Biology*, 372, 1022-1033.
- Chang, A., Scheer, M., Grote, A., Schomburg, I. & Schomburg, D. 2009. BRENDA, AMENDA and FRENDA the enzyme information system: new content and tools in 2009. *Nucleic Acids Research* 37, D588-D592.
- Chen, Y.-T., Hong, P.-F., Wen, L. & Lin, C.-T. 2014. Molecular cloning and characterization of a thioredoxin from Taiwanofungus camphorata. *Botanical Studies*, 55, 1-8.
- Chibani, K., Tarrago, L., Schürmann, P., Jacquot, J.-P. & Rouhier, N. 2011. Biochemical properties of poplar thioredoxin z. *FEBS Letters*, 585, 1077-1081.
- Clarke, D. J., Murray, E., Faktor, J., Mohtar, A., Vojtesek, B., Mackay, C. L., Smith, P. L. & Hupp, T. R. 2016. Mass spectrometry analysis of the oxidation states of the pro-oncogenic protein anterior gradient-2 reveals covalent dimerization via an intermolecular disulphide bond. *Biochimica et Biophysica Acta (BBA) - Proteins and Proteomics*, 1864, 551-561.
- Collet, J.-F. & Messens, J. 2010. Structure, Function, and Mechanism of thioredoxin proteins. *Antioxidants and redox signaling*, 13, 1205-1216.

- Collins, J. A., Wood, S. T., Nelson, K. J., Rowe, M. A., Carlson, C. S., Chubinskaya, S., Poole, L. B., Furdai, C. M. & Loeser, R. F. 2016. Oxidative Stress Promotes Peroxiredoxin Hyperoxidation and Attenuates Pro-survival Signaling in Aging Chondrocytes. *Journal of Biological Chemistry*, 291, 6641-6654.
- Cumming, R. C., Andon, N. L., Haynes, P. A., Park, M., Fischer, W. H. & Schubert, D. 2004. Protein Disulfide Bond Formation in the Cytoplasm during Oxidative Stress. *Journal of Biological Chemistry*, 279, 21749-21758.
- Cunniff, B., Snider, G. W., Fredette, N., Hondal, R. J. & Heintz, N. H. 2013. A direct and continuous assay for the determination of thioredoxin reductase activity in cell lysates. *Analytical Biochemistry*, 443, 10.1016/j.ab.2013.08.013.
- D'autreaux, B. & Toledano, M. B. 2007. ROS as signalling molecules: mechanisms that generate specificity in ROS homeostasis. *Nature Reviews Molecular Cell Biology* 8, 813-824.
- Da Silva Dantas, A., Patterson, M. J., Smith, D. A., Maccallum, D. M., Erwig, L. P., Morgan, B. A. & Quinn, J. 2010. Thioredoxin Regulates Multiple Hydrogen Peroxide-Induced Signaling Pathways in *Candida albicans*. *Molecular and Cellular Biology*, 30, 4550-4563.
- Dalle-Donne, I., Rossi, R., Colombo, G., Giustarini, D. & Milzani, A. 2009. Protein S-glutathionylation: a regulatory device from bacteria to humans. *Trends in biochemical sciences*, 34, 85-96.
- Das, K. C. & Das, C. K. 2000. Thioredoxin, a Singlet Oxygen Quencher and Hydroxyl Radical Scavenger: Redox Independent Functions. *Biochemical and Biophysical Research Communications*, 277, 443-447.
- Das, K. C., Guo, X.-L. & White, C. W. 1999. Induction of thioredoxin and thioredoxin reductase gene expression in lungs of newborn primates by oxygen. *American Journal of Physiology - Lung Cellular and Molecular Physiology*, 276, L530-L539.
- Day, A. M., Brown, J. D., Taylor, S. R., Rand, J. D., Morgan, B. A. & Veal, E. A. 2012. Inactivation of a Peroxiredoxin by Hydrogen Peroxide Is Critical for Thioredoxin-Mediated Repair of Oxidized Proteins and Cell Survival. *Molecular Cell*, 45, 398-408.
- Demple, B., Herman, T. & Chen, D. S. 1991. Cloning and expression of APE, the cDNA encoding the major human apurinic endonuclease: definition of a family of DNA repair enzymes. *Proceedings of the National Academy of Sciences of the United States of America*, 88, 11450-11454.

- Dennison, C. 2003. *A guide to protein isolation*, Netherlands, Kluwer academic publishers.
- Depuydt, M., Leonard, S. E., Vertommen, D., Denoncin, K., Morsomme, P., Wahni, K., Messens, J., Carroll, K. S. & Collet, J.-F. 2009. A Periplasmic Reducing System Protects Single Cysteine Residues from Oxidation. *Science*, 326, 1109-1111.
- Dey, P. M. & Harborne, J. B. 1997. *Plant Biochemistry*, Academic Press.
- Du, Y., Zhang, H., Lu, J. & Holmgren, A. 2012. Glutathione and Glutaredoxin Act as a Backup of Human Thioredoxin Reductase 1 to Reduce Thioredoxin 1 Preventing Cell Death by Aurothioglucose. *The Journal of Biological Chemistry*, 287, 38210-38219.
- Dwivedi, G. & Kemp, M. L. 2012. Systemic Redox Regulation of Cellular Information Processing. *Antioxidants and redox signaling*, 16, 374-380.
- Eagling, B. D. 2015. *Modelling and analysis of peroxiredoxin kinetics for systems biology applications*. MSc, University of KwaZulu-Natal.
- Fan, C., Zheng, W., Fu, X., Li, X., Wong, Y. S. & Chen, T. 2014. Enhancement of auranofin-induced lung cancer cell apoptosis by selenocystine, a natural inhibitor of TrxR1 in vitro and in vivo. *Cell Death & Disease*, 5, e1191.
- Fan, J., Yu, H., Lv, Y. & Yin, L. 2016. Diagnostic and prognostic value of serum thioredoxin and DJ-1 in non-small cell lung carcinoma patients. *Tumor Biology*, 37, 1949-1958.
- Feng, C., Wang, H., Lu, N., Chen, T., He, H., Lu, Y. & Tu, X. M. 2014. Log-transformation and its implications for data analysis. *Shanghai Archives of Psychiatry*, 26, 105-109.
- Flohé, L. 2010. Chapter 1 - Changing Paradigms in Thiology: From Antioxidant Defense Toward Redox Regulation. In: ENRIQUE, C. & LESTER, P. (eds.) *Methods in Enzymology*. Academic Press.
- Flohé, L. 2013. The fairytale of the GSSG/GSH redox potential. *Biochimica et Biophysica Acta (BBA) - General Subjects*, 1830, 3139-3142.
- Frijhoff, J., Winyard, P. G., Zarkovic, N., Davies, S. S., Stocker, R., Cheng, D., Knight, A. R., Taylor, E. L., Oettrich, J., Ruskovska, T., Gasparovic, A. C., Cuadrado, A., Weber, D., Poulsen, H. E., Grune, T., Schmidt, H. H. H. W. & Ghezzi, P. 2015. Clinical Relevance of Biomarkers of Oxidative Stress. *Antioxidants and redox signaling*, 23, 1144-1170.
- Fujino, G., Noguchi, T., Takeda, K. & Ichijo, H. 2006. Thioredoxin and protein kinases in redox signaling. *Seminars in Cancer Biology*, 16, 427-435.
- Gasdaska, P. Y., Gasdaska, J. R., Cochran, S. & Powis, G. 1995. Cloning and sequencing of a human thioredoxin reductase. *FEBS Letters*, 373, 5-9.

- Gasdaska, P. Y., Oblong, J. E., Cotgreave, I. A. & Powis, G. 1994. The predicted amino acid sequence of human thioredoxin is identical to that of the autocrine growth factor human adult T-cell derived factor (ADF): Thioredoxin mRNA is elevated in some human tumors. *Biochimica et Biophysica Acta (BBA) - Gene Structure and Expression*, 1218, 292-296.
- Gilda, J. E., Ghosh, R., Cheah, J. X., West, T. M., Bodine, S. C. & Gomes, A. V. 2015. Western Blotting Inaccuracies with Unverified Antibodies: Need for a Western Blotting Minimal Reporting Standard (WBMRS). *PLoS ONE*, 10, e0135392.
- Gleason, F. K., Lim, C. J., Gerami-Nejad, M. & Fuchs, J. A. 1990. Characterization of Escherichia coli thioredoxins with altered active site residues. *Biochem*, 29, 3701-3709.
- Go, Y.-M. & Jones, D. P. 2001. Thioredoxin Redox Western Analysis. *Current Protocols in Toxicology*. John Wiley & Sons, Inc.
- Go, Y.-M. & Jones, D. P. 2013. The redox proteome. *The Journal of Biological Chemistry*, 288, 26512-26520.
- Goldring, J. P. D. & Coetzer, T. H. T. 2003. Isolation of chicken immunoglobulins (IgY) from egg yolk*. *Biochemistry and Molecular Biology Education*, 31, 185-187.
- Gorlatov, S. N. & Stadtman, T. C. 1998. Human thioredoxin reductase from HeLa cells: Selective alkylation of selenocysteine in the protein inhibits enzyme activity and reduction with NADPH influences affinity to heparin. *Proceedings of the National Academy of Sciences of the United States of America*, 95, 8520-8525.
- Grimaldi, P., Ruocco, M., Lanzotti, M., Ruggiero, A., Ruggiero, I., Arcari, P., Vitagliano, L. & Masullo, M. 2008. Characterisation of the components of the thioredoxin system in the archaeon *Sulfolobus solfataricus*. *Extremophiles*, 12, 553-562.
- Grogan, T. M., Fenoglio-Prieser, C., Zeheb, R., Bellamy, W., Frutiger, Y., Vela, E., Stemmerman, G., Macdonald, J., Richter, L., Gallegos, A. & Powis, G. 2000. Thioredoxin, a putative oncogene product, is overexpressed in gastric carcinoma and associated with increased proliferation and increased cell survival. *Human Pathology*, 31, 475-481.
- Gygi, S. P., Rist, B., Gerber, S. A., Turecek, F., Gelb, M. H. & Aebersold, R. 1999. Quantitative analysis of complex protein mixtures using isotope-coded affinity tags. *Nature Biotechnology*, 17, 994-999.

- Halvey, P. J., Watson, W. H., Hansen, J. M., Go, Y.-M., Samali, A. & Jones, D. P. 2005. Compartmental oxidation of thiol–disulphide redox couples during epidermal growth factor signalling. *Biochemical Journal*, 386, 215-219.
- Hansen, J. M., Zhang, H. & Jones, D. P. 2006. Differential oxidation of thioredoxin-1, thioredoxin-2, and glutathione by metal ions. *Free radical biology and medicine*, 40, 138-45.
- Hansen, R. E. & Winther, J. R. 2009. An introduction to methods for analyzing thiols and disulfides: Reactions, reagents, and practical considerations. *Analytical Biochemistry*, 394, 147-158.
- Harju, S., Fedosyuk, H. & Peterson, K. 2004. Rapid isolation of yeast genomic DNA: Bust n' Grab. *BMC Biotechnology*, 4, 8.
- Harman, D. 1956. Aging: A Theory Based on Free Radical and Radiation Chemistry. *Journal of Gerontology*, 11, 298-300.
- Hawkes, H.-J. K., Karlenius, T. C. & Tonissen, K. F. 2014. Regulation of the human thioredoxin gene promoter and its key substrates: A study of functional and putative regulatory elements. *Biochimica et Biophysica Acta (BBA) - General Subjects*, 1840, 303-314.
- Hedström, E., Eriksson, S., Zawacka-Pankau, J., Arnér, E. S. & Selivanova, G. 2009. p53-dependent inhibition of TrxR1 contributes to the tumor-specific induction of apoptosis by RITA. *Cell cycle*, 8, 3584-3591.
- Heuck, A. P. & Wolosiuk, R. A. 1997a. Di-fluoresceinthiocarbamyl-insulin: A Fluorescent Substrate for the Assay of Protein Disulfide Oxidoreductase Activity. *Analytical Biochemistry*, 248, 94-101.
- Heuck, A. P. & Wolosiuk, R. A. 1997b. Fluoresceinthiocarbamyl-insulin: A potential analytical tool for the assay of disulfide bond reduction. *Journal of Biochemical and Biophysical Methods* 34, 213-225.
- Hirt, R. P., Müller, S., Martin Embley, T. & Coombs, G. H. 2002. The diversity and evolution of thioredoxin reductase: new perspectives. *TRENDS in Parasitology*, 18, 302-308.
- Hofmeyr, J.-H. S. 1995. Metabolic regulation: A control analytic perspective. *Journal of Bioenergetics and Biomembranes*, 27, 479-490.
- Hofmeyr, J.-H. S. & Cornish-Bowden, A. 2000. Regulating the cellular economy of supply and demand. *FEBS Letters*, 476, 47-51.

- Holden, P. & Horton, W. A. 2009. Crude subcellular fractionation of cultured mammalian cell lines. *BMC Research Notes*, 2, 243-243.
- Holmgren, A. 1979a. Reduction of disulfides by thioredoxin. Exceptional reactivity of insulin and suggested functions of thioredoxin in mechanism of hormone action. *Journal of Biological Chemistry*, 254, 9113-9119.
- Holmgren, A. 1979b. Thioredoxin catalyzes the reduction of insulin disulfides by dithiothreitol and dihydrolipoamide. *Journal of Biological Chemistry*, 254, 9627-9632.
- Holmgren, A. 1985. Thioredoxin. *Annual Review of Biochemistry*, 54, 237-271.
- Holmgren, A. 1995. Thioredoxin structure and mechanism: conformational changes on oxidation of the active-site sulfhydryls to a disulfide. *Structure*, 3, 239-243.
- Holmgren, A. & Bjornstedt, M. 1995. Thioredoxin and thioredoxin reductase. *Methods in Enzymology*, 252, 199-208.
- Holmgren, A. & Lu, J. 2010. Thioredoxin and thioredoxin reductase: Current research with special reference to human disease. *Biochemical and Biophysical Research Communications* 396, 120-124.
- Hornberg, J. J., Bruggeman, F. J., Westerhoff, H. V. & Lankelma, J. 2006. Cancer: A Systems Biology disease. *Biosystems*, 83, 81-90.
- Hu, Q. & Wang, G. 2016. Mitochondrial dysfunction in Parkinson's disease. *Translational Neurodegeneration*, 5, 14.
- Hugo, M., Van Laer, K., Reyes, A. M., Vertommen, D., Messens, J., Radi, R. & Trujillo, M. 2014. Mycothiol/Mycoredoxin 1-dependent reduction of the peroxiredoxin AhpE from *Mycobacterium tuberculosis*. *Journal of Biological Chemistry*, 289, 5228-5239.
- Ikeh, M. a. C., Kastora, S. L., Day, A. M., Herrero-De-Dios, C. M., Tarrant, E., Waldron, K. J., Banks, A. P., Bain, J. M., Lydall, D., Veal, E. A., Maccallum, D. M., Erwig, L. P., Brown, A. J. P. & Quinn, J. 2016. Pho4 mediates phosphate acquisition in *Candida albicans* and is vital for stress resistance and metal homeostasis. *Molecular Biology of the Cell*, 27, 2784-2801.
- Jeon, S.-J. & Ishikawa, K. 2002. Identification and characterization of thioredoxin and thioredoxin reductase from *Aeropyrum pernix* K1. *European Journal of Biochemistry*, 269, 5423-5430.
- Ji, H. 2010. Lysis of Cultured Cells for Immunoprecipitation. *Cold Spring Harbor Protocols*, 2010, pdb.prot5466.

- Jiao, J. A., Yee, B. C., Kobrehel, K. & Buchanan, B. B. 1992. Effect of thioredoxin-linked reduction on the activity and stability of the Kunitz and Bowman-Birk soybean trypsin inhibitor protein. *Journal of Agricultural and Food Chemistry* 40, 2333-2336.
- Jones, D. P. 2006. Redefining oxidative stress. *Antioxidants and redox signaling*, 8, 1865-1879.
- Jones, D. P. 2010. Redox sensing: orthogonal control in cell cycle and apoptosis signalling. *J Intern Med*, 268, 432-48.
- Jones, D. P. & Go, Y.-M. 2011. Mapping the cysteine proteome: analysis of redox-sensing thiols. *Current Opinion in Chemical Biology*, 15, 103-112.
- Jones, D. T., Pugh, C. W., Wigfield, S., Stevens, M. F. G. & Harris, A. L. 2006. Novel thioredoxin inhibitors paradoxically increase hypoxia-inducible factor-A expression but decrease functional transcriptional activity, DNA binding, and degradation. *Clinical Cancer Research*, 12, 5384-5394.
- Jortzik, E., Farhadi, M., Ahmadi, R., Tóth, K., Lohr, J., Helmke, B. M., Kehr, S., Unterberg, A., Ott, I., Gust, R., Deborde, V., Davioud-Charvet, E., Réau, R., Becker, K. & Herold-Mende, C. 2014. Antiglioma activity of GoPI-sugar, a novel gold(I)-phosphole inhibitor: Chemical synthesis, mechanistic studies, and effectiveness in vivo. *Biochimica et Biophysica Acta (BBA) - Proteins and Proteomics*, 1844, 1415-1426.
- Josefsen, K. & Nielsen, H. 2011. Northern Blotting Analysis. *In: NIELSEN, H. (ed.) RNA: Methods and Protocols*. Totowa, NJ: Humana Press.
- Joudrier, P., Gautier, M. F., De Lamotte, F. & Kobrehel, K. 2005. The thioredoxin h system: potential applications. *Biotechnology Advances*, 23, 81-85.
- Juttner, J., Olde, D., Langridge, P. & Baumann, U. 2000. Cloning and expression of a distinct subclass of plant thioredoxins. *European Journal of Biochemistry*, 267, 7109-7117.
- Karlenius, T. C. & Tonissen, K. F. 2010. Thioredoxin and Cancer: A Role for Thioredoxin in all States of Tumor Oxygenation. *Cancers*, 2, 209-232.
- Kawahara, N., Tanaka, T., Yokomizo, A., Nanri, H., Ono, M., Wada, M., Kohno, K., Takenaka, K., Sugimachi, K. & Kuwano, M. 1996. Enhanced Coexpression of Thioredoxin and High Mobility Group Protein 1 Genes in Human Hepatocellular Carcinoma and the Possible Association with Decreased Sensitivity to Cisplatin. *Cancer Research*, 56, 5330-5333.

- Kim, J.-A., Park, S., Kim, K., Rhee, S. G. & Kang, S. W. 2005. Activity assay of mammalian 2-cys peroxiredoxins using yeast thioredoxin reductase system. *Analytical Biochemistry*, 338, 216-223.
- Komalapriya, C., Kaloriti, D., Tillmann, A. T., Yin, Z., Herrero-De-Dios, C., Jacobsen, M. D., Belmonte, R. C., Cameron, G., Haynes, K., Grebogi, C., De Moura, A. P. S., Gow, N. a. R., Thiel, M., Quinn, J., Brown, A. J. P. & Romano, M. C. 2015. Integrative Model of Oxidative Stress Adaptation in the Fungal Pathogen *Candida albicans*. *PLoS ONE*, 10, e0137750.
- Kranner, I., Birtić, S., Anderson, K. M. & Pritchard, H. W. 2006. Glutathione half-cell reduction potential: A universal stress marker and modulator of programmed cell death? *Free Radical Biology and Medicine*, 40, 2155-2165.
- Krnajski, Z., Gilberger, T.-W., Walter, R. D. & Müller, S. 2001. The malaria parasite *Plasmodium falciparum* possesses a functional thioredoxin system. *Molecular and Biochemical Parasitology*, 112, 219-228.
- Kumar, J. K., Tabor, S. & Richardson, C. C. 2004. Proteomic analysis of thioredoxin-targeted proteins in *Escherichia coli*. *Proceedings of the National Academy of Sciences of the United States of America*, 101, 3759-3764.
- Le Gal, K., Ibrahim, M. X., Wiel, C., Sayin, V. I., Akula, M. K., Karlsson, C., Dalin, M. G., Akyürek, L. M., Lindahl, P., Nilsson, J. & Bergo, M. O. 2015. Antioxidants can increase melanoma metastasis in mice. *Science Translational Medicine*, 7, 308re8-308re8.
- Lee, M. H., Han, J. H., Lee, J.-H., Choi, H. G., Kang, C. & Kim, J. S. 2012. Mitochondrial Thioredoxin-Responding Off-On Fluorescent Probe. *Journal of the American Chemical Society*, 134, 17314-17319.
- Leichert, L. I. & Jakob, U. 2004. Protein thiol modifications visualized in vivo. *PLoS biology*, 2, e333.
- Li, J., Cheng, Z.-J., Liu, Y., Yan, Z.-L., Wang, K., Wu, D., Wan, X.-Y., Xia, Y., Lau, W. Y., Wu, M.-C. & Shen, F. 2015. Serum thioredoxin is a diagnostic marker for hepatocellular carcinoma. *Oncotarget*, 6, 9551-9563.
- Li, Y., Gong, H., Sun, Y., Yan, J., Cheng, B., Zhang, X., Huang, J., Yu, M., Guo, Y., Zheng, L. & Huang, K. 2012. Dissecting the role of disulfide bonds on the amyloid formation of insulin. *Biochemical and Biophysical Research Communications*, 423, 373-378.
- Lillig, C. H. & Holmgren, A. 2007. Thioredoxin and related molecules—from biology to health and disease. *Antioxidants and redox signaling*, 9, 25-47.

- Lim, H. W. & Lim, C.-J. 1995. Direct reduction of DTNB by *E. coli* thioredoxin reductase. *Journal of Biochemistry and Molecular Biology*, 28, 17-20.
- Lim, J. B., Huang, B. K., Deen, W. M. & Sikes, H. D. 2015. Analysis of the lifetime and spatial localization of hydrogen peroxide generated in the cytosol using a reduced kinetic model. *Free Radical Biology and Medicine*, 89, 47-53.
- Lin, K., O'Brien, K. M., Trujillo, C., Wang, R., Wallach, J. B., Schnappinger, D. & Ehrt, S. 2016. Mycobacterium tuberculosis Thioredoxin Reductase Is Essential for Thiol Redox Homeostasis but Plays a Minor Role in Antioxidant Defense. *PLOS Pathogens*, 12, e1005675.
- Lin, T.-Y. 2010. Protein-protein interaction as a powering source of oxidoreductive reactivity. *Molecular BioSystems* 6, 1454-1462.
- Liu, Y., Duan, D., Yao, J., Zhang, B., Peng, S., Ma, H., Song, Y. & Fang, J. 2014. Dithiaarsanes Induce Oxidative Stress-Mediated Apoptosis in HL-60 Cells by Selectively Targeting Thioredoxin Reductase. *Journal of Medicinal Chemistry*, 57, 5203-5211.
- Liu, Y., Ma, H., Zhang, L., Cui, Y., Liu, X. & Fang, J. 2016. A small molecule probe reveals declined mitochondrial thioredoxin reductase activity in a Parkinson's disease model. *Chemical Communications*, 52, 2296-2299.
- Lopert, P., Day, B. J. & Patel, M. 2012. Thioredoxin Reductase Deficiency Potentiates Oxidative Stress, Mitochondrial Dysfunction and Cell Death in Dopaminergic Cells. *PLoS ONE*, 7, e50683.
- Loscalzo, J. & Barabasi, A.-L. 2011. Systems biology and the future of medicine. John Wiley & Sons, Inc.
- Lothrop, A. P., Snider, G. W., Ruggles, E. L., Patel, A. S., Lees, W. J. & Hondal, R. J. 2014. Selenium as an Electron Acceptor during the Catalytic Mechanism of Thioredoxin Reductase. *Biochemistry*, 53, 654-663.
- Lovell, M. A., Xie, C., Gabbita, S. P. & Markesbery, W. R. 2000. Decreased thioredoxin and increased thioredoxin reductase levels in alzheimer's disease brain. *Free Radical Biology and Medicine*, 28, 418-427.
- Lu, J. & Holmgren, A. 2014. The thioredoxin antioxidant system. *Free Radical Biology and Medicine*, 66, 75-87.
- Lu, J., Papp, L. V., Fang, J., Rodriguez-Nieto, S., Zhivotovsky, B. & Holmgren, A. 2006. Inhibition of Mammalian Thioredoxin Reductase by Some Flavonoids: Implications for Myricetin and Quercetin Anticancer Activity. *Cancer Research*, 66, 4410-4418.

- Lu, J., Vlamis-Gardikas, A., Kandasamy, K., Zhao, R., Gustafsson, T. N., Engstrand, L., Hoffner, S., Engman, L. & Holmgren, A. 2013. Inhibition of bacterial thioredoxin reductase: an antibiotic mechanism targeting bacteria lacking glutathione. *The FASEB Journal*, 27, 1394-1403.
- Lundberg, M., Curbo, S., Reiser, K., Masterman, T., Braesch-Andersen, S., Areström, I. & Ahlberg, N. 2014. Methodological Aspects of ELISA Analysis of Thioredoxin 1 in Human Plasma and Cerebrospinal Fluid. *PLoS ONE*, 9, e103554.
- Luthman, M. & Holmgren, A. 1982. Rat liver thioredoxin and thioredoxin reductase: purification and characterization. *Biochemistry*, 21, 6628-6633.
- Maeda, K., Hägglund, P., Björnberg, O., Winther, J. R. & Svensson, V. 2010. Kinetic and thermodynamic properties of two barley thioredoxin h isozymes, HvTrxh1 and HvTrxh2. *FEBS Lett.*, 584, 3376-3380.
- Mahmood, T. & Yang, P.-C. 2012. Western Blot: Technique, Theory, and Trouble Shooting. *North American Journal of Medical Sciences*, 4, 429-434.
- Makmura, L., Hamann, M., Areopagita, A., Furuta, S., Munoz, A. & Momand, J. 2001. Development of a sensitive assay to detect reversibly oxidized protein cysteine sulfhydryl groups. *Antioxidants and redox signaling*, 3, 1105-1118.
- Manns, J. M. 2005. SDS-Polyacrylamide Gel Electrophoresis (SDS-PAGE) of Proteins. *Current Protocols in Microbiology*. John Wiley & Sons, Inc.
- Mark, D. F. & Richardson, C. C. 1976. *Escherichia coli* thioredoxin: A subunit of bacteriophage T7 DNA polymerase. *Proceedings of the National Academy of Sciences*, 73, 780-784.
- Mashamaite, L. N., Rohwer, J. M. & Pillay, C. S. 2015. The glutaredoxin mono- and di-thiol mechanisms for deglutathionylation are functionally equivalent: implications for redox systems biology. *Bioscience Reports*, 35, e00173.
- Matsuzawa, A. & Ichijo, H. 2008. Redox control of cell fate by MAP kinase: physiological roles of ASK1-MAP kinase pathway in stress signaling. *Biochimica et Biophysica Acta (BBA) - General Subjects*, 1780, 1325-1336.
- Mccord, J. M. & Fridovich, I. 1969a. Superoxide Dismutase: AN ENZYMIC FUNCTION FOR ERYTHROCUPREIN (HEMOCUPREIN). *Journal of Biological Chemistry*, 244, 6049-6055.
- Mccord, J. M. & Fridovich, I. 1969b. The Utility of Superoxide Dismutase in Studying Free Radical Reactions: I. RADICALS GENERATED BY THE INTERACTION OF

- SULFITE, DIMETHYL SULFOXIDE, AND OXYGEN. *Journal of Biological Chemistry*, 244, 6056-6063.
- Mccord, J. M. & Fridovich, I. 1970. The Utility of Superoxide Dismutase in Studying Free Radical Reactions: II. THE MECHANISM OF THE MEDIATION OF CYTOCHROME c REDUCTION BY A VARIETY OF ELECTRON CARRIERS. *Journal of Biological Chemistry*, 245, 1374-1377.
- Metcalf, C., Ramasubramoni, A., Pula, G., Harper, M. T., Mundell, S. J. & Coxon, C. H. 2016. Thioredoxin Inhibitors Attenuate Platelet Function and Thrombus Formation. *PLoS ONE*, 11, e0163006.
- Metzler, D. E. & Metzler, C. M. 2001. *Biochemistry: The chemical reactions of living cells*. 2nd edition ed.: Academic Press.
- Meuillet, E. J., Mahadevan, D., Berggren, M., Coon, A. & Powis, G. 2004. Thioredoxin-1 binds to the C2 domain of PTEN inhibiting PTEN's lipid phosphatase activity and membrane binding: a mechanism for the functional loss of PTEN's tumor suppressor activity. *Archives of Biochemistry and Biophysics*, 429, 123-133.
- Meyer, Y., Buchanan, B. B., Vignols, F. & Reichheld, J. P. 2009. Thioredoxins and glutaredoxins: unifying elements in redox biology. *Annual review of genetics*, 43, 335-367.
- Meyer, Y., Siala, W., Bashandy, T., Riondet, C., Vignols, F. & Reichheld, J. P. 2008. Glutaredoxins and thioredoxins in plants. *Biochimica et Biophysica Acta (BBA) - Molecular Cell Research*, 1783, 589-600.
- Miranda-Vizuet, A., Damdimopoulos, A. E., Gustafsson, J.-Å. & Spyrou, G. 1997. Cloning, expression, and characterization of a novel *Escherichia coli* thioredoxin. *Journal of Biological Chemistry*, 272, 30841-30847.
- Miyazaki, K., Noda, N., Okada, S., Hagiwara, Y., Miyata, M., Sakurabayashi, I., Yamaguchi, N., Sugimura, T., Terada, M. & Wakasugi, H. 1998. Elevated serum level of Thioredoxin in patients with Hepatocellular Carcinoma. *Biotherapy*, 11, 277-288.
- Montano, S. J., Lu, J., Gustafsson, T. N. & Holmgren, A. 2014. Activity assays of mammalian thioredoxin and thioredoxin reductase: Fluorescent disulfide substrates, mechanisms, and use with tissue samples. *Analytical Biochemistry*, 449, 139-146.
- Montrichard, F., Alkhalifioui, F., Yano, H., Vensel, W. H., Hurkman, W. J. & Buchanan, B. B. 2009. Thioredoxin targets in plants: The first 30 years. *Journal of Proteomics*, 72, 452-474.

- Mukherjee, A. & Martin, S. G. 2008. The thioredoxin system: a key target in tumour and endothelial cells. *British Journal of Radiology*, 81, S57-68.
- Mustacich, D. & Powis, G. 2000. Thioredoxin reductase. *Biochemical Journal*, 346, 1-8.
- Nakamura, H., De Rosa, S., Roederer, M., Anderson, M. T., Dubs, J. G., Yodoi, J., Holmgren, A., Herzenberg, L. A. & Herzenberg, L. A. 1996. Elevation of plasma thioredoxin levels in HIV-infected individuals. *International Immunology*, 8, 603-611.
- Nelson, K. J. & Parsonage, D. 2011. Measurement of Peroxiredoxin Activity. *Current Protocols in Toxicology*, 0 7, Unit7.10-Unit7.10.
- Nielsen, J. 2003. It Is All about Metabolic Fluxes. *Journal of Bacteriology*, 185, 7031-7035.
- Nikkanen, L., Toivola, J. & Rintamäki, E. 2016. Crosstalk between chloroplast thioredoxin systems in regulation of photosynthesis. *Plant, Cell & Environment*, 39, 1691-1705.
- Nkabyo, Y. S., Ziegler, T. R., Gu, L. H., Watson, W. H. & Jones, D. P. 2002. Glutathione and thioredoxin redox during differentiation in human colon epithelial (Caco-2) cells. *American journal of physiology. Gastrointestinal and liver physiology.*, 283, G1352-G1359.
- Nordberg, J., Zhong, L., Holmgren, A. & Arnér, E. S. J. 1998. Mammalian Thioredoxin Reductase Is Irreversibly Inhibited by Dinitrohalobenzenes by Alkylation of Both the Redox Active Selenocysteine and Its Neighboring Cysteine Residue. *Journal of Biological Chemistry*, 273, 10835-10842.
- Obiero, J., Pittet, V., Bonderoff, S. A. & Sanders, D. a. R. 2010. Thioredoxin system from *Deinococcus radiodurans*. *Journal of Bacteriology*, 192, 494-501.
- Olin-Sandoval, V., González-Chávez, Z., Berzunza-Cruz, M., Martínez, I., Jasso-Chávez, R., Becker, I., Espinoza, B., Moreno-Sánchez, R. & Saavedra, E. 2012. Drug target validation of the trypanothione pathway enzymes through metabolic modelling. *FEBS Journal*, 279, 1811-1833.
- Olivier, B. G., Rohwer, J. M. & Hofmeyr, J.-H. S. 2005. Modelling cellular systems with PySCeS. *Bioinformatics*, 21, 560-561.
- Padayachee, L. & Pillay, C. S. 2016. The thioredoxin system and not the Michaelis–Menten equation should be fitted to substrate saturation datasets from the thioredoxin insulin assay. *Redox Report*, 21, 170-179.
- Park, B.-J., Cha, M.-K. & Kim, I.-H. 2014. Thioredoxin 1 as a serum marker for breast cancer and its use in combination with CEA or CA15-3 for improving the sensitivity of breast cancer diagnoses. *BMC Research Notes*, 7, 7-7.

- Park, J. H., Kim, Y. S., Lee, H. L., Shim, J. Y., Lee, K. S., Oh, Y. J., Shin, S. S., Choi, Y. H., Park, K. J., Park, R. W. & Hwang, S. C. 2006. Expression of peroxiredoxin and thioredoxin in human lung cancer and paired normal lung. *Respirology*, 11, 269-275.
- Pascal, L. E., True, L. D., Campbell, D. S., Deutsch, E. W., Risk, M., Coleman, I. M., Eichner, L. J., Nelson, P. S. & Liu, A. Y. 2008. Correlation of mRNA and protein levels: Cell type-specific gene expression of cluster designation antigens in the prostate. *BMC Genomics*, 9, 1-13.
- Peltoniemi, M. J., Karala, A.-R., Jurvansuu, J. K., Kinnula, V. L. & Ruddock, L. W. 2006. Insights into deglutathionylation reactions: Different intermediates in the glutaredoxin and protein disulfide isomerase catalyzed reactions are defined by the γ -linkage present in glutathione. *Journal of Biological Chemistry*, 281, 33107-33114.
- Peng, S., Zhang, B., Meng, X., Yao, J. & Fang, J. 2015a. Synthesis of Piperlongumine Analogues and Discovery of Nuclear Factor Erythroid 2-Related Factor 2 (Nrf2) Activators as Potential Neuroprotective Agents. *Journal of Medicinal Chemistry*, 58, 5242-5255.
- Peng, S., Zhang, B., Yao, J., Duan, D. & Fang, J. 2015b. Dual protection of hydroxytyrosol, an olive oil polyphenol, against oxidative damage in PC12 cells. *Food & Function*, 6, 2091-2100.
- Perier, C. & Vila, M. 2012. Mitochondrial Biology and Parkinson's Disease. *Cold Spring Harbor Perspectives in Medicine*, 2, a009332.
- Persson, T., Popescu, B. O. & Cedazo-Minguez, A. 2014. Oxidative Stress in Alzheimer's Disease: Why Did Antioxidant Therapy Fail? *Oxidative Medicine and Cellular Longevity*, 2014, 427318.
- Pham-Huy, L. A., He, H. & Pham-Huy, C. 2008. Free Radicals, Antioxidants in Disease and Health. *International Journal of Biomedical Science : IJBS*, 4, 89-96.
- Pigiet, V. P. & Conley, R. R. 1977. Purification of thioredoxin, thioredoxin reductase and glutathione reductase by affinity chromatography. *Journal of Biological Chemistry*, 252, 6367-6372.
- Pillay, C. S., Eagling, B. D., Driscoll, S. R. E. & Rohwer, J. M. 2016. Quantitative measures for redox signaling. *Free Radical Biology and Medicine*, 96, 290-303.
- Pillay, C. S., Hofmeyr, J.-H. S., Mashamaite, L. N. & Rohwer, J. M. 2013. From Top-Down to Bottom-Up: Computational Modeling Approaches for Cellular Redoxin Networks. *Antioxidants and redox signaling*, 18, 2075-2086.

- Pillay, C. S., Hofmeyr, J.-H. S. & Rohwer, J. M. 2011. The logic of kinetic regulation in the thioredoxin system. *BMC Systems Biology*, 5, 15.
- Pillay, C. S., Hofmeyr, J. H., Olivier, B. G., Snoep, J. L. & Rohwer, J. M. 2009. Enzymes or redox couples? The kinetics of thioredoxin and glutaredoxin reactions in a systems biology context. *Biochem J*, 417, 269-75.
- Planavsky, N. J., Asael, D., Hofmann, A., Reinhard, C. T., Lalonde, S. V., Knudsen, A., Wang, X., Ossa Ossa, F., Pecoits, E., Smith, A. J. B., Beukes, N. J., Bekker, A., Johnson, T. M., Konhauser, K. O., Lyons, T. W. & Rouxel, O. J. 2014. Evidence for oxygenic photosynthesis half a billion years before the Great Oxidation Event. *Nature Geoscience*, 7, 283-286.
- Poole, L. B. & Nelson, K. J. 2008. Discovering mechanisms of signaling-mediated cysteine oxidation. *Current Opinion in Chemical Biology*, 12, 18-24.
- Poole, L. B., Reynolds, C. M., Wood, Z. A., Karplus, P. A., Ellis, H. R. & Li Calzi, M. 2000. AhpF and other NADH:peroxiredoxin oxidoreductases, homologues of low Mr thioredoxin reductase. *European Journal of Biochemistry*, 267, 6126-6133.
- Potamitou, A., Holmgren, A. & Vlamis-Gardikas, A. 2002. Protein Levels of Escherichia coli Thioredoxins and Glutaredoxins and Their Relation to Null Mutants, Growth Phase, and Function. *Journal of Biological Chemistry*, 277, 18561-18567.
- Quiñonez-Flores, C. M., González-Chávez, S. A., Del Río Nájera, D. & Pacheco-Tena, C. 2016. Oxidative Stress Relevance in the Pathogenesis of the Rheumatoid Arthritis: A Systematic Review. *BioMed Research International*, 2016, 14.
- Raniga, P. V., Di Trapani, G., Vuckovic, S., Bhatia, M. & Tonissen, K. F. 2015. Inhibition of thioredoxin 1 leads to apoptosis in drug-resistant multiple myeloma. *Oncotarget*, 6, 15410-15424.
- Ren, W. & Ai, H.-W. 2013. Genetically Encoded Fluorescent Redox Probes. *Sensors (Basel, Switzerland)*, 13, 15422-15433.
- Requejo, R., Chouchani, E. T., Hurd, T. R., Menger, K. E., Hampton, M. B. & Murphy, M. P. 2010. Chapter 8 - Measuring Mitochondrial Protein Thiol Redox State. In: ENRIQUE, C. & LESTER, P. (eds.) *Methods in Enzymology*. Academic Press.
- Rinalducci, S., Murgiano, L. & Zolla, L. 2008. Redox proteomics: basic principles and future perspectives for the detection of protein oxidation in plants. *Journal of Experimental Botany*, 59, 3781-3801.

- Robson, C. N. & Hickson, I. D. 1991. Isolation of cDNA clones encoding a human apurinic/aprimidinic endonuclease that corrects DNA repair and mutagenesis defects in *E. coli* xth (exonuclease III) mutants. *Nucleic Acids Research*, 19, 5519–5523.
- Robson, C. N., Milne, A. M., Pappin, D. J. & Hickson, I. D. 1991. Isolation of cDNA clones encoding an enzyme from bovine cells that repairs oxidative DNA damage in vitro: homology with bacterial repair enzymes. *Nucleic Acids Research*, 19, 1087–1092.
- Rohwer, J. M., Viljoen, C., Christensen, C. D., Mashamaite, L. N. & Pillay, C. S. 2016. Identifying the conditions necessary for the thioredoxin ultrasensitive response. *Perspectives in Science*, 9, 53-59.
- Rouhier, N., Gelhaye, E. & Jacquot, J. P. 2004. Plant glutaredoxins: still mysterious reducing systems. *Cellular and Molecular Life Sciences* 61, 1266-1277.
- Sabel'nikov, A. G., Avdeeva, A. V. & Il'iashenko, B. I. 1977. *Escherichia coli* cell competence induced by calcium cations. *Genetika*, 13, 1281-1288.
- Saccoccia, F., Angelucci, F., Boumis, G., Carotti, D., Desiato, G., Miele, A. E. & Bellelli, A. 2014. Thioredoxin Reductase and its Inhibitors. *Current Protein & Peptide Science*, 15, 621-646.
- Sambrook, J., Fritsch, E. F. & Maniatis, T. 1989. *Molecular cloning: a laboratory manual*, New York, Cold Spring Harbor Laboratory Press.
- Sauer, U. 2006. Metabolic networks in motion: (13)C-based flux analysis. *Molecular Systems Biology*, 2, 62-62.
- Sayin, V. I., Ibrahim, M. X., Larsson, E., Nilsson, J. A., Lindahl, P. & Bergo, M. O. 2014. Antioxidants Accelerate Lung Cancer Progression in Mice. *Science Translational Medicine*, 6, 221ra15-221ra15.
- Schägger, H. 2006. Tricine-SDS-PAGE. *Nature Protocols*, 1, 16-22.
- Schägger, H. & Von Jagow, G. 1987. Tricine-sodium dodecyl sulfate-polyacrylamide gel electrophoresis for the separation of proteins in the range from 1 to 100 kDa. *Analytical Biochemistry*, 166, 368-379.
- Sengupta, R. & Holmgren, A. 2012. The role of thioredoxin in the regulation of cellular processes by S-nitrosylation. *Biochimica et Biophysica Acta (BBA) - General Subjects*, 1820, 689-700.
- Serrato, A. J., Pérez-Ruiz, J. M. & Cejudo, F. J. 2002. Cloning of thioredoxin h reductase and characterization of the thioredoxin reductase-thioredoxin h system from wheat. *Biochemical Journal*, 367, 491-497.

- Sessions, A. L., Doughty, D. M., Welander, P. V., Summons, R. E. & Newman, D. K. 2009. The Continuing Puzzle of the Great Oxidation Event. *Current Biology*, 19, R567-R574.
- Shiio, Y. & Aebersold, R. 2006. Quantitative proteome analysis using isotope-coded affinity tags and mass spectrometry. *Nature Protocols*, 1, 139-145.
- Si, M.-R., Zhang, L., Yang, Z.-F., Xu, Y.-X., Liu, Y.-B., Jiang, C.-Y., Wang, Y., Shen, X.-H. & Liu, S.-J. 2014. NrdH Redoxin Enhances Resistance to Multiple Oxidative Stresses by Acting as a Peroxidase Cofactor in *Corynebacterium glutamicum*. *Applied and Environmental Microbiology*, 80, 1750-1762.
- Sigma-Aldrich. 1994. *Suitability assay of thioredoxin* [Online]. Available: http://www.sigmaaldrich.com/etc/medialib/docs/Sigma/Enzyme_Assay/thioredoxinsuit.Par.0001.File.tmp/thioredoxinsuit.pdf [Accessed].
- Sivashanmugam, A., Murray, V., Cui, C., Zhang, Y., Wang, J. & Li, Q. 2009. Practical protocols for production of very high yields of recombinant proteins using *Escherichia coli*. *Protein Science : A Publication of the Protein Society*, 18, 936-948.
- Sobhakumari, A., Love-Homan, L., Fletcher, E. V. M., Martin, S. M., Parsons, A. D., Spitz, D. R., Knudson, C. M. & Simons, A. L. 2012. Susceptibility of Human Head and Neck Cancer Cells to Combined Inhibition of Glutathione and Thioredoxin Metabolism. *PLoS ONE*, 7, e48175.
- Soini, Y., Kahlos, K., Napankangas, U., Kaarteenaho-Wiik, R., Saily, M., Koistinen, P., Paaakko, P., Holmgren, A. & Kinnula, V. L. 2001. Widespread Expression of Thioredoxin and Thioredoxin Reductase in Non-Small Cell Lung Carcinoma. *Clinical Cancer Research*, 7, 1750-1757.
- Sommer, A. & Traut, R. R. 1974. Diagonal Polyacrylamide-Dodecyl Sulfate Gel Electrophoresis for the Identification of Ribosomal Proteins Crosslinked with Methyl-4-Mercaptobutyrimidate. *Proceedings of the National Academy of Sciences of the United States of America*, 71, 3946-3950.
- Speranza, M. L., Ronchi, S. & Minchiotti, L. 1973. Purification and characterization of yeast thioredoxin reductase. *Biochim Biophys Acta*, 327, 274-281.
- Stantchev, T. S., Paciga, M., Lankford, C. R., Schwartzkopff, F., Broder, C. C. & Clouse, K. A. 2012. Cell-type specific requirements for thiol/disulfide exchange during HIV-1 entry and infection. *Retrovirology*, 9, 97.
- Stark, A. M., Pfannenschmidt, S., Tscheslog, H., Maass, N., Rosel, F., Mehdorn, H. M. & Held-Feindt, J. 2006. Reduced mRNA and protein expression of BCL-2 versus

- decreased mRNA and increased protein expression of BAX in breast cancer brain metastases: a real-time PCR and immunohistochemical evaluation. *Neurological Research*, 28, 787-793.
- Štefanková, P., Perečko, D., Barák, I. & Kollárová, M. 2006. The thioredoxin system from *Streptomyces coelicolor*. *Journal of Basic Microbiology*, 46, 47-55.
- Steinhubl, S. R. 2008. Why Have Antioxidants Failed in Clinical Trials? *The American Journal of Cardiology*, 101, S14-S19.
- Subramaniam, S. R. & Chesselet, M.-F. 2013. Mitochondrial dysfunction and oxidative stress in Parkinson's disease. *Progress in neurobiology*, 0, 17-32.
- Tairum, C. A., Jr., De Oliveira, M. A., Horta, B. B., Zara, F. J. & Netto, L. E. 2012. Disulfide biochemistry in 2-Cys peroxiredoxin: Requirement of Glu50 and Arg146 for the reduction of yeast Tsa1 by thioredoxin. *The Journal of Molecular Biology* 424, 28-41.
- Takemoto, T., Zhang, Q.-M. & Yonei, S. 1998. Different mechanisms of thioredoxin in its reduced and oxidized forms in defense against hydrogen peroxide in *Escherichia coli*. *Free Radical Biology and Medicine*, 24, 556-562.
- Terzer, M., Maynard, N. D., Covert, M. W. & Stelling, J. 2009. Genome-scale metabolic networks. *Wiley Interdisciplinary Reviews: Systems Biology and Medicine* 1, 285-97.
- Toledano, M. B., Kumar, C., Le Moan, N., Spector, D. & Tacnet, F. 2007. The system biology of thiol redox system in *Escherichia coli* and yeast: Differential functions in oxidative stress, iron metabolism and DNA synthesis. *FEBS lett*, 581, 3598-3607.
- Tomalin, L. E., Day, A. M., Underwood, Z. E., Smith, G. R., Dalle Pezze, P., Rallis, C., Patel, W., Dickinson, B. C., Bähler, J., Brewer, T. F., Chang, C. J.-L., Shanley, D. P. & Veal, E. A. 2016. Increasing extracellular H₂O₂ produces a bi-phasic response in intracellular H₂O₂, with peroxiredoxin hyperoxidation only triggered once the cellular H₂O₂-buffering capacity is overwhelmed. *Free Radical Biology and Medicine*, 95, 333-348.
- Trotter, E. W. & Grant, C. M. 2003. Non-reciprocal regulation of the redox state of the glutathione-glutaredoxin and thioredoxin systems. *EMBO Reports*, 4, 184-188.
- Ungerstedt, J., Du, Y., Zhang, H., Nair, D. & Holmgren, A. 2012. In vivo redox state of Human thioredoxin and redox shift by the histone deacetylase inhibitor suberoylanilide hydroxamic acid (SAHA). *Free Radical Biology and Medicine*, 53, 2002-2007.
- Urig, S. & Becker, K. 2006. On the potential of thioredoxin reductase inhibitors for cancer therapy. *Seminars in Cancer Biology*, 16, 452-465.

- Wang, E. 2010. *A roadmap of cancer systems biology*, Canada, CRC Press.
- Watson, W. H. & Jones, D. P. 2003. Oxidation of nuclear thioredoxin during oxidative stress. *FEBS Letters*, 543, 144-147.
- Watson, W. H., Pohl, J., Montfort, W. R., Stuchlik, O., Reed, M. S., Powis, G. & Jones, D. P. 2003. Redox Potential of Human Thioredoxin 1 and Identification of a Second Dithiol/Disulfide Motif. *Journal of Biological Chemistry*, 278, 33408-33415.
- Watson, W. H., Yang, X., Choi, Y. E., Jones, D. P. & Kehrer, J. P. 2004. Thioredoxin and its role in Toxicology. *Toxicol Sci*, 78, 3-14.
- Welsh, S. J., Williams, R. R., Birmingham, A., Newman, D. J., Kirkpatrick, D. L. & Powis, G. 2003. The Thioredoxin Redox Inhibitors 1-Methylpropyl 2-Imidazolyl Disulfide and Pleurotin Inhibit Hypoxia-induced Factor 1 α and Vascular Endothelial Growth Factor Formation 1. *Molecular Cancer Therapeutics*, 2, 235-243.
- Williams, C. 1995. Mechanism and structure of thioredoxin reductase from Escherichia coli. *The FASEB Journal*, 9, 1267-1276.
- Williams, C. H., Jr 1976. Flavin-containing dehydrogenases. New York: Academic Press.
- Williams, C. H., Zanetti, G., Arscott, L. D. & Mcallister, J. K. 1967. Lipoamide Dehydrogenase, Glutathione Reductase, Thioredoxin Reductase, and Thioredoxin. *Journal of Biological Chemistry*, 242, 5226-5231.
- Wouters, M. A., Fan, S. W. & Haworth, N. L. 2010. Disulfides as redox switches: from molecular mechanisms to functional significance. *Antioxidants and redox signaling*, 12, 53-91.
- Wu, M.-H., Song, F.-Y., Wei, L.-P., Meng, Z.-Y., Zhang, Z.-Q. & Qi, Q.-D. 2014. Serum Levels of Thioredoxin Are Associated with Stroke Risk, Severity, and Lesion Volumes. *Molecular Neurobiology*, 1-9.
- Wu, Y., Yang, L. & Zhong, L. 2010. Decreased serum levels of thioredoxin in patients with coronary artery disease plus hyperhomocysteinemia is strongly associated with the disease severity. *Atherosclerosis*, 212, 351-355.
- Wynn, R., Cocco, M. J. & Richards, F. M. 1995. Mixed disulfide intermediates during the reduction of disulfides by Escherichia coli thioredoxin. *Biochem*, 34, 11807-11813.
- Xia, K., Manning, M., Hesham, H., Lin, Q., Bystroff, C. & Colón, W. 2007. Identifying the subproteome of kinetically stable proteins via diagonal 2D SDS/PAGE. *Proceedings of the National Academy of Sciences of the United States of America*, 104, 17329-17334.

- Yamada, Y., Nakamura, H., Adachi, T., Sannohe, S., Oyamada, H., Kayaba, H., Yodoi, J. & Chihara, J. 2003. Elevated serum levels of thioredoxin in patients with acute exacerbation of asthma. *Immunology Letters*, 86, 199-205.
- Yang, X. & Ma, K. 2010. Characterization of a Thioredoxin-Thioredoxin Reductase System from the Hyperthermophilic Bacterium *Thermotoga maritima*. *Journal of Bacteriology*, 192, 1370-1376.
- Yoo, M.-H., Carlson, B. A., Tsuji, P., Irons, R., Gladyshev, V. N. & Hatfield, D. L. 2010. Alteration of Thioredoxin Reductase 1 Levels in Elucidating Cancer Etiology. *Methods in Enzymology*, 474, 255-275.
- Yoo, M.-H., Xu, X.-M., Carlson, B. A., Patterson, A. D., Gladyshev, V. N. & Hatfield, D. L. 2007. Targeting Thioredoxin Reductase 1 Reduction in Cancer Cells Inhibits Self-Sufficient Growth and DNA Replication. *PLoS ONE*, 2, e1112.
- Zako, T., Sakono, M., Hashimoto, N., Ihara, M. & Maeda, M. 2009. Bovine insulin filaments induced by reducing disulfide bonds show a different morphology, secondary structure, and cell toxicity from intact insulin amyloid fibrils. *Biophysical Journal* 3331-3340.
- Zander, T., Phadke, N. D. & Bardwell, J. C. 1998. Disulfide bond catalysts in *Escherichia coli*. *Methods in Enzymology*, 290, 59-74.
- Zhang, B., Duan, D., Ge, C., Yao, J., Liu, Y., Li, X. & Fang, J. 2015a. Synthesis of Xanthohumol Analogues and Discovery of Potent Thioredoxin Reductase Inhibitor as Potential Anticancer Agent. *Journal of Medicinal Chemistry*, 58, 1795-1805.
- Zhang, L., Duan, D., Liu, Y., Ge, C., Cui, X., Sun, J. & Fang, J. 2014. Highly Selective Off-On Fluorescent Probe for Imaging Thioredoxin Reductase in Living Cells. *Journal of the American Chemical Society*, 136, 226-233.
- Zhang, Q.-B., Gao, S.-J. & Zhao, H.-X. 2015b. Thioredoxin: A novel, independent diagnosis marker in children with autism. *International Journal of Developmental Neuroscience*, 40, 92-96.
- Zhang, X. Y., Chen, D. C., Xiu, M. H., Wang, F., Qi, L. Y., Sun, H. Q., Chen, S., He, S. C., Wu, G. Y., Haile, C. N., Kosten, T. A., Lu, L. & Kosten, T. R. 2009. The novel oxidative stress marker thioredoxin is increased in first-episode schizophrenic patients. *Schizophrenia Research*, 113, 151-157.
- Zhong, L., Arnér, E. S. J. & Holmgren, A. 2000. Structure and mechanism of mammalian thioredoxin reductase: The active site is a redox-active selenolthiol-selenenylsulfide

formed from the conserved cysteine-selenocysteine sequence. *Proceedings of the National Academy of Sciences of the United States of America*, 97, 5854-5859.

Appendix

Details of the kinetic parameters obtained for the insulin disulfide bond reduction by *Escherichia coli* and by baker's yeast are summarized in Table S1.

Table S1: The Michaelis-Menten parameters and second-order rate constants (k_2) for the disulfide bond reduction of insulin from computational modeling of the *E. coli* thioredoxin system and by the baker's yeast thioredoxin system at varying thioredoxin reductase (TR) concentrations.

Organism	Apparent Michaelis-Menten parameters					Redox couple model	
	TR	$K_m \pm \text{SE}$	$k_{\text{cat}} \pm \text{SE}$	k_{cat}/K_m	r^2	$k_2 \pm \text{SE}$	r^2
	(μM)	(μM)	(s^{-1})	($\mu\text{M}^{-1}.\text{s}^{-1}$)		($\mu\text{M}^{-1}.\text{s}^{-1}$)	
<i>Escherichia coli</i>	0.1	34.56 ± 3.89	0.75 ± 0.02	0.02	0.989	0.02 ± 0.0001	0.997
	0.5	172.10 ± 4.24	3.88 ± 0.04	0.02	0.999	0.02 ± 0.0003	0.999
	1.0	330.28 ± 12.81	7.53 ± 0.17	0.02	0.999	0.02 ± 0.0003	0.999
<i>Saccharomyces cerevisiae</i>	0.05	114.64 ± 17.55	0.11 ± 0.01	0.001	0.97	0.001 ± 0.0001	0.97
	0.15	77.44 ± 20.20	0.15 ± 0.01	0.002	0.92	0.002 ± 0.0003	0.94
	0.25	87.82 ± 11.92	0.18 ± 0.01	0.002	0.98	0.002 ± 0.0001	0.98

Kinetic modeling experiments were carried out using the open source Python Simulator for Cellular Systems (PySCeS) modeling software (Olivier *et al.*, 2005) (<http://pysces.sourceforge.net>). The following modeling files were used to analyze the *E.coli* (File 1) and the baker's yeast (File 2) thioredoxin systems. In these models, thioredoxin reductase was modeled with a two-substrate Michaelis-Menten kinetic expression and insulin reduction was modeled with mass-action kinetics.

File 1: The PySCeS code used for modeling the *E. coli* thioredoxin system

```
FIX: NADPH NADP ISS ISH
```

```
#all data in uM, time = per second
```

```
R1: NADPH + TrxSS = NADP + TrxSH
```

```
kcat1 * TR * (NADPH / Knadph) * (TrxSS / Ktrxss) / ((1 + NADPH / Knadph + NADP / Knadp) * (1 + TrxSS / Ktrxss))
```

```
R2: TrxSH + ISS = ISH + TrxSS
```

```
k2 * TrxSH * ISS
```

```
#Metabolites
```

```
NADP= 1
```

```
NADPH= 400
```

```
TrxSS= 0.05
```

```
TrxSH= 0.05
```

```
ISS= 30
```

```
ISH= 1
```

```
#Rate parameters
```

```
Knadph= 1.2
```

```
Ktrxss= 2.8
```

```
kcat1= 22.8
```

```
TR= 0.1
```

```
Knadp= 15
```

```
k2= 4
```

File 2: The PySCeS code used for modeling the baker's yeast thioredoxin system

FIX: NADPH NADP InSH InSS

#all data in uM, time = per second

R1: NADPH + TrxSS = NADP + TrxSH

$(kcat1 * TR * (NADPH / Knadph) * (TrxSS / K1trxss)) / ((1 + NADPH / Knadph) * (1 + TrxSS / K1trxss))$

R2: TrxSH + InSS = TrxSS + InSH

$k2 * TrxSH * InSS$

#Species

NADPH= 400

NADP= 1

InSH= 1

InSS= 20

TrxSH= 0.75

TrxSS= 0.75

Rate parameters

kcat= 66.6

TR= 0.05

Knadph= 1.2

K1trxss= 4.4

k2 = 0.03

The following modeling files were used to simulate a core model of the *E.coli* thioredoxin system (Pillay *et al.*, 2011). For the incorporation of a competitive inhibitor, all the parameters, rates, reactions and concentrations remained the same as those seen in File 3 with the exception of reaction 1 (R1) and the addition of an inhibition constant ($K_i = 0.52 \mu\text{M}$) (Lu *et al.*, 2013) (File 4).

File 3: The PySCeS code used for a core model of the *E.coli* thioredoxin system

FIX: NADP NADPH H2O2 H2O PAPS PAP SO3 MetSO Met PSH PSS

#all data in uM, time = per second

R1: NADPH + TrxSS = NADP + TrxSH

$(kcat1 * TR * (NADPH / Knadph) * (TrxSS / K1trxss)) / ((1 + NADPH / Knadph) * (1 + TrxSS / K1trxss))$

R2: TrxSH + PSS = TrxSS + PSH

$k2 * TrxSH * PSS$

R3: MetSO + TrxSH = Met + TrxSS

$(kcat3 * MSR * MetSO * TrxSH) / (K3trxsh * MetSO + Kmetso * TrxSH + MetSO * TrxSH)$

R4: PAPS + TrxSH = SO3 + PAP + TrxSS

$0.156 * PAPS * TrxSH$

R5: H2O2 + TpxSH = H2O + TpxSS

$k5 * H2O2 * TpxSH$

R6: TrxSH + TpxSS = TrxSS + TpxSH

$k6 * TrxSH * TpxSS$

#Metabolite Concentrations

NADPH = 137.0

NADP = 1.0

TrxSH = 1.0

TrxSS = 1.0

PSS = 4.23

PSH = 1.0

MetSO = 970.0

Met = 48300.0

PAPS = 0.07

SO3 = 1.0

PAP = 1.0

H2O2 = 0.02

H2O = 1.0

TpxSH = 4.88

TpxSS = 1.0

#Kinetic Parameters

TR = 4.74

kcat1 = 22.75

Knadph = 1.2

K1trxss = 2.8

k2 = 0.064

MSR = 2.35

kcat3 = 3.7

Kmetso = 1900.0

K3trxsh = 10.0

PR = 0.345

kcat4 = 3.5

Kpaps = 22.5

K4trxsh = 13.7

k5 = 44.0

k6 = 3000.0

File 4: The modified PySCeS code used for a core model of the *E.coli* thioredoxin system with the incorporation of a competitive inhibitor



$$\frac{(k_{cat1} * TR * (\text{NADPH}/K_{nadph}) * (\text{TrxSS}/K_{1trxss}))}{((1 + \text{NADPH}/K_{nadph}) * ((1 + \text{TrxSS}/K_{1trxss}) + (i/k_i)))}$$

The co-response analysis revealed a non-linear relationship between the reductive thioredoxin redox charge and the flux with increasing concentrations of NADPH and thioredoxin reductase (Figure 4.5). This non-linear relationship occurred as a consequence of the saturation of the Tpx redox cycle and therefore increasing the concentration of hydrogen peroxide should result in an increased demand for reduced Tpx causing an increase in the flux and a linear relationship between the reductive thioredoxin redox charge and the flux should be obtained. To test this hypothesis, co-response plots were generated with increasing NADPH and thioredoxin reductase concentrations as previously performed. However, the hydrogen peroxide concentration was increased from 0.02 μM to 20 μM (Figure S1). Under conditions of perturbed reductive supply, at an increased hydrogen peroxide concentration, the redox potential (Figure S1 A), the redox ratio (Figure S1 B) as well as the reductive thioredoxin redox charge (Figure S1 D) closely correlated with the flux.

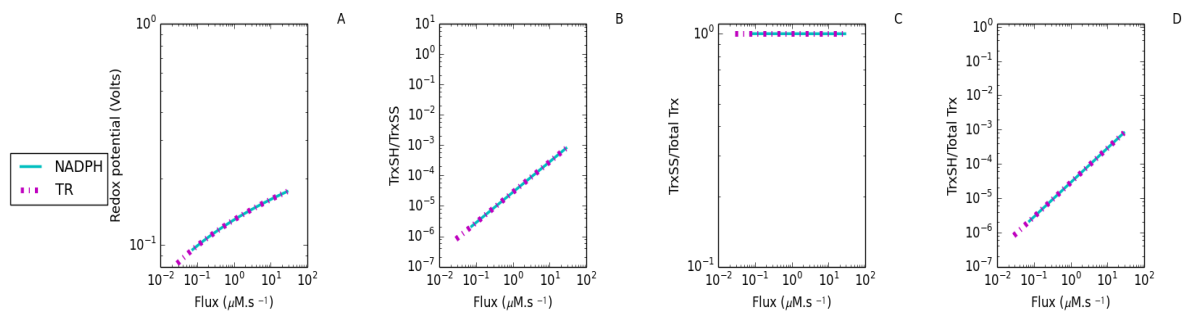


Figure S1. Co-response analysis revealed a linear relationship between the reductive thioredoxin redox charge and the flux when the demand for Tpx was increased. Co-response plots were generated with varying concentrations of NADPH (—) and thioredoxin reductase (---) at a higher hydrogen peroxide concentration and the relationship with the redox potential (A), redox ratio (B), oxidative thioredoxin redox charge (C) and reductive thioredoxin redox charge (D) was determined.

In addition to the plots generated using the initial linear regions within the *in vitro* curves (Figure 4.11-4.12), qualitative (Figure S2) and co-response plots (Figure S3) using the entire *in vitro* dataset were also generated.

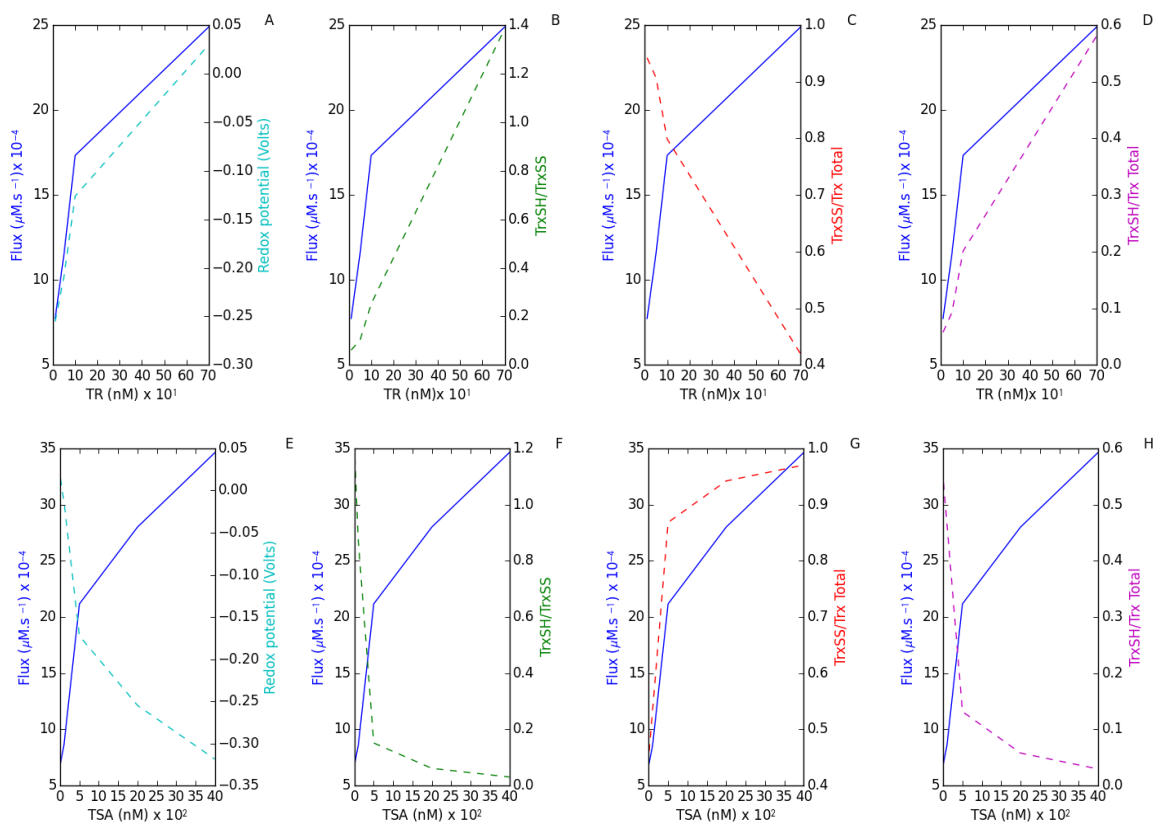


Figure S2. The reductive thioredoxin redox charge correlates with the flux as the reductive supply from thioredoxin reductase increased while the oxidative thioredoxin redox charge correlates with the flux with increasing peroxiredoxin concentrations. *In vitro* assays with varying concentrations of thioredoxin reductase and peroxiredoxin were performed to determine the relationship between the flux (blue) and redox potential (cyan, A and E), redox ratio (green, B and F), oxidative thioredoxin redox charge (red, C and G) and reductive thioredoxin redox charge (magenta, D and H).

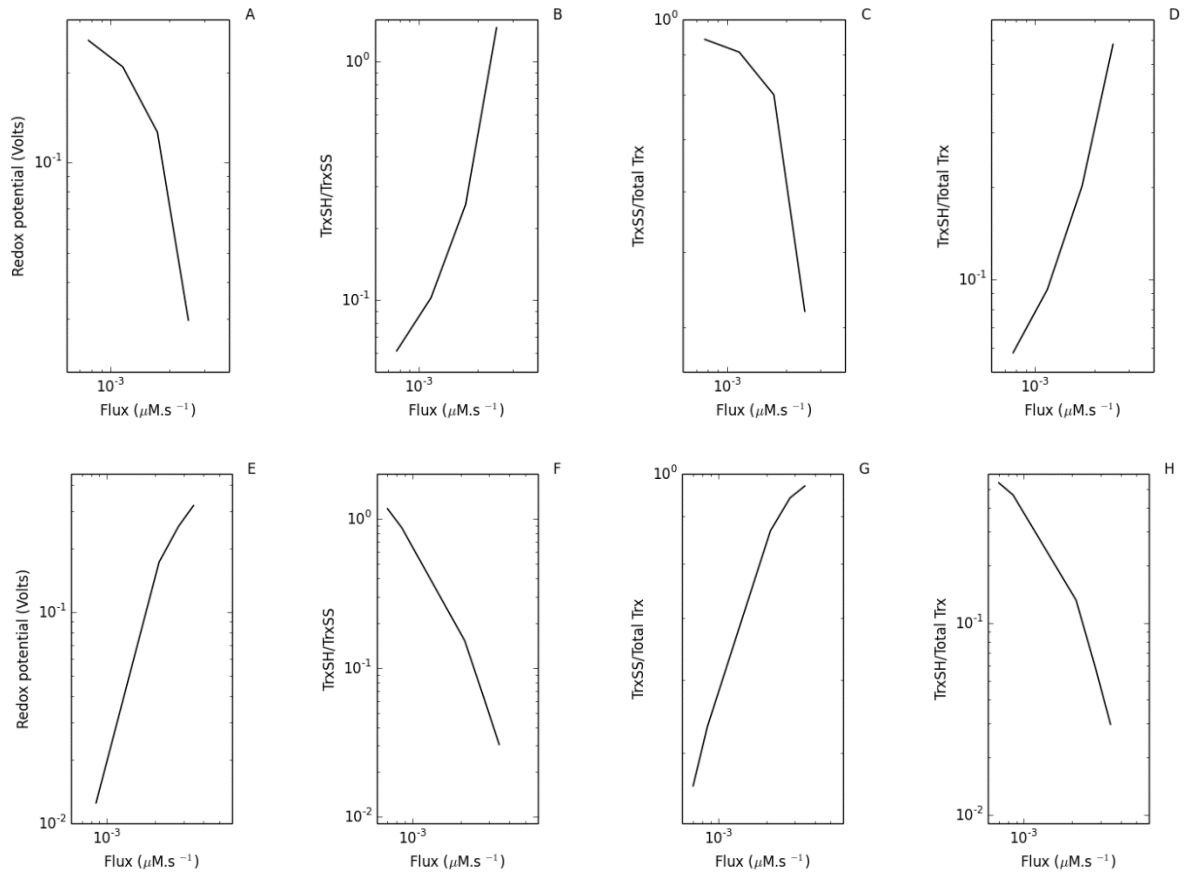


Figure S3. Co-response plots generated from *in vitro* assay and western blot data confirming that the the reductive thioredoxin redox charge correlates with the flux with perturbations in reductive supply and the oxidative thioredoxin redox charge correlates with the flux with perturbations in oxidative demand. Co-response plots were generated with varying concentrations of thioredoxin reductase (A-D) and peroxiredoxin (E-H) and the relationship with the redox potential (A and E), redox ratio (B and F), oxidative thioredoxin redox charge (C and G) and reductive thioredoxin redox charge (D and H) was determined.

A realistic model of the red blood cell was used to determine if the proposed novel measure, thioredoxin redox charge was a surrogate measure for flux. The reactions included in the model are illustrated below (Figure S4, Table S2). The kinetic parameters and parameter values are given in Table S2.

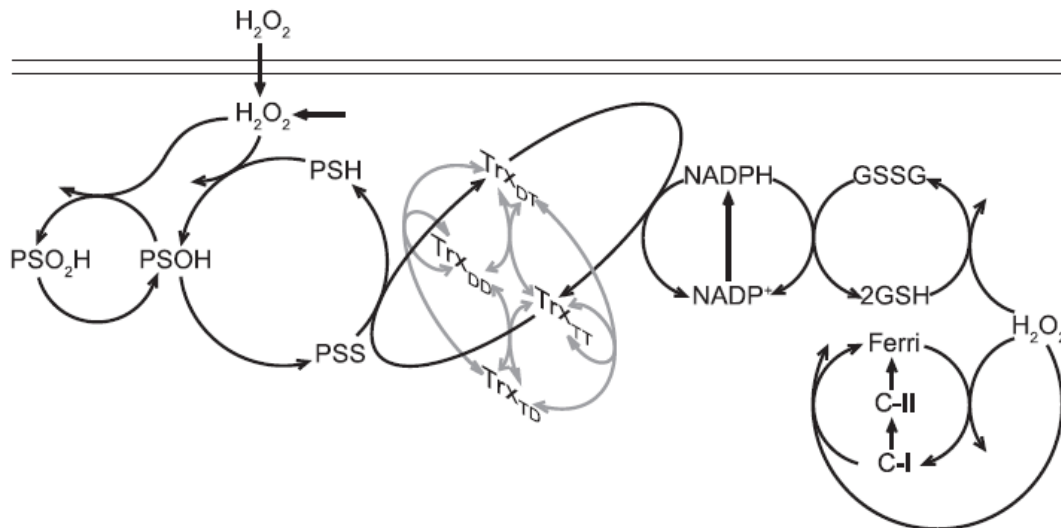


Figure S4. Reactions used to create a realistic model of hydrogen peroxide metabolism in human erythrocytes (Benfeitas *et al.*, 2014). The model includes the reactions for the (i) generation of intracellular hydrogen peroxide from both endogenous and exogenous sources; (ii) hydrogen peroxide consumption via catalase, peroxiredoxin 2 and glutathione peroxidase; (iii) peroxiredoxin 2 sulfinylation and reduction of the sulfinic to the sulfenic form; (iv) Trx1 oxidation by peroxiredoxin 2, reduction via thioredoxin reductase and reactions between the active-site dithiol and the regulatory dithiol; (v) glutathione reductase mediated reduction of glutathione disulfide (GSSG); and (vi) NADP^+ reduction to NADPH by the hexose monophosphate shunt. Permission to reproduce this figure was granted by the Elsevier publishing company.

Table S2. Reaction rates and parameters considered in the creation of the realistic human erythrocyte model (Benfeitás *et al.*, 2014). (Permission to reproduce this table was granted by the Elsevier publishing company)

Reaction	Reaction rates (v) and parameters
$\rightarrow \text{H}_2\text{O}_2$	$v_{\text{prod}} = 3.5 \times 10^{-8} \text{ M s}^{-1}$
$\text{eH}_2\text{O}_2 \rightarrow \text{H}_2\text{O}_2$	$k_p = 10.9 \text{ s}^{-1}$ ^a
$\text{H}_2\text{O}_2 \rightarrow \text{eH}_2\text{O}_2$	$k_p = 10.9 \text{ s}^{-1}$ ^a
$\text{H}_2\text{O}_2 + 2 \text{ GSH} \rightarrow \text{GSSG} + 2 \text{ H}_2\text{O}$	$\nu = 1/((\phi_1/[\text{H}_2\text{O}_2]) + (\phi_2/[\text{GSH}]))$ $\phi_1 = 3.99 \times 10^{-2} \text{ s}$ $\phi_2 = 9.72 \text{ s}$
$\text{GSSG} + \text{NADPH} + \text{H}^+ \rightarrow 2 \text{ GSH} + \text{NADP}^+$	$\nu = V_{\text{Max, GSR}} / (1 + (K_{\text{M,GSR,NADPH}}/[\text{NADPH}]) + (K_{\text{M,GSR,GSSG}}/[\text{GSSG}]))$ $V_{\text{Max,GSR}} = 4.9 \times 10^{-5} \text{ M s}^{-1}$ $K_{\text{M,GSR,NADPH}} = 8.5 \times 10^{-6} \text{ M}$ $K_{\text{M,GSR,GSSG}} = 6.5 \times 10^{-5} \text{ M}$
Ferricatalase + $\text{H}_2\text{O}_2 \rightarrow$ compound I + H_2O	$k_{\text{Ferri}} = 6 \times 10^6 \text{ M}^{-1} \text{ s}^{-1}$
Compound I + $\text{H}_2\text{O}_2 \rightarrow$ ferricatalase + $\text{O}_2 + \text{H}_2\text{O}$	$k_{\text{Cl}} = 1.8 \times 10^7 \text{ M}^{-1} \text{ s}^{-1}$
Compound I \rightarrow compound II	$k_{\text{ClInac}} = 1.1 \times 10^{-2} \text{ s}^{-1}$
Compound II \rightarrow ferricatalase	$k_{\text{ClI}} = 7.39 \times 10^4 \text{ s}^{-1}$
$\text{PSHPSH} + \text{H}_2\text{O}_2 \rightarrow \text{PSOHPSH} + \text{H}_2\text{O}$	$2k_{\text{Ox}} = 2 \times 10^8 \text{ M}^{-1} \text{ s}^{-1}$ ^b
$\text{PSOHPSH} \rightarrow \text{PSSPSH} + \text{H}_2\text{O}$	$k_{\text{Cond}} = 1.7 \text{ s}^{-1}$
$\text{PSOHPSH} + \text{H}_2\text{O}_2 \rightarrow \text{PSOHPSOH} + \text{H}_2\text{O}$	$k_{\text{Ox}} = 10^8 \text{ M}^{-1} \text{ s}^{-1}$
$\text{PSOHPSH} + \text{H}_2\text{O}_2 \rightarrow \text{PSO}_2\text{HPSH} + \text{H}_2\text{O}$	$k_{\text{Sulf}} = 1.2 \times 10^4 \text{ M}^{-1} \text{ s}^{-1}$
$\text{PSSPSH} + \text{H}_2\text{O}_2 \rightarrow \text{PSSPSOH} + \text{H}_2\text{O}$	$k_{\text{Ox}} = 10^8 \text{ M}^{-1} \text{ s}^{-1}$
$\text{PSSPSH} + \text{Trx1}_{\text{TT}} \rightarrow \text{PSHPSH} + \text{Trx1}_{\text{DT}}$	$k_{\text{Red}} = 2.1 \times 10^5 \text{ M}^{-1} \text{ s}^{-1}$
$\text{PSSPSH} + \text{Trx1}_{\text{TD}} \rightarrow \text{PSHPSH} + \text{Trx1}_{\text{DD}}$	$k_{\text{Red}} = 2.1 \times 10^5 \text{ M}^{-1} \text{ s}^{-1}$
$\text{PSOHPSOH} \rightarrow \text{PSSPSOH} + \text{H}_2\text{O}$	$2k_{\text{Cond}} = 3.4 \text{ s}^{-1}$ ^b
$\text{PSOHPSOH} + \text{H}_2\text{O}_2 \rightarrow \text{PSO}_2\text{HPSOH} + \text{H}_2\text{O}$	$2k_{\text{Sulf}} = 2.4 \times 10^4 \text{ M}^{-1} \text{ s}^{-1}$
$\text{PSSPSOH} \rightarrow \text{PSSPSS} + \text{H}_2\text{O}$	$k_{\text{Cond}} = 1.7 \text{ s}^{-1}$
$\text{PSSPSOH} + \text{H}_2\text{O}_2 \rightarrow \text{PSO}_2\text{HPSS} + \text{H}_2\text{O}$	$k_{\text{Sulf}} = 1.2 \times 10^4 \text{ M}^{-1} \text{ s}^{-1}$
$\text{PSSPSOH} + \text{Trx1}_{\text{TT}} \rightarrow \text{PSOHPSH} + \text{Trx1}_{\text{DT}}$	$k_{\text{Red}} = 2.1 \times 10^5 \text{ M}^{-1} \text{ s}^{-1}$
$\text{PSSPSOH} + \text{Trx1}_{\text{TD}} \rightarrow \text{PSOHPSH} + \text{Trx1}_{\text{DD}}$	$k_{\text{Red}} = 2.1 \times 10^5 \text{ M}^{-1} \text{ s}^{-1}$
$\text{PSSPSS} + \text{Trx1}_{\text{TT}} \rightarrow \text{PSSPSH} + \text{Trx1}_{\text{DT}}$	$2k_{\text{Rad}} = 4.2 \times 10^5 \text{ M}^{-1} \text{ s}^{-1}$ ^b
$\text{PSSPSS} + \text{Trx1}_{\text{TD}} \rightarrow \text{PSSPSH} + \text{Trx1}_{\text{DD}}$	$2k_{\text{Rad}} = 4.2 \times 10^5 \text{ M}^{-1} \text{ s}^{-1}$ ^b
$\text{PSO}_2\text{HPSH} + \text{H}_2\text{O}_2 \rightarrow \text{PSO}_2\text{HPSOH} + \text{H}_2\text{O}$	$k_{\text{Ox}} = 10^8 \text{ M}^{-1} \text{ s}^{-1}$
$\text{PSO}_2\text{HPSH} \rightarrow \text{PSOHPSH}$	$k_{\text{Srx}} = 10^{-4} \text{ s}^{-1}$
$\text{PSO}_2\text{HPSOH} \rightarrow \text{PSO}_2\text{HPSS} + \text{H}_2\text{O}$	$k_{\text{Cond}} = 1.7 \text{ s}^{-1}$
$\text{PSO}_2\text{HPSOH} + \text{H}_2\text{O}_2 \rightarrow \text{PSO}_2\text{HPSO}_2\text{H} + \text{H}_2\text{O}$	$k_{\text{Sulf}} = 1.2 \times 10^4 \text{ M}^{-1} \text{ s}^{-1}$
$\text{PSO}_2\text{HPSOH} \rightarrow \text{PSOHPSOH}$	$k_{\text{Srx}} = 10^{-4} \text{ s}^{-1}$
$\text{PSO}_2\text{HPSS} + \text{Trx1}_{\text{TT}} \rightarrow \text{PSO}_2\text{HPSH} + \text{Trx1}_{\text{DT}}$	$k_{\text{Red}} = 2.1 \times 10^5 \text{ M}^{-1} \text{ s}^{-1}$
$\text{PSO}_2\text{HPSS} + \text{Trx1}_{\text{TD}} \rightarrow \text{PSO}_2\text{HPSH} + \text{Trx1}_{\text{DD}}$	$k_{\text{Red}} = 2.1 \times 10^5 \text{ M}^{-1} \text{ s}^{-1}$
$\text{PSO}_2\text{HPSS} \rightarrow \text{PSSPSOH}$	$k_{\text{Srx}} = 10^{-4} \text{ s}^{-1}$
$\text{PSO}_2\text{HPSO}_2\text{H} \rightarrow \text{PSO}_2\text{HPSOH}$	$2k_{\text{Srx}} = 2 \times 10^{-4} \text{ s}^{-1}$ ^b
$\text{iPSHPSH} + \text{H}_2\text{O}_2 \rightarrow \text{iPSOHPSH}$	$k_{\text{Ox}} = 10^8 \text{ M}^{-1} \text{ s}^{-1}$
$\text{iPSOHPSH} \rightarrow \text{iPSSPSH}$	$k_{\text{Cond}} = 1.7 \text{ s}^{-1}$
$\text{iPSOHPSH} + \text{H}_2\text{O}_2 \rightarrow \text{iPSO}_2\text{HPSH}$	$k_{\text{Sulf}} = 1.2 \times 10^4 \text{ M}^{-1} \text{ s}^{-1}$
$\text{iPSO}_2\text{HPSH} \rightarrow \text{iPSOHPSH}$	$k_{\text{Srx}} = 10^{-4} \text{ s}^{-1}$
$\text{iPSSPSH} + \text{Trx1}_{\text{TT}} \rightarrow \text{iPSHPSH} + \text{Trx1}_{\text{DT}}$	$k_{\text{Red}} = 2.1 \times 10^5 \text{ M}^{-1} \text{ s}^{-1}$
$\text{iPSSPSH} + \text{Trx1}_{\text{TD}} \rightarrow \text{iPSHPSH} + \text{Trx1}_{\text{DD}}$	$k_{\text{Red}} = 2.1 \times 10^5 \text{ M}^{-1} \text{ s}^{-1}$
$\text{PSHPSH} \rightleftharpoons \text{iPSHPSH}$	$K_{\text{Prx2}} = 166.9$
$\text{PSOHPSH} \rightleftharpoons \text{iPSOHPSH}$	$K_{\text{Prx2}} = 166.9$
$\text{PSSPSH} \rightleftharpoons \text{iPSSPSH}$	$K_{\text{Prx2}} = 166.9$
$\text{PSO}_2\text{HPSH} \rightleftharpoons \text{iPSO}_2\text{HPSH}$	$K_{\text{Prx2}} = 166.9$
$\text{iPSHPSH} \rightleftharpoons \text{iPSHiPSH}$	$K_{\text{Prx2}} = 166.9$
$\text{Trx1}_{\text{DT}} + \text{NADPH} + \text{H}^+ \rightarrow \text{Trx1}_{\text{TT}} + \text{NADP}^+$	$\nu = V_{\text{Max,TdxR}} / (1 + (K_{\text{M,TdxR,NADPH}}/[\text{NADPH}]) + (K_{\text{M,TdxR,Trx1DT}}/[\text{Trx1}_{\text{DT}}]))$ $V_{\text{Max,TdxR}} = 1.0 \times 10^{-5} \text{ M s}^{-1}$ $K_{\text{M,TdxR,NADPH}} = 6 \times 10^{-6} \text{ M}$ $K_{\text{M,TdxR,Trx1DT}} = 1.83 \times 10^{-6} \text{ M}$
$\text{Trx1}_{\text{DD}} + \text{Trx1}_{\text{TT}} \rightarrow 2 \text{ Trx1}_{\text{TD}}$	$k_{\text{Tdxb}} = 4.2 \times 10^3 \text{ M}^{-1} \text{ s}^{-1}$
$2 \text{ Trx1}_{\text{TD}} \rightarrow \text{Trx1}_{\text{DD}} + \text{Trx1}_{\text{TT}}$	$2k_{\text{Tdxa}} = 4.2 \times 10^5 \text{ M}^{-1} \text{ s}^{-1}$ ^b
$\text{Trx1}_{\text{DT}} + \text{Trx1}_{\text{TD}} \rightarrow \text{Trx1}_{\text{DD}} + \text{Trx1}_{\text{TT}}$	$k_{\text{Tdxa}} = 2.1 \times 10^5 \text{ M}^{-1} \text{ s}^{-1}$
$\text{Trx1}_{\text{DD}} + \text{Trx1}_{\text{TT}} \rightarrow 2 \text{ Trx1}_{\text{DT}}$	$k_{\text{Tdxa}} = 2.1 \times 10^5 \text{ M}^{-1} \text{ s}^{-1}$
$2 \text{ Trx1}_{\text{DT}} \rightarrow \text{Trx1}_{\text{DD}} + \text{Trx1}_{\text{TT}}$	$2k_{\text{Tdxb}} = 8.4 \times 10^3 \text{ M}^{-1} \text{ s}^{-1}$ ^b
$\text{Trx1}_{\text{DD}} + \text{Trx1}_{\text{DT}} \rightarrow \text{Trx1}_{\text{DD}} + \text{Trx1}_{\text{TD}}$	$k_{\text{Tdxb}} = 4.2 \times 10^3 \text{ M}^{-1} \text{ s}^{-1}$
$\text{Trx1}_{\text{DD}} + \text{Trx1}_{\text{TD}} \rightarrow \text{Trx1}_{\text{DD}} + \text{Trx1}_{\text{DT}}$	$k_{\text{Tdxa}} = 2.1 \times 10^5 \text{ M}^{-1} \text{ s}^{-1}$
$\text{Trx1}_{\text{TT}} + \text{Trx1}_{\text{TD}} \rightarrow \text{Trx1}_{\text{TT}} + \text{Trx1}_{\text{DT}}$	$k_{\text{Tdxa}} = 2.1 \times 10^5 \text{ M}^{-1} \text{ s}^{-1}$
$\text{Trx1}_{\text{TT}} + \text{Trx1}_{\text{DT}} \rightarrow \text{Trx1}_{\text{TT}} + \text{Trx1}_{\text{TD}}$	$k_{\text{Tdxb}} = 4.2 \times 10^3 \text{ M}^{-1} \text{ s}^{-1}$
$\text{Trx1}_{\text{DD}} + \text{NADPH} + \text{H}^+ \rightarrow \text{Trx1}_{\text{TD}} + \text{NADP}^+$	$\nu = V_{\text{Max,TdxR}} / (1 + (K_{\text{M,TdxR,NADPH}}/[\text{NADPH}]) + (K_{\text{M,TdxR,Trx1DD}}/[\text{Trx1}_{\text{DD}}]))$ $V_{\text{Max,TdxR}} = 1.0 \times 10^{-5} \text{ M s}^{-1}$ $K_{\text{M,TdxR,NADPH}} = 6 \times 10^{-6} \text{ M}$ $K_{\text{M,TdxR,Trx1DD}} = 1.83 \times 10^{-3} \text{ M}$
$\text{NADP}^+ \rightarrow \text{NADPH} + \text{H}^+$	$\nu = V_{\text{Max,TMS}}[\text{NADP}^+] / (K_{\text{M,HMS,NADP}^+} + [\text{NADP}^+])$ $V_{\text{Max,HMS}} = 2.4 \times 10^{-6} \text{ M s}^{-1}$ $K_{\text{M,HMS,NADP}^+} = 4.5 \times 10^{-7} \text{ M}$
$\text{NADPH} \rightleftharpoons \text{NADPH}_{\text{bound}}$	$K_{\text{NADPH}} = 9.6$
$\text{NADP}^+ \rightleftharpoons \text{NADP}_{\text{bound}}^+$	$K_{\text{NADP}^+} = 1.8$
Conservation relationships	
$[\text{GSH}] + (2 \times [\text{GSSG}]) = [\text{GS}]_{\text{tot}}$	$[\text{GS}]_{\text{tot}} = 3.2 \times 10^{-3} \text{ M}$
$[\text{Ferricatalase}] + [\text{compound I}] + [\text{compound II}] = [\text{Cat}]_{\text{tot}}$	$[\text{Cat}]_{\text{tot}} = 2.44 \times 10^{-5} \text{ M}$
$[\text{PSHPSH}] + [\text{PSOHPSH}] + [\text{PSSPSH}] + [\text{PSO}_2\text{HPSH}] + [\text{PSOHPSOH}] + [\text{PSSPSOH}] + [\text{PSSPSS}] + [\text{PSO}_2\text{HPSOH}] + [\text{PSO}_2\text{HPSS}] + [\text{PSO}_2\text{HPSO}_2\text{H}] + [\text{iPSHPSH}] + [\text{iPSOHPSH}] + [\text{iPSSPSH}] + [\text{iPSO}_2\text{HPSH}] + [\text{iPSHiPSH}] = [\text{Prx2 dimers}]_{\text{tot}}$	$[\text{Prx2 dimers}]_{\text{tot}} = 2.85 \times 10^{-4} \text{ M}$
$[\text{Trx1}_{\text{TT}}] + [\text{Trx1}_{\text{TD}}] + [\text{Trx1}_{\text{DT}}] + [\text{Trx1}_{\text{DD}}] = [\text{Trx}]_{\text{tot}}$	$[\text{Trx}]_{\text{tot}} = 5.6 \times 10^{-7} \text{ M}$
$[\text{NADPH}] + [\text{NADPH}_{\text{bound}}] + [\text{NADP}^+] + [\text{NADP}_{\text{bound}}^+] = [\text{NADP}]_{\text{tot}}$	$[\text{NADP}]_{\text{tot}} = 2.8 \times 10^{-5} \text{ M}$

A realistic model of peroxiredoxin oxidation events in *S. pombe* was used to determine if the proposed novel measure, thioredoxin redox charge was a surrogate measure for flux. The reactions included in the model are illustrated below (Figure S5, Table S3). The kinetic parameters and values are given in Table S3.

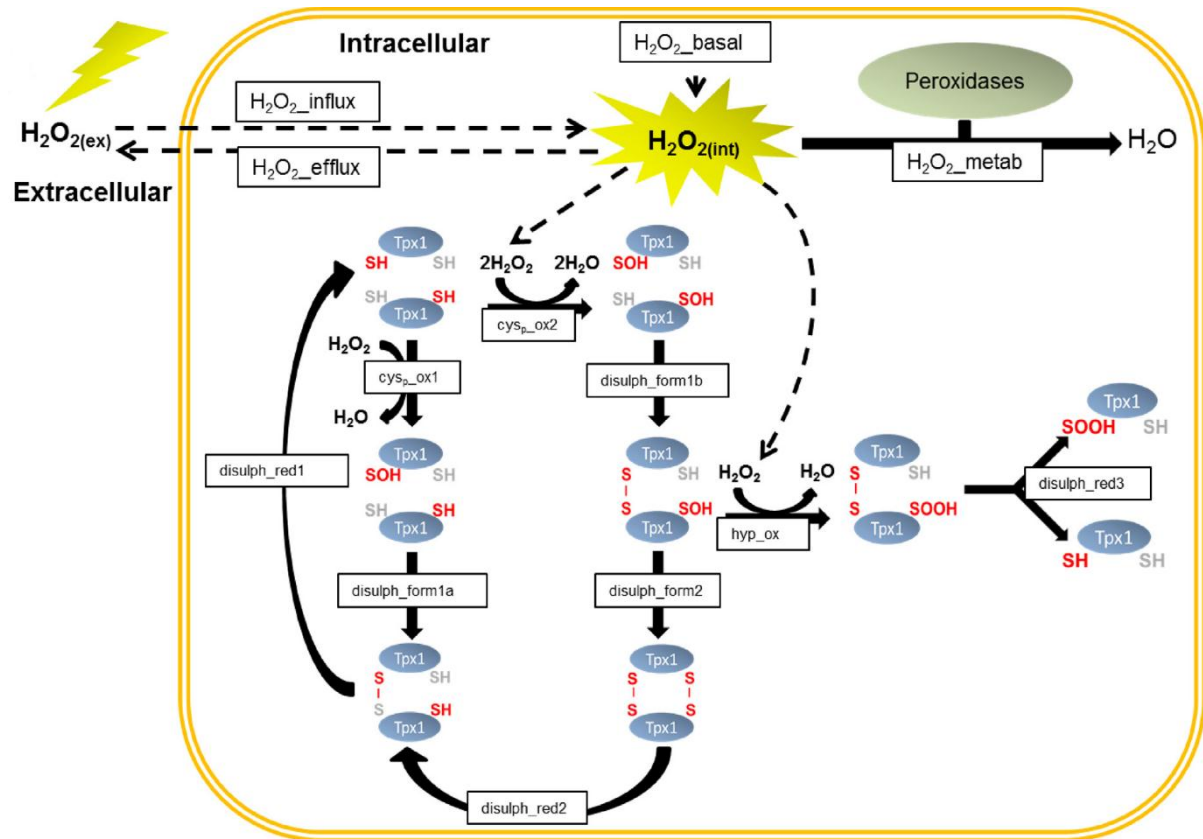


Figure S5. Reactions used to create a realistic model of peroxiredoxin oxidation (Tpx1) in *Schizosaccharomyces pombe* upon exposure to different concentrations of hydrogen peroxide (Tomalin *et al.*, 2016). The model contains 9 Tpx1 oxidation states which are interconverted by the indicated reactions. The rates of hydrogen peroxide influx and efflux as well as the removal of hydrogen peroxide from the intracellular compartment were also included in the model. Permission to reproduce this figure was not required as the article was published under a creative commons license.

Table S3. Reaction parameters used in the creation of the peroxiredoxin oxidation model (Tomalin *et al.*, 2016). Permission to reproduce this table was not required as the article was published under a creative commons license.

Parameter	Value	Units	Source	95% Confidence Interval
[Tpx1SH]	4	μM	Marguerat et al, (2012)	NA
[Trx1red]	0.7	μM	Marguerat et al, (2012)	NA
$k_{\text{H}_2\text{O}_2\text{perm}}$	1.72×10^{-5}	l s^{-1}	Parameter Estimation	$1.65 \times 10^{-5} - 1.8 \times 10^{-5}$
$V_{\text{max_H}_2\text{O}_2\text{metab}}$	59	$\mu\text{M s}^{-1}$	Parameter Estimation	51 - 70
$K_{\text{m_H}_2\text{O}_2\text{metab}}$	0.007	μM	Parameter Estimation	0.003 - 0.053
$k_{\text{cys_ox}}$	20	$\mu\text{M}^{-1} \text{s}^{-1}$	Peskin et al, (2013)	NA
$k_{\text{disulph_form1}}$	1.01	$\mu\text{M}^{-1} \text{s}^{-1}$	Parameter Estimation	0.25 - 10.97
$k_{\text{disulph_form2}}$	3.44	s^{-1}	Parameter Estimation	1.47 - 42.93
$k_{\text{disulph_red1}}$	0.190	$\mu\text{M}^{-1} \text{s}^{-1}$	Parameter Estimation	0.087 - 1.538
$k_{\text{disulph_red2}}$	0.143	$\mu\text{M}^{-1} \text{s}^{-1}$	Parameter Estimation	0.058 - 1.312
$k_{\text{disulph_red3}}$	0.029	$\mu\text{M}^{-1} \text{s}^{-1}$	Parameter Estimation	0.017 - 0.048
$k_{\text{Trx_red}}$	34	$\mu\text{M}^{-1} \text{s}^{-1}$	Oliveira et al, (2010)	NA
$k_{\text{hyp_ox}}$	0.012	$\mu\text{M}^{-1} \text{s}^{-1}$	Peskin et al, (2013)	NA
Vol_{ex}	0.05	l	Measured	NA
Vol_{int}	$5.20\text{E-}05$	l	Measured	NA
V_{basal}	5.28	$\mu\text{M s}^{-1}$	Parameter Estimation	1.48 - 16.20

References

- Benfeitás, R., Selvaggio, G., Antunes, F., Coelho, P. M. B. M. & Salvador, A. 2014. Hydrogen peroxide metabolism and sensing in human erythrocytes: A validated kinetic model and reappraisal of the role of peroxiredoxin II. *Free Rad Biol Med*, 74, 35-49.
- Lu, J., Vlamis-Gardikas, A., Kandasamy, K., Zhao, R., Gustafsson, T. N., Engstrand, L., Hoffner, S., Engman, L. & Holmgren, A. 2013. Inhibition of bacterial thioredoxin reductase: an antibiotic mechanism targeting bacteria lacking glutathione. *The FASEB Journal*, 27, 1394-1403.
- Olivier, B. G., Rohwer, J. M. & Hofmeyr, J.-H. S. 2005. Modelling cellular systems with PySCeS. *Bioinformatics*, 21, 560-561.
- Pillay, C. S., Hofmeyr, J.-H. S. & Rohwer, J. M. 2011. The logic of kinetic regulation in the thioredoxin system. *BMC Syst Biol*, 5, 15.

Tomalin, L. E., Day, A. M., Underwood, Z. E., Smith, G. R., Dalle Pezze, P., Rallis, C., Patel, W., Dickinson, B. C., Bähler, J., Brewer, T. F., Chang, C. J.-L., Shanley, D. P. & Veal, E. A. 2016. Increasing extracellular H₂O₂ produces a bi-phasic response in intracellular H₂O₂, with peroxiredoxin hyperoxidation only triggered once the cellular H₂O₂-buffering capacity is overwhelmed. *Free Radical Biology and Medicine*, 95, 333-348.